University of Alberta

Bitumen-Montmorillonite Interactions in Aqueous Media

by

Christopher Charles Repka

A thesis submitted to the Faculty of Graduate Studies and Research
in partial fulfillment of the requirements for the degree of

Master of Science
in
Materials Engineering

Department of Chemical and Materials Engineering

Edmonton, Alberta
Spring 2007

Your file Votre référence
ISBN: 978-0-494-30010-7
Our file Notre référence
ISBN: 978-0-494-30010-7

Abstract

Certain oil sand ores are deemed to be "poor processing". Markers of poor processability include high levels of fine particles or elevated concentrations of di-valent cations such as calcium and magnesium. On an industrial level, it is often difficult to obtain good bitumen recovery and/or froth quality from poor processing ores.

The tendency of montmorillonite to slime coat onto bitumen in various electrolytes (including potassium, calcium, magnesium, and bicarbonate ions) was observed from zeta potential distribution measurements.

Atomic absorption spectroscopy (AAS) was used to examine the precipitation behavior of calcium and magnesium as a function of both pH and bicarbonate concentration to help understand the action of bicarbonate ions in extraction systems.

Finally, Denver Cell extraction tests were performed to evaluate the effects of montmorillonite and calcium addition on bitumen recovery and froth quality for two different types of ore.

Acknowledgements

First and foremost, I wish to thank Drs. Zhenghe Xu and Jacob Masliyah for their guidance and their support during this project and throughout my entire graduate studies. I am grateful for the opportunity they have given me to study under them and the trust they have placed in me.

I wish to thank my fellow group members from the Oil Sands Research Group who have provided insight and friendship during my time with them. In particular, I wish to thank Jianjun Liu, Xinlin Ding, Liyan Zhang, Haihong Li, Jun Long, and Jim Skwarok for their assistance and their input into this project.

Several people from the oil sands industry also provided feedback regarding my work and put forth new ideas for me to consider. In no particular order, I wish to thank Brad Komishke, Mike Lipsett, Cliff Peters, Edward Maharajh, and Paul Hart.

Charles and Kathy Repka (my parents) and Chunfen Han (my girlfriend) gave me the moral support and encouragement to pursue and complete my Master's degree. I will be forever grateful to them for their faith and confidence in me.

Finally, I wish to thank the NSERC Industrial Research Chair in Oil Sands Engineering for providing the funding for this project. The taxpayers of Alberta, who subsidized both my undergraduate and graduate educations, also have my gratitude.

Table of Contents

1 Introduction and Literature Review **1**

1.1 The Oil Sands of Alberta 1

1.2 Bitumen Production in Surface Mining Operations 2

1.2.1 Large Scale Bitumen Production 2

1.2.2 Bitumen Production on a Smaller Scale 5

1.2.2.1 Liberation 5

1.2.2.2 Aeration and Flotation 7

1.3 The Impacts of Fine Particles and Solution Chemistry on Bitumen Extraction 13

1.3.1 Observations of Poor Processability 13

1.3.2 Causes of Poor Processability 16

1.3.2.1 Coagulation of Clays/Viscosity Increase of the Slurry 16

1.3.2.2 Water Chemistry Changes 17

1.3.2.3 Impediment of Liberation 18

1.3.2.4 Hetero-Coagulation: Emulsification and Slime Coating 18

1.4 Inter-Particle Forces and the Zeta Potential 22

1.4.1 DLVO Forces 22

1.4.1.1 The van der Waals Force 22

1.4.1.2 The Electrostatic Force 23

1.4.2 Non-DLVO Forces 26

1.5 Montmorillonite 27

1.6 Objectives of the Current Work 32

2. Experimental Principles **34**

2.1 Electrophoresis and Zeta Potential Distribution Measurements 34

2.1.1 The Electrophoresis Phenomenon 34

2.1.2 Zeta Potential Distributions 38

2.1.2.1 Background of the Technique 38

2.1.2.2 Applications of the Technique 40

2.2 Atomic Absorption Spectroscopy 42

2.2.1 Theory of Atomic Absorption Spectroscopy 42

2.2.2 Atomic Absorption Instrumentation 44

2.3 Laboratory Flotation 45

3. Zeta Potential Distribution Measurements **47**

3.1 Experimental Techniques 47

3.1.1 Experimental Apparatus 47

3.1.2 Materials 47

3.1.3 Experimental Procedure 48

3.1.3.1 Special Considerations at 35°C 51

3.2 Average Zeta Potential as a Function of pH 52

3.3 The Effects of Di-valent Cations on Slime Coating 55

3.3.1 Measurements in 1 mM KCl 55

3.3.2 Measurements in 1 mM KCl and 1 mM $CaCl_2$ 57

3.3.3 Measurements in 1 mM KCl and 1 mM $MgCl_2$ 60

3.3.4 Measurements in 1 mM KCl, 0.5 mM $CaCl_2$, and 0.5 mM $MgCl_2$ 62

3.3.5 Tests Performed Using Bitumen Extracted from Ore 64

3.4 Negation of Slime Coating 67

3.4.1 Sodium Bicarbonate 68

3.4.1.1 Effect of Sodium Bicarbonate in the Presence of Calcium 68

3.4.1.2 Effects of Sodium Bicarbonate in the Presence of Magnesium 73

3.4.1.3 Effects of Sodium Bicarbonate in the Presence of a System Containing Calcium and Magnesium 78

3.4.1.4 Sodium Bicarbonate as a Remedial Agent 80

3.4.2 Sodium Hydroxide 83

3.5 Slime Coating at Higher Temperatures 85

3.6 Summary 90

4. Precipitation of Calcium and Magnesium Ions from Solutions **92**

4.1 Experimental Techniques 92

4.1.1 Experimental Apparatus 92

4.1.2 Materials 92

4.1.3 Experimental Procedure 92

4.2 Precipitation in Solutions Containing 1 mM $CaCl_2$ 94

4.3 Precipitation in Solutions Containing 1 mM $MgCl_2$ 96

4.4 Relationship with Zeta Potential Distribution Results 98

4.5 Summary 99

5. Processability of Ores Doped with Di-Valent Ions and Montmorillonite **101**

5.1 Experimental Techniques 101

5.1.1 Experimental Apparatus 101

5.1.2 Materials 101

5.1.3 Experimental Procedure 102

5.2 Low Temperature Experiments 104

5.2.1 Good Ore Processability 105

5.2.2 Poor Ore Processability 107

5.2.3 Tailings Water Chemistry 110

5.3 High Temperature Experiments 112

5.3.1 Good Ore Processability 112

5.3.2 Poor Ore Processability 115

5.3.3 Tailings Water Chemistry 117

5.4 Summary 118

6. Conclusion and Recommendations for Future Work **120**

6.1 Summary of the Current Work 120

6.1.1 Zeta Potential Distributions 121

6.1.2 Atomic Absorption Spectroscopy 122

6.1.3 Denver Cell Flotation 122

6.2 Recommendations for Future Work 123

References **125**

Appendix A 135

Appendix B 137

List of Tables

Table 3.1	Exchangeable amounts of various ions from montmorillonite clay.	48
Table 3.2	Particle size distribution results (d_{10}, d_{50} , and d_{90}) of a bitumen emulsion and a montmorillonite suspension.	50
Table 5.1	Ore characteristics.	102
Table 5.2	Manipulated variables in the flotation tests.	104
Table 5.3	Analysis of the tailings water from tests performed at 35°C using good ore.	110
Table 5.4	Analysis of the tailings water from tests performed at 35°C using poor ore.	111
Table 5.5	Analysis of the tailings water from tests performed at 65°C using good ore.	118
Table 5.6	Analysis of the tailings water from tests performed at 65°C using poor ore.	118
Table B1	Ionic composition of the sample electrolyte.	138
Table B2	κa values for the components used in the sample electrolyte at 25°C.	137

List of Figures

Figure 1.1	A simple process flow sheet of an oil sands mining and bitumen extraction operation.	4
Figure 1.2	Interfacial forces acting on a liquid drop in a mineral flotation system.	9
Figure 1.3	Schematic of a bitumen extraction system with no slime coating (a), and a system with slime coating (b). Air bubbles are illustrated as hollow white circles, bitumen drops as solid black circles, and fine particles as the small solid grey circles.	19
Figure 1.4	Schematic of calcium acting as a bridge between bitumen and clay.	20
Figure 1.5	Sketches of the ionic distribution (top) and potential distribution (bottom) surrounding a particle immersed in an aqueous medium.	26
Figure 1.6	Octahedral units.	28
Figure 1.7	Tetrahedral units.	28
Figure 1.8	The typical structure of a 2:1 smectite clay including the exchangeable hydrated cations.	31
Figure 1.9	Simple schematic of a clay platelet illustrating the negatively charged basal plane and the positively charged edge surfaces.	32
Figure 2.1	Velocity profile in a "closed cell" electrophoresis or electro-osmosis experiment.	37
Figure 2.2	Hypothetical zeta potential distribution measurements including	

	individual measurements (a), no-interaction (b), strong attraction (c), strong attraction with insufficient coating particles (d), and weak attraction (e).	40
Figure 2.3	Layout of an atomic absorption spectrometer system.	45
Figure 2.4	Schematic of Denver Cell and Agitair unit operation.	46
Figure 3.1	Average zeta potential of bitumen at various pH values in three electrolytes.	53
Figure 3.2	Average zeta potential of montmorillonite at various pH values in three electrolytes.	53
Figure 3.3	Zeta potential distribution measurements of bitumen and montmorillonite in 1 mM KCl at pH 8.5 measured individually (a), and as a 1:1 mixture (b).	56
Figure 3.4	Zeta potential distributions of bitumen and montmorillonite in 1 mM KCl and 1 mM CaCl2 at pH 8.5 individually (a), with a 10:1 B:M ratio (b), and with a 1:1 B:M ratio (c).	58
Figure 3.5	Zeta potential distributions of bitumen and montmorillonite in 1 mM KCl and 1 mM $MgCl_2$ at pH 8.5 individually (a), with a 10:1 B:M ratio (b), and with a 1:1 B:M ratio (c).	61
Figure 3.6	Zeta potential distributions of bitumen and montmorillonite in 1 mM KCl, 0.5 mM $CaCl_2$, and 0.5 mM $MgCl_2$ at pH 8.5 individually (a), with a 10:1 B:M ratio (b), and with a 1:1 B:M ratio (c).	63
Figure 3.7	Zeta potential distributions of a bitumen/fines mixture extracted	

from a good processing ore and montmorillonite in 1 mM KCl measured individually (a), and in a 1:1 mixture (b). 65

Figure 3.8 Zeta potential distributions of a bitumen/fines mixture extracted from a good processing ore and montmorillonite in 1 mM KCl with1 mM $CaCl_2$ measured individually (a), and in a 1:1 mixture (b). 66

Figure 3.9 Zeta potential distributions of bitumen and montmorillonite measured separately in 1 mM KCl and 1 mM $CaCl_2$ without added bicarbonate (a) and with 7.1 mM of bicarbonate (b). 69

Figure 3.10 Zeta potential distributions of 1:1 binary mixtures of bitumen and montmorillonite in 1 mM KCl and 1 mM $CaCl_2$ without added bicarbonate (a), and with 7.1 mM of bicarbonate (b). 70

Figure 3.11 Zeta potential distributions of bitumen and montmorillonite measured separately in 1 mM KCl and 1 mM $CaCl_2$ without added bicarbonate (a) and with 16.4 mM of bicarbonate (b). 71

Figure 3.12 Zeta potential distributions of 1:1 binary mixtures of bitumen and montmorillonite in 1 mM KCl and 1 mM $CaCl_2$ without added bicarbonate (a), and with 16.4 mM of bicarbonate (b). 72

Figure 3.13 Zeta potential distributions of bitumen and montmorillonite measured separately in 1 mM KCl and 1 mM $MgCl_2$ without added bicarbonate (a) and with 7.1 mM of bicarbonate (b). 74

Figure 3.14 Zeta potential distributions of 1:1 binary mixtures of bitumen and montmorillonite in 1 mM KCl and 1 mM $MgCl_2$ without

added bicarbonate (a), and with 7.1 mM of bicarbonate (b). 75

Figure 3.15 Zeta potential distributions of bitumen and montmorillonite measured separately in 1 mM KCl and 1 mM $MgCl_2$ without added bicarbonate (a) and with 16.4 mM of bicarbonate (b). 76

Figure 3.16 Zeta potential distributions of 1:1 binary mixtures of bitumen and montmorillonite in 1 mM KCl and 1 mM $MgCl_2$ without added bicarbonate (a), and with 16.4 mM of bicarbonate (b). 77

Figure 3.17 Zeta potential distributions of bitumen and montmorillonite measured separately in 1 mM KCl with 0.5 mM $CaCl_2$ and 0.5 mM $MgCl_2$ without added bicarbonate (a) and with 16.4 mM of bicarbonate (b). 78

Figure 3.18 Zeta potential distributions of 1:1 binary mixtures of bitumen and montmorillonite in 1 mM KCl with 0.5 mM $CaCl_2$ and 0.5 mM $MgCl_2$ without added bicarbonate (a) and with 16.4 mM of bicarbonate (b). 80

Figure 3.19 Zeta potential distributions of bitumen and montmorillonite in 1 mM KCl and 1 mM $CaCl_2$ at pH 8.5 with a 1:1 B:M ratio (a), of the same mixture after 16.4 mM bicarbonate addition (b), and from the previous results with 16.4 mM bicarbonate pre-treatment (c). 82

Figure 3.20 Zeta potential distributions of bitumen and montmorillonite in 1 mM KCl with 1 mM $MgCl_2$ and 12.5 mM NaOH measured individually (a), and in a 1:1 mixture (b). 84

Figure 3.21 Zeta potential distribution "shift" of bitumen in 1 mM KCl and 1 mM $MgCl_2$ at 35°C. 86

Figure 3.22 Electrophoretic mobility vs. particle size calculated using Smoluckowski's Equation and Henry's Solution at a constant true zeta potential of -60 mV. 88

Figure 3.23 Zeta potential vs. particle size calculated using Smoluchowski's Equation and Henry's solution at a constant electrophoretic mobility of – 5.7 micron/sec/V/cm. 89

Figure 4.1 Solubility of calcium as a function of pH with and without bicarbonate addition. The total amount of added calcium was 1 mM. The square symbols represent the case without bicarbonate addition, the open circles represent the case with 7.1 mM bicarbonate, and the open triangles represent 16.4 mM bicarbonate. 94

Figure 4.2 Solubility of a 1 mM $CaCl_2$ solution at pH 8.5 as a function of bicarbonate concentration. The squares and the open circles represent the two experimental runs. 95

Figure 4.3 Solubility of magnesium as a function of pH with and without bicarbonate addition. The total amount of added magnesium was 1 mM. The square symbols represent the case without bicarbonate addition, the open circles represent the case with 7.1 mM bicarbonate, and the open triangles represent 16.4 mM bicarbonate. 97

Figure 4.4 Solubility of a 1 mM $MgCl_2$ solution at pH 8.5 as a function of bicarbonate concentration. 98

Figure 5.1 Primary (white) and total (gray) recovery from a good processing ore at 35°C 105

Figure 5.2 The bitumen/solids ratio of the primary (white) and secondary (gray) froths from a good processing ore at 35°C 107

Figure 5.3 Primary (white) and total (gray) recovery from a poor processing ore at 35°C 108

Figure 5.4 The bitumen/solids ratio of the primary (white) and secondary (gray) froths from a poor processing ore at 35°C 109

Figure 5.5 Primary (white) and total (grey) recovery from a good processing ore at 65°C 113

Figure 5.6 The bitumen/solids ratio of the primary (white) and secondary (gray) froths from a good processing ore at 65°C 114

Figure 5.7 Primary (white) and total (grey) recovery from a poor processing ore at 65°C 115

Figure 5.8 The bitumen/solids ratio of the primary (white) and secondary (gray) froths from a poor processing ore at 65°C 117

Nomenclature

Abbreviations

AAS	Atomic absorption spectrometer/spectroscopy
AFM	Atomic force microscope/microscopy
bbl	Barrel(s) of oil
BEU	Batch extraction unit
B:M	Bitumen to montmorillonite mass ratio
B/S	Bitumen to solids ratio
CCD	Closed circuit display
CEC	Cation exchange capacity
CSS	Cyclic steam stimulation
DLVO	Derjaguin-Landau-Verwey-Overbeek
FFR	Fast field reversal
HCL	Hollow cathode lamp
IPS	Inclined plate settler
LHES	Laboratory hydrotransport extraction system
M	molar (mol/L)
meq	Milliequivalents
ppm	Parts per million
PSC	Primary separation cell
PSV	Primary separation vessel
rpm	Revolutions per minute
SAGD	Steam assisted gravity drainage

SIPS	Sample introduction pumping system
UK	United Kingdom
US	United States
VAPEX	Vapor extraction

Symbols

A	Hamaker's constant
a	Radius
B	Absorption
C_s	Concentration of surfactant in liquid near the surface of the bubble
c_i	Ionic concentration of ion i
D	Diffusion coefficient of the surfactant in water
d_{10}, d_{50}, d_{90}	10/50/90% Cut size of particles
e	Electronic charge
F_{VDW}, F_{elec}	Force
$f_1(\kappa a)$	Henry's function
g	Acceleration due to gravity
H	Surface to surface separation distance
h	Planck's constant
I	Faraday's constant
i	Speed of light
k	Boltzmann's constant

L	Length of the absorption layer
m_b, m_{ore}, m_s	Mass
N	Number of free atoms per unit volume
R	Universal gas constant
S_v	Spectral radiant intensity
T	Absolute temperature
t, t_e, t_r, t_t	Time
$\frac{U}{E_\infty}$	Electrophoretic mobility
v	Rise velocity
W	Energy
w_{n1}, w_{n2}	Energy of an electron in a given quantum state
x	Distance
Y_{xi}, $Y_{\infty i}$	Number density of ion i per unit volume
z_i	Valence of ion i
Γ_0	Amount of surfactant adsorbed per unit surface area of a bubble
γ_{lv}, γ_{ml}, γ_{mv}	Interfacial tension
ΔG	Free energy change
δ	Average thickness of the diffuse layer
$\varepsilon\varepsilon_0$	Di-electric constant
ζ	Zeta potential

θ	Contact angle
κ	Debye-Hückel parameter
Λ	A parameter taking into account the effect of surfactants on rise velocity
λ_0	Characteristic wavelength for internal molecular motion
μ	Viscosity
ρ, ρ_1	Density
τ	Atomic absorption coefficient
υ	Resonance frequency
Φ_0, Φ_{tr}	Radiant power
ψ_x, ψ_0	Electrostatic potential

1 Introduction and Literature Review

1.1 The Oil Sands of Alberta

The demand for oil is expected to increase drastically as the world industrializes at a rapid pace. Asia alone imported 12.2 million barrels of oil each day in 2002 to fuel the rapidly developing economies of India and mainland China as well as the industrialized economies of countries such as Japan, South Korea, and Taiwan (USCINCPAC, 2002). On our own continent, the United States has become heavily reliant on imported oil. To meet the increasing demand and to help mitigate the effects of political instability in regions of traditional oil exporters such as Venezuela, Iraq, Iran, and Saudi Arabia, new and accessible sources of oil will become increasingly important. The oil sands (tar sands) of Alberta are an accessible source of oil in a politically stable and highly developed nation. As early as 1979, the oil sands were described as "Canada's future oil supply" (Towson, 1979). Oil reserves in the oil sands are estimated to be 174.4 billion bbl that, when combined with Canada's conventional reserves of 4.5 billion bbl, make Canada second only to Saudi Arabia in total proven oil reserves (Radler, 2002). This resource has the potential to play a key role in helping the world meet its energy demands in the 21st century.

Alberta's oil sands are composed of sand, fine mineral particles (< 44 μm), water, and bitumen (Camp, 1976). Bitumen is a mixture of high molecular weight hydrocarbons that can be up-graded into synthetic crude oil after it has been separated from the sand, water, and fine particles. The oil sands are located in three main deposits in Alberta: the Peace River deposit northwest of Edmonton, the Athabasca/Wabasca deposit northeast of Edmonton, and the Cold Lake deposit east of Edmonton. The Athabasca deposit is the largest and most developed of all the deposits (Camp, 1976). Oil sands can be surface mined from deposits less than 75

meters (250 feet) deep. In-situ techniques such as steam assisted gravity drainage (SAGD), cyclic steam stimulation (CSS or "huff and puff") or VAPEX solvent extraction must be used when the deposit lies more than 75 meters below the surface. The Athabasca/Wabasca deposit is accessible by either surface mining or in-situ techniques while bitumen in the Cold Lake and Peace River deposits is only recoverable using in-situ methods (Canadian Energy Research Institute, 2004). Of all the oil sands in Alberta, it is estimated that only 7% are amenable to surface mining (Government of Alberta: Department of Energy, 2004). Despite this fact, surface mining is still the dominant technique used to recover bitumen today. The focus of this thesis will be on surface mineable oil sands.

1.2 Bitumen Production in Surface Mining Operations

1.2.1 Large Scale Bitumen Production

One of the earliest published research works on bitumen extraction from Alberta's surface mineable oil sands was from Clark and Pasternack in 1932 (Clark and Pasternack, 1932). Clark, using his pilot plant on the Clearwater River, demonstrated that satisfactory bitumen recovery could be obtained by using a caustic hot water extraction process. Although the process flow-sheets used by today's oil sands operators are slightly different from that described in Clark's pilot plant, the fundamental process is the same. First, oil sand is mixed or slurried with hot water and process aids, and mechanical energy is added to the slurry to help separate bitumen from sand grains. The liberated bitumen attaches to entrained air bubbles where it floats and is collected as froth.

Modern bitumen extraction processes must integrate a mining operation with the mineral processing operation that recovers the bitumen from the oil sands ore.

The complete process is described in a review paper by Masliyah et al. (2004). Mining is performed using truck/shovel or dragline/bucket wheel reclaimer methods. In the former method, ore is blended with water and process additives in a cyclofeeder or rotary breaker before being pumped through a hydrotransport pipeline to primary separators. In the latter method, ore is transported by a conveyor belt to the plant where the ore is mixed with water and additives in rotating drums before being sent to primary separators. In the primary separators (known as primary separation vessels (PSV), Sep-Cells, or primary separation cells (PSC)), the slurry is allowed to segregate into three zones. The contents and destinations of each zone are as follows:

1) The top zone contains an aerated, bitumen rich froth. This froth is sent to froth treatment to remove the entrained air, water, and solids. At the Syncrude and Suncor operations, froth is diluted with naphtha before passing through inclined plate settler (IPS) or centrifuge units. At Albian Sands, froth is diluted with a paraffinic solvent and is subjected to counter-current decantation. In all cases, the diluent is recovered and the clean bitumen is sent to upgrading where bitumen is converted to synthetic crude oil that can be used as refinery feed stock.

2) The middle zone of the primary separator contains a mixture of water, suspended solids, and small bitumen droplets. This zone is typically sent to some form of secondary recovery units such as mechanical flotation cells or hydrocyclones where the residual suspended bitumen can be recovered. The froth from these units is then sent back to the primary separators to be re-processed.

3) The bottom zone of the primary separator contains coarse sand and water which is eventually disposed of into tailings ponds. Small amounts of residual hydrocarbon may remain in this stream.

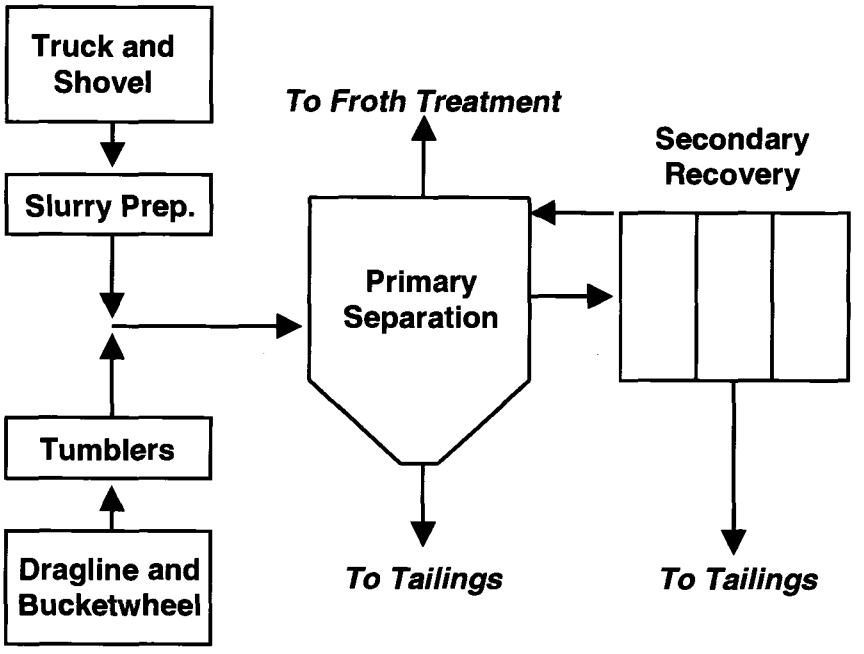

Figure 1.1: A simple process flow sheet of an oil sands mining and bitumen extraction operation.

A flow-sheet of the process is shown in Figure 1.1 above.

While the bitumen extraction process appears fairly straightforward at the macro-level, it is really the processes that occur at the micro-level that determine how effectively bitumen can be extracted from the ore. Such processes are determined by bitumen-sand interactions, bitumen-air interactions, and bitumen-fines interactions. Water chemistry plays a critical role in how well the process operates. The next section of this thesis will focus on how bitumen extraction occurs on a smaller scale.

1.2.2 Bitumen Production on a Smaller Scale

On the small scale, there are two fundamental processes which must occur in order for bitumen to be recovered as froth: liberation (separation) and flotation (aeration). During liberation, bitumen separates from the surface of sand grains and enters the fluid phase as a discrete entity. Flotation is the stage where bitumen attaches to air bubbles and is able to float into the froth because of the density difference between the aerated bitumen and water. Each process and the factors affecting them are discussed in the sections that follow.

1.2.2.1 Liberation

During liberation, water must displace bitumen on the surface of sand grains. One mechanism for bitumen displacement has been described by Takamura and Chow (1983). The authors speculated that water in the oil sands was present as pendular rings at grain to grain contact points and as a 10 nm film covering the sand surfaces. Bitumen recession from sand grain surfaces towards grain to grain contact points was observed when oil sand clumps were placed in hot water. The film of bitumen surrounding the sand grains became thinner and thinner until the disjoining pressure (resulting from the presence of the 10 nm water film) forced a complete detachment of bitumen from the sand surface. The disjoining pressure and the crumbling rate of oil sand pellets were found to increase in the presence of NaOH and decrease in the presence of Ca^{2+}. A higher disjoining pressure, or inter-facial repulsive force, is better for bitumen liberation as it stabilizes the water film and prevents bitumen-sand contact. More recently, Liu et al. (2003) studied the forces between bitumen and silica using atomic force microscopy (AFM). They found that the repulsive force between bitumen and silica increased with increasing pH.

Calcium additions had a two-pronged effect on bitumen-silica interactions: Ca^{2+} decreased the repulsive force and increased the adhesion force between bitumen and silica.

The important effects of NaOH on bitumen recovery were noted previously by Sanford and Seyer (1979), Sanford (1983), Schramm et al. (1984) and Schramm and Smith (1989). These authors attributed the important role of NaOH to the production of natural surfactants from compounds contained in bitumen. Sanford and Seyer (1979), using a batch extraction unit (BEU), speculated that the addition of NaOH to oil sands slurries ionized organic bitumen acids to give surface active salts, and that these surfactants changed the interfacial tensions between bitumen, water, and solids such that bitumen-solids separation was favored. Sanford (1983) tested the effects of various inorganic bases and surfactants on bitumen recovery. A maximum recovery was observed at varying dosages of bases such as NH_3, Na_2SiO_3, or $Na_5P_3O_{10}$ or surfactants such as sodium oleate or Tide® laundry detergent. Schramm et al. (1984) studied the effects of NaOH on the carboxylate surfactant concentration and the effects of carboxylic surfactants on bitumen recovery. The amount of total and free carboxylic surfactants in an oil sands extraction slurry increased with increasing NaOH addition. A maximum recovery was observed at a specific surfactant concentration, indicating that the potential exists to adversely affect bitumen recovery through over-dosage of process aids. The action of surfactants was further elucidated by Schramm et al. (1985, 2003) who performed electrokinetic measurements that correlated the maximum zeta potential of bitumen with the optimal free surfactant concentration for bitumen recovery, indicating that surfactants control the bitumen/solution charge through adsorption at the interface. In their latter study,

Schramm also observed that the maximum recovery was observed at the minimum of interfacial tension between bitumen froth and aqueous tailings water.

The presence of surfactants and other dissolved species is, of course, not the only factor controlling bitumen separation from sand grains. Mechanical energy input, such as fluid shear, is also an important pre-requisite for bitumen recovery in oil sands extraction systems (Sanford, 1983), although the exact role of mechanical energy input is not yet clear. Adequate thermal energy input is also required if satisfactory bitumen recovery is to be achieved. Schramm et al. (Schramm, Stasiuk, Yarranton, Maini, and Shelfantook, 2003) speculated that the main effect of thermal energy input was to reduce the viscosity of bitumen. Their tests indicated that adequate bitumen recoveries could be achieved at temperatures as low as 25°C provided that a diluent (kerosene) was added at high levels. The viscosity reduction might allow bitumen to recede from sand grains more easily.

1.2.2.2 Aeration and Flotation

Once the bitumen has been separated from the sand and entered the aqueous phase, it must attach to air bubbles in order to achieve sufficient buoyant force to float into the froth. Thermodynamically, the conditions for air bubble attachment to a mineral surface, such as a bitumen surface, are expressed by Young's equation (1.1) and the Dupre relationship (1.2) (Ives, 1984; King, 1982), given below, where γ_{mv}, γ_{ml}, and γ_{lv} are the mineral/vapor, mineral/liquid, and liquid/vapor interfacial tensions, respectively, while θ is the contact angle as illustrated in Figure 1.2.

$$\cos\theta = \frac{\gamma_{mv} - \gamma_{ml}}{\gamma_{lv}} \qquad [1.1]$$

The free energy change resulting from displacement of water by air on the mineral surface is denoted as ΔG.

$$\Delta G = \gamma_{mv} - (\gamma_{ml} - \gamma_{lv}) \qquad [1.2]$$

Combination of 1.1 and 1.2 leads to the thermodynamic condition of flotation, given by equation 1.3. Since the free energy change must be negative for bubble adhesion to occur, equation 1.3 stipulates that for any mineral-liquid system with $0°<\theta<180°$, bubble adhesion is theoretically possible.

$$\Delta G = \gamma_{lv}(\cos\theta - 1) < 0 \qquad [1.3]$$

From equations 1.1-1.3, one can easily see how the interfacial tensions between the various phases control not only the separation of bitumen from sand grains, but also the aeration of liberated bitumen droplets/globules. The reader should be reminded, at this point, that the above equations only hold for equilibrium conditions where gravitational effects, surface roughness, contamination, or non-equilibrium adsorption are not present.

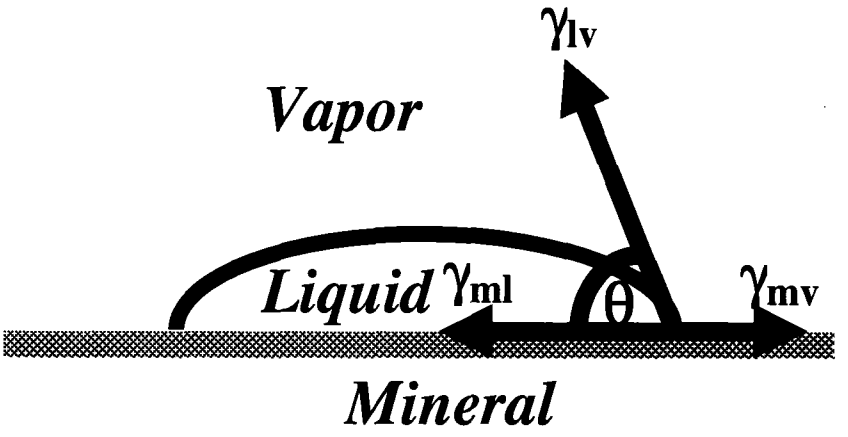

Figure 1.2: Interfacial forces acting on a liquid drop in a mineral flotation system.

At present, more information is available in the oil sands literature on the topic of liberation than on the topic of flotation. This is unfortunate, as it has been shown that the flotation step is the rate limiting step in the bitumen recovery process (Wallwork et al., 2004). While some aspects of mineral aeration may be applicable to oil sands, oil sands are an inherently different substance than metallic minerals and therefore the discussion of some literature specific to bitumen aeration is appropriate in this thesis. One difference between metallic mineral processing and oil sand processing is that the viscosity of bitumen can change with temperature. It is thus possible that bitumen not only attaches to air bubbles (as minerals do) but it is also possible that bitumen can spread over an air bubble and completely engulf it. One study by Moran et al. (2000) looked at the statistical probability of bitumen spreading over an air bubble when air was contacted with a bitumen droplet. While the Dupre relationship predicts that the spreading of bitumen over an air bubble is thermodynamically favorable, it also assumes that a three-phase contact point is already present between bitumen, water, and air. Moran speculated that various

colloidal forces between bitumen and air are present, which impede the formation of a three-phase contact point. The probability of aeration increased with an increase in aqueous phase ionic strength and decreased in the presence of clays which, it was speculated, created a steric barrier to bitumen-air contact. Induction time measurements on bitumen-air attachment have also been carried out (Gu et al, 2003). The induction time, t, is the sum of the times required for the water film between bitumen and air to thin (t_t), rupture (t_r), and for the three phase contact line to expand (t_e). In general, flotation recovery and induction time are inversely related. The trends observed in their experiments indicate that induction time decreases with a moderate increase in temperature (from 25°C to 50°C). The induction time was higher when the experiments were performed in process water rather than in de-ionized water. The highest induction time was observed when the experiments were carried out in process water doped with an additional 50 ppm Ca^{2+} and 0.5% fine solids.

Following aeration, bitumen rises into the froth under the buoyancy imparted by the attached air. The rise velocity of aerated bitumen is a difficult problem to solve from a theoretical standpoint. Many correlations have been developed such as those by Levich (1.4) and Frumkin and Levich (1.5) (Klassen and Mokrousov, 1963). The latter equation (1.5) deals specifically with the rise velocity of bubbles in the presence of surfactants.

$$v = \frac{2a^2 g(\rho - \rho_1)}{9\mu} \qquad [1.4]$$

$$v = \frac{2a^2 g(\rho - \rho_1)\left(\mu + \frac{\Lambda}{3}\right)}{3\mu(2\mu + \Lambda)} \qquad [1.5]$$

In these equations v is the rise velocity, a is the radius of the bubble, g is the acceleration due to gravity, ρ is the density of the fluid, ρ_1 is the density of the bubble, and μ is the viscosity of water. The parameter Λ in equation 1.5 is defined as:

$$\Lambda = \frac{2\Gamma_0 \delta}{Da} \cdot \frac{d\gamma_{lv}}{dC_s} \qquad [1.6]$$

where Γ_0 is the amount of surfactant adsorbed per unit surface area of the bubble, δ is average thickness of the diffuse layer, D is the diffusion coefficient of the surfactant in water, and C_s is the concentration of surfactant in liquid near the surface of the bubble. As seen in the above equations, the two most important parameters controlling rise velocity are the fluid viscosity and the density difference between the fluid and bubble. The effects of viscosity on rise velocity of bitumen have been examined by Schramm (1989) who concluded that an increase in viscosity caused by the presence of interacting fine particles can effectively hinder bitumen recovery. The authors also noted that viscosity does not need be constant throughout the entire separator, and that the addition of NaOH had a significant impact on viscosity and hence rise velocity. A Luba Tube sampling technique was used by other researchers (Ng et al., 2000) to examine the bitumen-air aggregate size and the bitumen loading on bubbles in a pilot plant PSV. It was discovered that the aggregate size and bitumen loading were highly dependent on the type of ore processed. For estuarine ores the average aggregate diameter was 1 mm and was loaded with approximately 0.9 mg of bitumen while for marine ores the average size of aggregates was 0.33-0.69 mm and each carried approximately 0.017-0.137 mg of bitumen. The small diameter of aggregates from marine ores and the large aggregate diameter from estuarine ores

correlated well with the low recovery obtained from marine ores and high recovery obtained from estuarine ores. Differences between the aeration characteristics of estuarine ores and marine ores were studied by Zhou et al. (2000) who looked at the phenomenon of air holdup or, in other words, the volume of air in a given volume of flotation suspension. Air holdup was higher in extracts from marine ores than in extracts from estuarine ores, higher when NaOH was added to the process as compared to the case without NaOH addition, and higher in turbid (fines containing) extracts than in clear extracts. The idea that marine ores release more surfactants may seem to contradict the notion that lower recoveries are usually obtained from marine ores. This further complicates the role of surfactants in the bitumen extraction system and may show that surfactants perform other actions such as stabilizing oil in water emulsions (i.e. reverse emulsions) and air bubbles, thus creating another barrier for air bubble/bitumen attachment.

The presence of "indigenous air" (air naturally entrapped in oil sands) and its effects on bitumen extraction have been examined by Flynn et al. (2001). Experimental data obtained from jar flotation tests appear to support the claim that a small amount of indigenous air is present in oil sand, but also that this air is not sufficient to provide good bitumen recovery. Bitumen recovery increased when additional air was added to the system, and the timing of the air addition did not appear to affect recovery. This work somewhat contrasts the work of Drelich et al. (1995). While Drelich also concurred that additional air input was necessary for bitumen recovery, he believed that (in addition to the aeration stage) air also assisted during bitumen liberation. Drelich thus proposed that air be added near the beginning of an extraction process. The discrepancy between the results of Flynn and Drelich may be due to the different oil sands ores and experimental procedures used. Flynn

used ores from the Syncrude lease in the Athabasca deposit while Drelich used Utah oil sands which have fundamentally different physical and chemical properties.

1.3 The Impacts of Fine Particles and Solution Chemistry on Bitumen Extraction

Laboratory research and industrial experience have indicated that two of the most important parameters affecting the bitumen extraction process are the fine particle content of the ore and the water chemistry of the system. These components have the potential to affect both bitumen liberation and flotation. The effects of fine clay particles and dissolved ions, particularly divalent cations such as calcium and magnesium, are discussed in this section. An entire section is warranted since the theory and results discussed here will provide the motivation for this thesis.

1.3.1 Observations of Poor Processability

The detrimental effects of calcium ions, magnesium ions, and fine particles on bitumen recovery were established as early as Clark's and Pasternack's 1932 paper (Clark and Pasternack, 1932). In this paper, it was noted that the addition of small amounts of magnesium chloride, magnesium sulfate, or magnesium oxide had a detrimental impact on bitumen recovery. A similar detrimental effect was observed with the addition of calcium chloride and calcium oxide, but not with calcium carbonate. Clark also added bentonite (montmorillonite) clay to the process and observed that "Half of one percent of it [clay addition] decreased the yield and increased the tendency for it [the clay] to stay in the plant water. One to two percent caused marked loss of yield and dispersion of bitumen as well as increased content of mineral matter [in the froth]". Clark noted that the presence of other clays affected bitumen recovery adversely, but only when added in much higher quantities.

More recent work has also shown the detrimental impact of di-valent ions and/or fine particles on bitumen recovery. Sanford (1983) observed a decrease in bitumen recovery with increasing fines content in pilot plant runs but found no correlation between the amount of di-valent ions present and the bitumen recovery obtained. Sanford also discovered through recovery tests that one cannot accurately re-create the processability of high-fines ores by blending fine particles with low-fines ores. BEU tests performed by Baptista (1989b) showed that the amount of primary froth obtained was inversely related to the milliequivalents (meq) of calcium, calcium+magnesium, and calcium+magnesium+sodium exchanged from the clays of the various oil sands. A similar trend relating bitumen recovery to the exchangeable ions was observed in pilot plant tests by the same author (1989a), although the results obtained appear to contradict the earlier results of Sanford (1983) who found that ore processability decreases as the fines content increases. Baptista observed that the fines content of the ore was not the determining factor of ore processability. In his tests, he found that the oil sand with the highest recovery was also the oil sand containing the most fines while the ore with the lowest recovery was characterized as having an average fines content. The presence of degraded illite has also been shown to have a detrimental impact on bitumen recovery (Wallace et al., 2004).

Several researchers have carried out systematic studies to further elucidate the characteristics of poor processing ores by modifying good ores or creating "model oil sands". In this approach, the manipulated variables can be carefully defined and controlled. Any changes in processability can then be attributed directly to the manipulated variable(s). Kasongo et al. (2000) performed Denver cell flotation tests using estuarine ores doped with clay (illite, kaolinite, or montmorillonite) in the presence of various amounts of calcium. No effects on primary recovery or flotation

kinetics were observed when 40 ppm of calcium or 1 wt % of any of the three clays were added to the system. However, in the presence of 30 ppm or higher of calcium ions and 1 wt % montmorillonite, primary recovery dropped sharply, illustrating a synergetic effect of calcium ions and montmorillonite clay. No depression was observed with kaolinite or illite in the presence of calcium ions. Recently, jar tests were performed using "model oil sands" synthesized by mixing bitumen, sand, fine particles, and water (Chong et al., 2003; Fong et al., 2004). Chong et al. found that, in the absence of NaOH, a decrease in the fine quartz content resulted in an increase in recovery. The authors also noted that a small amount of fines was beneficial for bitumen recovery in comparison to the case with no fines. The presence of an appropriate amount of fine particles was believed to prevent the attachment of larger sand grains to liberated bitumen. Such larger sand grains would weigh the bitumen down and drag it into the tailings. Fong et al. (Fong et al., 2004) found that the addition of sodium ions up to 2000 ppm and the corresponding sulfate or chloride ion concentrations of 2000 and 3080 ppm, respectively, had no impact on bitumen recovery when compared to the blank test. However, the addition of fine silica (d_{50} = 13 μm), ultra-fine silica (d_{50} = 1.2 μm), 1% illite clay, or 15 ppm or less calcium in the process water had a detrimental impact on bitumen recovery. For all these cases, bitumen recovery was restored at a higher NaOH dosage. Bitumen recovery was permanently lost when montmorillonite was added at concentrations from 0.05-1 wt%, when kaolinite (acid or sodium form) was added at 1-5 wt%, or when magnesium or calcium ions were present in the process water at levels above 9 and 30 ppm, respectively.

1.3.2 Causes of Poor Processability

Numerous explanations for the cause(s) of poor processability have been put forward. Most of the explanations fall into one of several categories.

1.3.2.1 Coagulation of Clays/Viscosity Increase of the Slurry

According to Equations 1.4 and 1.5, the rise velocity of bitumen should decrease as the viscosity of the slurry increases. The viscosity of the slurry increases as the clay platelets become less dispersed. Since the residence time of a bitumen/air aggregate inside primary separators is finite, a slower rise velocity should lead to a lower bitumen recovery. This possibility was examined by Schramm (Schramm, 1989) who concluded that although viscosity is not uniform throughout the primary separation unit, an increase in suspension viscosity can hinder bitumen recovery. In addition, it is also possible that coagulated clay platelets form some kind of structure capable of trapping bitumen. This explanation was put forth by Baptista (Baptista, 1989a, 1989b) who, as discussed above, noted a decrease in bitumen recovery in oil sands containing clays rich in exchangeable calcium, calcium+magnesium, and calcium+magnesium+sodium. Baptista believed that clays with a high concentration of exchangeable calcium and magnesium were capable of coagulating to form bitumen trapping structures. While the concept appears to correlate with the recovery data obtained, no empirical evidence of the existence of coagulated clay structures capable of entrapping bitumen was provided by the author. The role of salinity in the gelation of ultra-fines suspensions has also been examined (Kotlyar et al., 1995). Floc size, settling characteristics, and degree of gelation were observed in the presence of NaCl and $NaHCO_3$. Faster settling rates and larger floc sizes were observed for the case with chloride present than for the case with bicarbonate present until a threshold

concentration of bicarbonate was reached. Past this threshold, the settling rate observed in the bicarbonate case increased drastically. It was determined that approximately 1.4 volume percent of ultra-fine solids was required for gelation to occur, independent of the type of anions present.

1.3.2.2 Water Chemistry Changes

Another notion exists that the presence of fine particles can adversely impact the chemistry of the water used for oil sand processing. For instance, fine silica was observed to decrease the pH of process water in the model oil sands tests described above. The pH decrease was attributed to an exchange of protons at the silica surface with hydroxyl ions in solution. The presence of acidic kaolinite decreased the pH of slurry water while montmorillonite increased the pH of slurry water. The decrease in pH with acidic kaolinite or fine silica would negatively impact bitumen recovery as it consumes alkalinity necessary for the generation of natural surfactants. The addition of montmorillonite might benefit bitumen extraction from an alkalinity standpoint, but will negatively affect it in terms of slime coating, as will be discussed in Section 1.3.2.4.

Smith and Schramm (1992) performed an analysis on the consumption of NaOH by mineral components in the oil sands. The idea that mineral components consume NaOH is supported by the idea that 1.25 meq of NaOH per 500 g of oil sand produces only 0.13 meq of surfactants. The NaOH loss was attributed by the authors to reactions with polyvalent carbonates, clays, and sulfates. Also stated was the possibility of some precipitation of carboxylate surfactants.

1.3.2.3 Impediment of Liberation

Some evidence exists that the presence of fine particles and divalent cations affects not only bitumen flotation but also bitumen liberation. Contact angle measurements (Basu et al., 2004) have shown that the addition of calcium ions or montmorillonite clay can adversely impact bitumen separation from a glass surface. No synergetic effect was observed in measurements performed in combinations of calcium ions and montmorillonite clays. The results obtained in a mixture of calcium and montmorillonite clay were similar to those obtained in calcium ions alone.

1.3.2.4 Hetero-Coagulation: Emulsification and Slime Coating

Emulsification by fines, or slime coating, occurs when fine particles adsorb onto the surface of bitumen during the aqueous extraction process. The fine particles adsorb onto bitumen, and not vice-versa, because the fine particles are less hydrophobic than bitumen, resulting in a lower energy state than that for bitumen to be exposed to the aqueous phase. The consequences of fine particle coagulation with bitumen are as follows:

1) Fine particles might act to stabilize emulsions of extremely small bitumen droplets by adsorbing on their surfaces and preventing coalescence with other bitumen droplets.
2) A layer of hydrophilic (or much less hydrophobic) particles coated on the outside of a bitumen drop might prevent effective bitumen/air attachment. As a result, the flotation recovery, kinetics, and froth quality might all be adversely affected. This is the phenomenon known as "slime coating".

A schematic of slime coating and the effects on bitumen recovery are shown in Figure 1.3. One of the first mechanistic studies of slime coating was performed by Sun (Sun, 1943) on mineral systems. Sun proposed an "ionic hypothesis" whereby the zeta potentials of the mineral and slime particles were the controlling factors of slime coating. According to this hypothesis, slime coating should be severe when the zeta potentials of both mineral and slime were opposite in sign and high in magnitude or when the zeta potential of the slime is low.

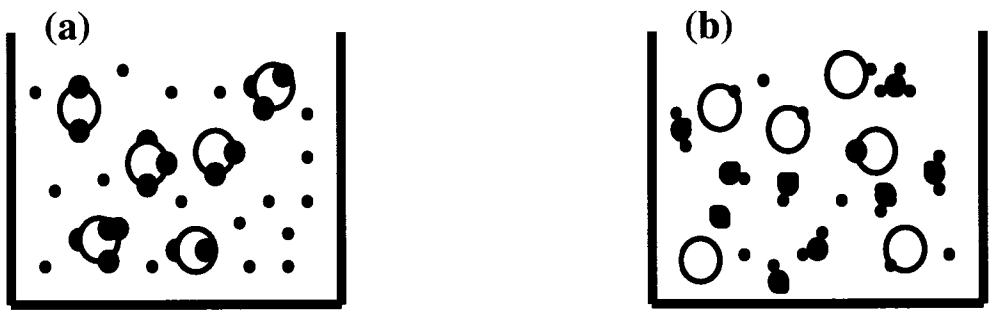

Figure 1.3: Schematic of a bitumen extraction system without slime coating (a), and with slime coating (b). Air bubbles are illustrated as hollow white circles, bitumen drops as solid black circles, and fine particles as the small solid grey circles.

No slime coating is expected when the zeta potentials of the slime and particles are high in magnitude and alike in sign. This hypothesis is in line with what would be predicted by the DLVO theory, explained in Section 1.4.1. The theory predicts that under conditions of electrostatic attraction or low electrostatic repulsion, the net force acting between particles is attractive in nature. Conversely, at conditions of high electrostatic repulsion, the electrostatic repulsive force overpowers the attractive van der Waals force and no attraction is observed between the two particles.

While Sun's hypothesis would hypothetically remain true for a system containing bitumen, fine particles, sand, and water, it has been shown that the zeta potential of most oil sands components are moderately negative in nature (Liu et al., 2002, 2003, 2004a, 2004b). If slime coating were to occur under such conditions, other mechanisms must be responsible. Several concepts discussing how this might occur are noted in the literature. The accepted ideas involve calcium or other di-valent cations acting as a "bridge" between clay platelets and bitumen. Hall and Tollefson (1982), in their paper on tailings, brought forth the idea that calcium bridging complexes form between clays and minerals. A simple schematic (Figure 1.4) shows one possibility of chemical bonding between bitumen and a clay particle. It should also be noted that at this time, there is no general agreement amongst the oil sands research community as to exactly how bitumen and fines are physically or chemically bonded to each other.

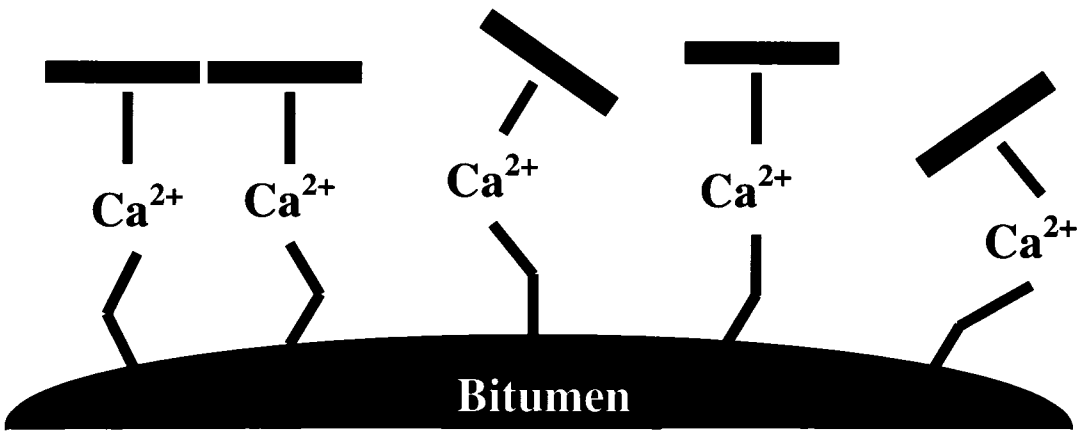

Figure 1.4: Schematic of calcium acting as a bridge between bitumen and clay.

Another possibility brought up in the literature is that somehow certain solids become coated with toluene insoluble organic material. The presence of this material would impart a bi-wettable, or surface active, property to the clay particles. Czarnecka and Gillott (1980) observed that bitumen and various bitumen fractions strongly adsorb on the external surface of clay minerals, causing those minerals to become less hydrophilic. Generally, slightly more organic matter was adsorbed on calcium saturated clay than sodium saturated clays. Bensebaa et al. (2000) and Sparks et al. (2003) hypothesized that bitumen solids from oil sands deposits are partially coated with toluene insoluble organic material such as humic and asphaltene like components. Such surface active solids can stabilize water in oil, or conversely, oil in water emulsions such as fine bitumen droplets suspended in the middlings of the primary separation unit.

Regardless of the exact causes of slime coating or other mineral-bitumen hetero-coagulation, it is necessary from a scientific standpoint to verify that such a phenomenon actually exists. One technique used to observe the presence of slime coating is to measure zeta potential distributions. The technique will be discussed in detail in Section 2.1. Liu et al. (2002, 2004b) observed the presence of a slime coating of montmorillonite on bitumen in the presence of 40 ppm calcium using zeta potential distribution measurements. Slime coatings were not observed in the presence of a combination of calcium and kaolinite clay. These findings correlate well with the recovery tests of Kasongo et al. (2000). Liu et al. (2004a) also performed zeta potential distribution measurements on fines from good processing ores and those from poor processing ores. When measurements were performed in 40 ppm calcium or in process water from extraction tests, the fines obtained from poor

processing ores were found to coat onto bitumen and emulsified froth while those from good processing ores did not.

Colloidal force measurements using an atomic force microscope (AFM) have also been used to examine the net force existing between bitumen and clays or real oil sand fines (Liu et al., 2004a, 2004b). Stronger attractive forces conducive to slime coating were measured between bitumen and montmorillonite than between bitumen and kaolinite. Similarly, when real oil sand fines were examined using the AFM, stronger adhesion forces were observed for fines from poor processing ores than those from good processing ores.

1.4 Inter-Particle Forces and the Zeta Potential

The previous sections explained how an oil sands extraction system is fundamentally controlled by the various inter-particle forces that exist in the system. A more thorough examination of various colloidal forces, as well as the zeta potential, is warranted as it supports the foundation of this thesis.

1.4.1 DLVO Forces

On the colloidal scale, the two well understood and quantified forces acting between suspended particles are the van der Waals (London) forces and the electrostatic (coulombic) force. These two types of forces are collectively known as the "DLVO", or Derjaguin-Landau-Verwey-Overbeek, forces.

1.4.1.1 The van der Waals Force

In any instance, electrons in a molecule or atom may become momentarily concentrated in one region. As a result of this instantaneous electron distribution, the

atom/molecule becomes temporarily polarized. This momentary polarization of one atom/molecule induces dipoles in neighboring atoms or molecules. This attraction between the dipole and the neighboring induced dipole is a major component of van der Waals forces (Petrucci and Harwood, 1997). The van der Waals interaction energy between two bodies can be calculated by a "pairwise summation" of intermolecular forces between two bodies (Hunter, 2001). For the case of two spheres of radius a, with a surface to surface separation of H, the van-der Waals interaction force is given by Equation 1.7 when $r_1, r_2 >> H$ (Hunter, 2001).

$$F_{VDW} = \frac{Aa}{12H^2} \qquad a >> H \qquad [1.7]$$

The constant A is known as the Hamaker constant. The Hamaker constant is calculated from the material properties of particles 1 and 2 and the properties of the suspending medium. It is worth noting that equation 1.7 is valid only when the center to center distance of the two particles is much less than a characteristic wavelength for internal molecular motion, λ_0. A typical value of λ_0 is 100 nm (Masliyah, 1994). When the center to center distance becomes a significant fraction of λ_0 the van der Waals interactions, which are known as retarded van der Waals interactions, will be lower than those calculated by equation 1.7. Equations for the retarded van der Waals interactions are available in the literature, but are beyond the scope of this thesis.

1.4.1.2 The Electrostatic Force

When solid particles or emulsion droplets are introduced into an aqueous phase, a spontaneous separation of charge will occur between the two phases in contact and the surface of the particle/droplet will become positively or negatively

charged. Causes of this charge separation include, but are not limited to, ionization of surface groups, differential solution of ions from the surface of a sparingly soluble crystal, isomorphous substitution, specific ion adsorption, and charged crystal surfaces (Everett, 1988). In order for the condition of system electro-neutrality to be maintained, the charge generated on the surface of the particle must be balanced by a build-up of opposite charge in the solution surrounding the particle. This build up of charge surrounding the particle is expressed in two forms: the Stern or Helmholtz layer, consisting of ions bound to the surface, and the diffuse electric double layer which is not bound to the surface (Israelachvili, 1992). The distribution of ions throughout the electric double layer is expressed by the Boltzmann distribution (Equation 1.8) where Y_{xi} and $Y_{\infty i}$ are the number density of ion i per unit volume at a distance x from the surface of the particle and in the "bulk" solution, respectively, z_i is the valence of ion i, ψ_x is the electrostatic potential at point x, k is the Boltzmann constant, e is the electronic charge, and T is absolute temperature (Israelachvili, 1992).

$$Y_{xi} = Y_{\infty i} \exp\left(\frac{-z_i e \psi_x}{kT}\right) \qquad [1.8]$$

The electric potential gradient, expressed in terms of the variables defined above, is given by Equation 1.9. Equation 1.9 can be further simplified to equation 1.10, which is valid for low potentials (Israelachvili, 1992). Equation 1.10 thus defines the electric potential at any distance from the surface when the surface potential, ψ_0, is known. The electric potential at $x = \infty$ (the "bulk" solution) is generally defined as zero.

$$\sum_i Y_{xi} = \sum_i Y_{\infty i} + \frac{\varepsilon\varepsilon_0}{2kT}\left(\frac{d\psi}{dx}\right)_x^2 \qquad [1.9]$$

$$\psi_x \approx \psi_0 \exp(-\kappa x) \qquad [1.10]$$

The parameter κ is defined by equation 1.11 where I is Faraday's constant, c_i is the ionic concentration of ion i in mol/L, and z is the valence of the respective ions. Note that κ is dependent only upon the solution composition and concentration and is unaffected by the properties of the suspended phase. The term κ is also known as the Debye-Hückel parameter (Hunter, 2001).

$$\kappa = \left(\frac{2000I^2}{\varepsilon\varepsilon_0 RT}\right)^{1/2} \left(0.5\sum c_i z_i^2\right)^{1/2} \qquad [1.11]$$

As mentioned above, the Stern or Helmholtz layer contains the inner layer of ions that are bound to the surface of the particle. The boundary between the mobile inner layer (ions that will move with the particle as the particle travels through the solution) and the diffuse layer is known as the shear plane. The electric potential measured at the shear plane is referred to as the zeta potential (Masliyah, 1994). Schematics illustrating the relationship between ion and potential distribution are shown in Figure 1.5.

The electrostatic force between two spheres of radius a is given by Equation 1.12 (Israelachvili, 1992) where H is the surface to surface distance between the two spheres.

$$F_{elec} \approx 2\pi a\varepsilon\varepsilon_0\kappa\psi_0^2 \exp(-\kappa H) \qquad [1.12]$$

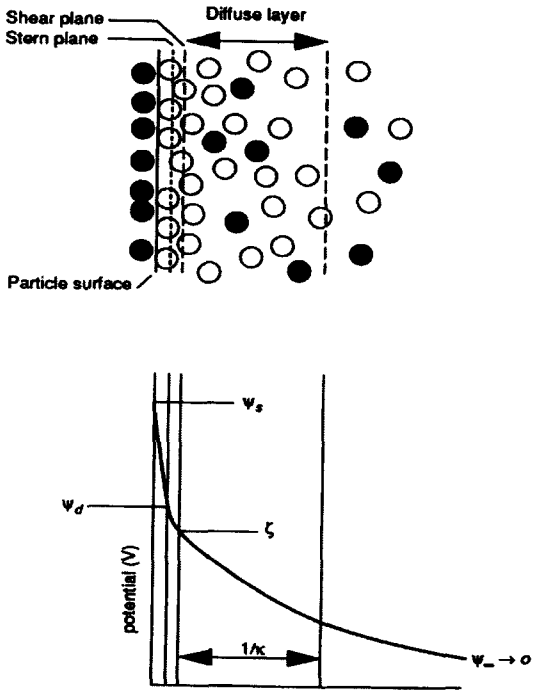

Figure 1.5: Sketches of the ionic distribution (top) and potential distribution (bottom) surrounding a particle immersed in an aqueous medium (Adapted from (Masliyah, 1994).

1.4.2 Non-DLVO Forces

Other colloidal forces which are not included in the DLVO theory may also exist. These forces have been summarized in a review paper by Johnson et al. (2000). One major non-DLVO force, the steric force, arises because of the presence of surface adsorbed molecules. Steric repulsion is thus a physical force, and is likely attributable to elastic compression of adsorbed molecules and a rise in osmotic pressure between

particles. The structural, or hydration, force is related to the presence of a strongly associated layer of water on the suspended particles, resulting in a strong short range repulsive force. The attractive "hydrophobic force" is not well understood, but may possibly be due to a re-structuring of water molecules around hydrophobic colloidal particles. The re-arrangement of water molecules creates a thermodynamically un-favorable "water cage" around the particle, resulting in an attraction between hydrophobic particles greater than that predicted by van der Waals forces alone. Bridging forces occur when flocculant molecules attach to more than one particle and "bridge" them together into large flocs.

1.5 Montmorillonite

Montmorillonite is a di-octahedral smectite clay mineral with a general formula of $Me_X^{+}(Ro_{2-X}^{3+}Ro_X^{2+})Si_4O_{10}(OH)_2 \cdot nH_2O$ where Me is usually Na or Ca and Ro is typically Al, Fe, or Mg (Eslinger and Pevear, 1988; Velde, 1977). In the past, the term clay defined minerals that were smaller than 2 μm in size. Today, the term is generally applied to minerals with a phyllosilicate sheet structure (Velde, 1992). Most clay minerals exist discretely in the form of platelets containing a large basal plane with small edge surfaces. Clay minerals are built from two structural groups: octahedral units and tetrahedral units. The octahedral unit contains two planes of closely packed oxygen or hydroxyl units with aluminum, iron, or magnesium embedded between the oxygen or hydroxyl planes. In this situation, the aluminum, iron, or magnesium ions would have a co-ordination number of 6 with respect to the oxygen or hydroxyl ions in the lattice. The other structural unit, the tetrahedral unit, consists of silica tetrahedrons. Each silica tetrahedron contains one silicon atom with four oxygen or hydroxyl units all lying at an equal distance from the central silicon

atom. The tetrahedrons are arranged to form a hexagonal network, with all apical tips of the tetrahedrons pointing in the same direction (Grim, 1968). Typical octahedral and tetrahedral units are shown in Figures 1.6 and 1.7, respectively.

Clays can be further classified into 1:1 or 2:1 layer types. Clays possessing a 1:1 layer type are a combination of 1 octahedral sheet and 1 tetrahedral sheet. The octahedral sheet is linked to the tetrahedral sheet via the apical oxygen from the tetrahedral sheet, which is shared between the two sheets. The apical oxygen thus also becomes part of the octahedral sheet, replacing a hydroxyl unit. Clays with a 2:1 layer type combine 2 tetrahedral sheets with 1 octahedral sheet. The 2:1 layer type is similar to the 1:1 layer type, but contains an additional tetrahedral layer which is inverted with respect to the other tetrahedral layer (Eslinger and Pevear, 1988). The layer structure of smectite clays, including montmorillonite, is the 2:1 type.

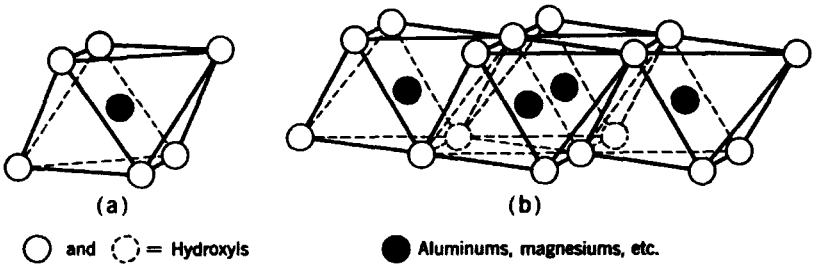

Figure 1.6: Octahedral units (from Grim, 1968).

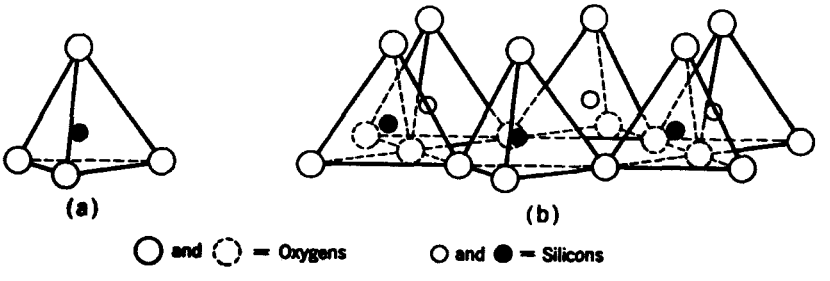

Figure 1.7: Tetrahedral units (from Grim, 1968).

Most crystalline solids do not have a perfect structure, and clays are no exception. One group of imperfections observed in smectite clays is substitutions. Substitutions are classified as octahedral, octahedral-tetrahedral, and interlayer (Velde, 1992). In octahedral substitutions, the substitution may be classified as stoichiometric (equivalent charge) or non-stoichiometric. Equivalent charge substitutions occur when the octahedral ion substituted has the same charge as the ion it is replacing (e.g. Mg^{2+} for Fe^{2+}, etc.). Non-stoichiometric substitutions occur when the ion substituted into the lattice contains a different charge than the ion it is replacing. Non-stoichiometric substitutions are often present when vacancies exist in other octahedral sites, as electrical neutrality must be maintained. When an ion of a different charge is substituted into an octahedral position and no cation vacancies are present in the octahedral sheet, another type of substitution must be made somewhere in the lattice. This may, for example, occur as a substitution into a tetrahedral site provided that electrostatic neutrality is maintained in the structure.

Interlayer substitutions are unique in that they are only present in clays with a 2:1 structure, such as montmorillonite. This occurs when an ion substitution in the lattice is balanced by the presence of another ion on the surface of the sheet structure. The presence of an interlayer charge may occur in a number of ways (Velde, 1992). One possibility is a trivalent ion substituted for Si^{4+} in the tetrahedral sheet, resulting in a net negative charge of -1 for the structure. The charge is balanced by the presence of a uni-valent ion such as Na^{+} or K^{+} between the two tetrahedral layers of adjacent sheet structures. Interlayer substitutions are also present as a result of the substitution of a di-valent ion for a tri-valent ion in the octahedral sheet or the presence of cation vacancies in the octahedral sheet. An 2:1 layer clay showing the inter-layer ions is given in Figure 1.8.

An important feature of smectite clays is that the charge imbalance on the tetrahedral-octahedral network is relatively low, and the inter-layer ion is thus only loosely held. The two most important results of this feature are the swelling capability and the cation exchange capacity of the clay (Velde, 1992). Smectite clays, such as montmorillonite, swell when placed into an aqueous (or other polar) solvent as the inter-layer cations become hydrated and "push" the 2:1 layers further apart. The cation exchange capacity, or CEC, denotes the ability of the clay to exchange ions from its inter-layer sites for those in an aqueous solution. The thermodynamic driving force for the CEC is the difference in chemical potential of the ion in solution and the same ion held between the layers. For example, inter-layer calcium ions may be replaced with sodium ions from solution if the chemical potential of both ions decreases as a result of the exchange. Cation exchange capacity is measured in meq per 100 g of clay.

Another interesting feature of clays is that the charge on the basal plane does not necessarily have to be the same as the charge on the edge surface. The charge density on the basal plane is determined by the type and degree of isomorphous ion substitutions in the clay platelet. As a result, the charge density on this surface is usually negative and is largely independent of the electrolyte composition. Surface charges on the edges of platelets are generated by the discontinuity of the crystal structure, resulting in an exposure of alumina and silica groups. The adsorption of potential determining ions on these surfaces creates positively or negatively charged surfaces at low and high pH values, respectively (van Olphen, 1977).

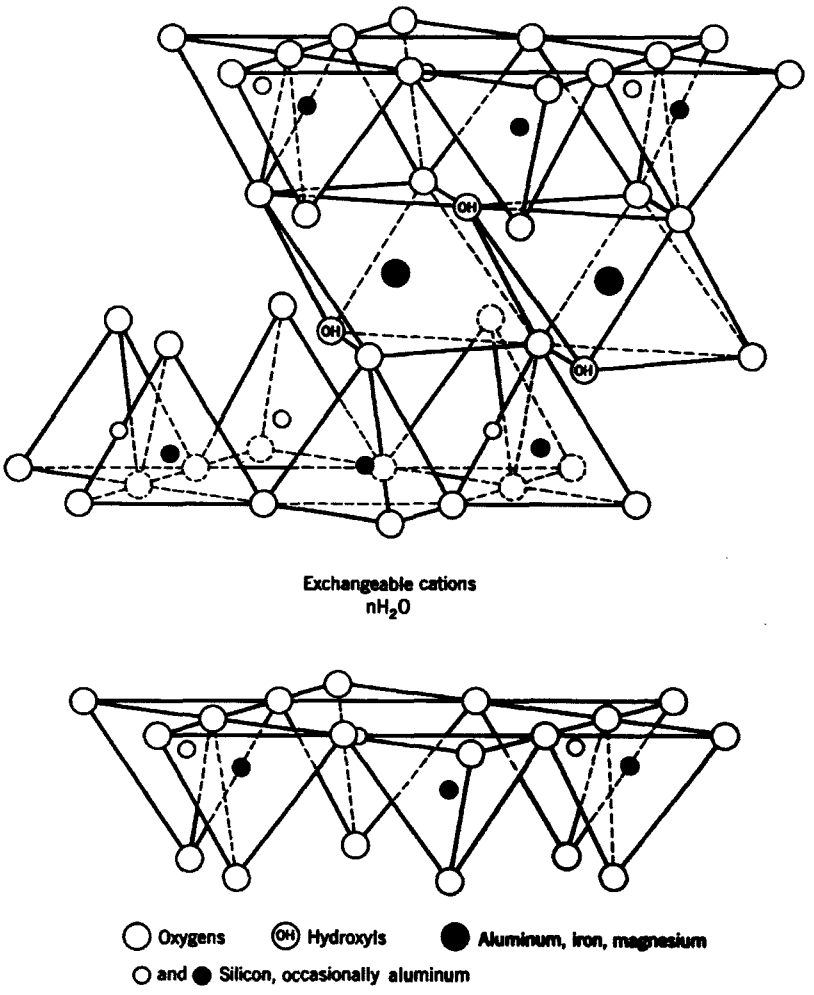

Figure 1.8: The typical structure of a 2:1 smectite clay including the exchangeable hydrated cations (from Grim, 1968).

An illustration of a clay platelet with opposing basal and edge charges is shown in Figure 1.9. It now becomes apparent that the zeta potential and other electrokinetic properties of clay minerals are actually dependent on the properties of two different surfaces. A true purist could argue that one cannot specifically refer to the "zeta potential of clay". In spite of this argument, the properties of the basal plane are generally predominant as the surface area is so much larger.

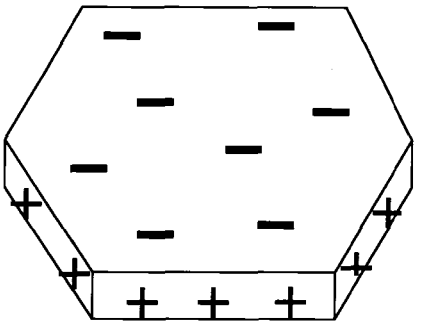

Figure 1.9: Simple schematic of a clay platelet illustrating the negatively charged basal plane and the positively charged edge surfaces. Adapted from Hunter et al. (Hunter, 2001).

1.6 Objectives of the Current Research

Previous research on the role of water chemistry in bitumen extraction, particularly on bitumen-montmorillonite interactions, has focused on calcium as the "bad-acting" ion. It was of interest to determine whether magnesium would also be able to induce slime coating of montmorillonite onto bitumen in the same way as calcium. For this purpose, the technique of zeta potential distribution measurement was employed. Zeta potential distribution measurements were also used to examine the effect of bicarbonate and sodium hydroxide on the interactions between bitumen and montmorillonite in solutions containing calcium, magnesium, or a combination of calcium and magnesium. The difference between the zeta potentials of solvent extracted bitumen and bitumen obtained without solvent extraction is also explored. Our attempts to obtain zeta potential distribution data at an elevated temperature (35°C) are outlined.

Another objective of the current work was to obtain a deeper understanding as to how pH and bicarbonate additions affect water chemistry as it may relate to hetero-coagulation. Specifically, the solubility of calcium and magnesium in aqueous

solutions was examined as a function of pH and bicarbonate concentration using atomic absorption spectroscopy.

Finally, Denver Cell flotation tests were performed to determine if a direct correlation exists between flotation test results and the results from the zeta potential distribution measurements. In particular, it was of interest to determine whether the water chemistry conditions that caused slime coating in the zeta potential distribution measurements would also cause a reduction in bitumen recovery and/or froth quality in flotation tests.

2 Experimental Principles

This chapter will discuss the theoretical aspects of the experimental techniques used. The details of the experimental procedures (test methods) will be described in the introductory section of each chapter containing pertinent results.

2.1 Electrophoresis and Zeta Potential Distribution Measurements

2.1.1 The Electrophoresis Phenomenon

Electrophoresis is the phenomenon whereby suspended particles carrying a surface charge undergo motion under the influence of an electric field. The moving particles will achieve a velocity such that a balance is achieved between the electrical forces acting to propel the particle and the viscous forces acting to slow the particle. In general, the velocity of a particle during electrophoresis is a function of the di-electric constant of the suspending medium, the permittivity of free space, the zeta potential of the particle, the strength of the electric field, and the viscosity of the continuous (suspending) phase. The velocity of the particles per unit electric field strength is known as the electrophoretic mobility. Hunter (Hunter, 1981) and Masliyah (Masliyah, 1994) summarized the various equations which relate electrophoretic mobility to the above mentioned parameters for various Debye lengths. For large Debye lengths ($\kappa a << 1$), the electrophoretic mobility is given by Equation 2.1 where U/E_∞ is the electrophoretic mobility, $\varepsilon\varepsilon_0$ is the di-electric constant of the suspending medium, ζ is the zeta potential of the particle, and μ is the viscosity of the suspending medium.

$$\frac{U}{E_\infty} = \frac{2\varepsilon\varepsilon_0\zeta}{3\mu} \qquad [2.1]$$

This equation is known as the Hückel equation. For a small Debye length (κa >> 1), an equation known as the Smoluchowski equation (2.2) is used.

$$\frac{U}{E_\infty} = \frac{\varepsilon\varepsilon_0\zeta}{\mu} \qquad [2.2]$$

While the Hückel and Smoluchowski equations are valid in the situations of κa << 1 and κa >>1, respectively, a more general solution is required for less extreme values of κa. Henry noted that the difference between Huckel's and Smoluchowski's equations arose from the different way in which the electric field was taken into account in the vicinity of the particle (Hunter, 1981). Henry superimposed the external field with the local field around the particle and obtained what is known as Henry's solution (2.3).

$$\frac{U}{E_\infty} = \frac{2\varepsilon\varepsilon_0\zeta}{3\mu} f_1(\kappa a) \qquad [2.3]$$

where $f_1(\kappa a)$ is known as Henry's function. Henry's function for spherical particles is given by equation 2.4.

$$f_1(\kappa a) = 1 + \frac{(\kappa a)^2}{16} - \frac{5(\kappa a)^3}{48} - \frac{(\kappa a)^4}{96} + \frac{(\kappa a)^5}{96} - \frac{(\kappa a)^4}{8}\exp(\kappa a)\left(1 - \frac{(\kappa a)^2}{12}\right)\int_\infty^{\kappa a}\frac{\exp(-x)}{x}dx \qquad [2.4]$$

Until this point, the focus has been on the charge or potential developed at the suspended particle-solution interface. In reality, most electrophoresis experiments are performed in rectangular or circular glass cells or capillaries. These cell or capillary surfaces also develop a charge when filled with the electrolyte. When an electric field is applied during electrophoresis, electro-osmosis (movement of the fluid due to an applied electrical field) will also occur. As a result of this phenomenon, it becomes important to be able to determine what component of a moving particle's velocity is due to electrophoresis and what component of its velocity arises from fluid forces acting on the particle. One way to solve the problem is to perform the electrophoresis measurement under "closed cell" or "closed tube" conditions whereby both ends of the electrophoresis cell are sealed. Under these conditions, the net volumetric flow rate within the cell must be zero. The electro-osmotic pressure developed at the cell walls is thus balanced by a counter-pressure in the middle of the cell (Hunter, 2001). For the case of a rectangular cell, a velocity profile similar to that shown in Figure 2.1 is typical. Assuming 1-dimensional fluid/particle motion, a symmetrical velocity profile is established within the cell. Two maximum fluid velocities are achieved at distances of approximately $3/\kappa$ from each of the two cell walls while the maximum velocity in the counter-flow direction is observed in the center of the cell. There are two planes inside the cell at which the fluid velocity is zero. These planes are indicated by the dotted lines in Figure 2.1 and are known as the "stationary layers" or "stationary planes". In most electrophoresis experiments, the zeta potential is measured at one of these two stationary layers so that the fluid force acting on the particles can be neglected when the zeta potential is being calculated (i.e. equations 2.1, 2.2, and 2.3 can be applied).

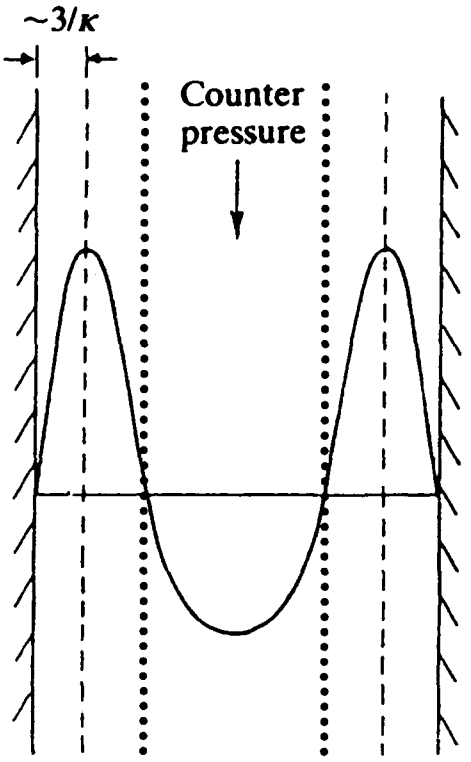

Figure 2.1: Velocity profile in a "closed cell" electrophoresis or electro-osmosis experiment (Modified from Hunter, 2001). The stationary layers are indicated by the dotted lines.

One method of measuring the zeta potential using electrophoresis is as follows: The sample suspension is loaded into a glass electrophoresis cell and the cell is sealed. An electric field is applied to the suspension by a pair of electrodes and the motion of the particle(s) in the stationary layer is captured using a microscope, a particle illumination system, and a CCD camera. The recording is transferred to a computer where image analysis software determines the electrophoretic mobility of each particle and can then convert mobility to zeta potential using one of the correlations discussed earlier. Although the exact experimental procedure will be discussed later in this thesis, it is important to note here that this method allows a measurement of

zeta potential distributions rather than a single zeta potential value. This ability to measure zeta potential distributions enables researchers to examine the interactions between components in multi-component suspensions.

2.1.2 Zeta Potential Distributions

2.1.2.1 Background of the Technique

Zeta potential distribution measurements are possible because some electrophoresis systems (like the one mentioned in the section above) are capable of determining the zeta potential of a number of particles simultaneously. For instance, if the movement of 60 particles is captured by the CCD camera, the computer will calculate the electrophoretic mobilities and zeta potentials of all 60 particles. Statistically, the particles will all be traveling at slightly different velocities in the cell and their calculated zeta potentials will be slightly different. The data produced can then be used to construct frequency vs. zeta potential histograms. For instance, if 6 of the above 60 particles have a zeta potential between -50.00 and -51.99 mV, then the bar corresponding to the abscissa co-ordinate of -50.00 to -51.99 will register a value of 10% on the ordinate. The average zeta potential and standard deviation can be calculated using the distribution data if an average value is desired.

The technique of zeta potential distribution measurements has been summarized in detail previously by Liu et al. (2002) and Xu et al. (2003), but will be repeated here for the convenience of the reader. Shown in Figure 2.2 are hypothetical, ideal cases representing various particle-particle interactions. Figure 2.2(a) shows the case where the zeta potential distributions of hypothetical components A and B are measured separately, and the results are plotted onto one graph. In this case, there is a significant amount of separation between the two distributions. This condition is a

necessary pre-requisite for this technique to be useful. If the distributions for components A and B are over-lapping or are very close when measured separately and plotted on the same graph, then the technique of zeta potential distributions will not provide any insight into the interactions between mixtures of components A and B. Figure 2.2(b) represents the case where a zeta potential distribution measurement is performed on a mixture of components A and B where there is no physico-chemical interaction between A and B (i.e. the system resembles a mechanical mixture). Since the surfaces of A and B are free of each other, both A and B peaks are still present. Upon careful examination, one will note that the peak positions have shifted slightly from their original positions such that the distance between the two peaks decreases. This shift is generally attributed to the hydrodynamic interactions occurring between moving A and B particles. In Figure 2.2(c), B particles are strongly attracted to the surface of A particles and have almost entirely coated the surface of A. As a result of this coating, the peak for A disappears and only the peak for B remains. A side benefit of this technique is that it can be used to determine which of the two phases is more hydrophilic (provided that measurements are performed in an aqueous phase). In this case, B is more hydrophilic than A as B coated the outside of A and not vice-versa. A similar case of strong attraction is observed in Figure 2.2(d), however in this case there are not enough B particles available in the system to completely cover the surfaces of all the A particles. As a result, the surface of most particles is a mixture of components A and B. A single peak residing between the independent peak values of A and B is typically observed. A measurement illustrating a weak attraction between A and B is shown in Figure 2.2(e). A single, slightly bi-modal distribution may be observed with some free B particles and some partially coated A particles present.

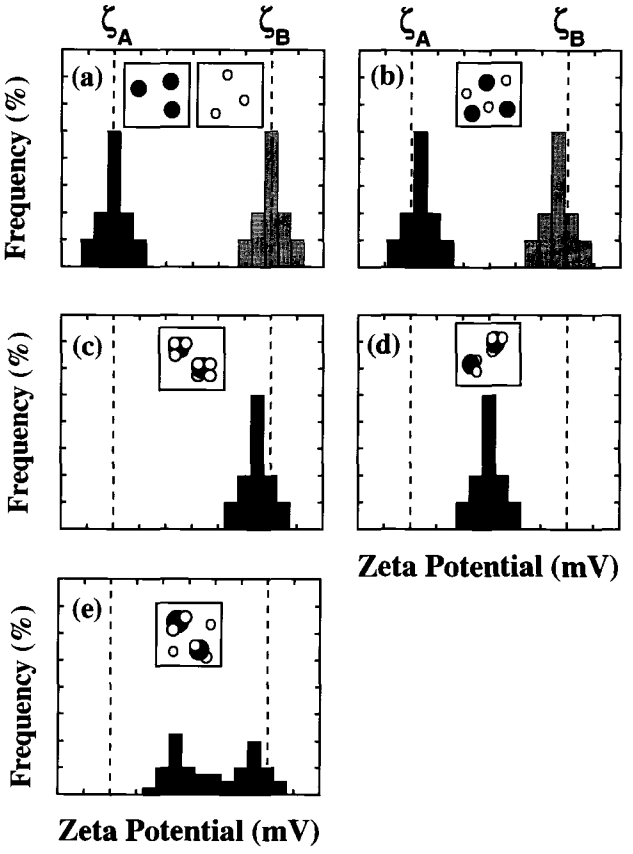

Figure 2.2: Hypothetical zeta potential distribution measurements including individual measurements (a), no-interaction (b), strong attraction (c), strong attraction with insufficient coating particles (d), and weak attraction (e).

2.1.2.2 Applications of the Technique

As discussed previously, the technique has been used in oil sands research to examine bitumen-kaolinite and bitumen-montmorillonite hetero-coagulation in the presence of KCl and $CaCl_2$ (Liu et al., 2002). Xu et al. (2003) used the technique to examine hetero-coagulation between coal and montmorillonite or kaolinite at various pH levels. They determined that montmorillonite slime coats onto coal at both pH 5

and 10, but that the slime coating was less severe at pH 10. Inconclusive zeta potential results were obtained for coal-kaolinite mixtures at pH 5 (peak overlap when measured individually), but the absence of a slime coating at pH 10 was confirmed. Zeta potential distributions obtained from electrophoretic light scattering experiments were used to look at hetero-coagulaton between various mineral systems such as the silica-silica/aminopropyl system (Skvarla, 1996a, 1996b), and the hematite-quartz system and magnesite-quartz systems (Skvarla, 1996b). Connah et al. of Malvern Instruments Ltd. (UK) and Malvern Instruments Inc. (US) developed an instrument that measures the zeta potential distribution of multi-component mixtures outside of the stationary layer by using a fast field reversal (FFR) technique (Connah, 2002). An FFR measurement takes advantage of the fact that electro-osmosis is almost absent immediately after the electric field is applied. By continually reversing the direction of the field at short intervals, electro-osmosis can be effectively negated. The team combined the principles of FFR and standard slow field reversal techniques and accurately measured the zeta potential distribution of various latex particles. The FFR measurement was used to calculate the mean particle mobility while the slow field reversal measured the electrophoretic mobility distribution of the sample. The difference in the mean of the two measurements was attributed to electro-osmosis and this value was used to correct the values of the slow field reversal measurement to create a zeta potential distribution. All of the team's experiments were performed at the center of the capillary cell rather than at the stationary layer.

Zeta potential distributions have also been used by researchers outside of the natural resource fields and to examine phenomena other than hetero-coagulation. For example, Boevé et al. (Boeve et al., 1994) used zeta potential distribution measurements in the field of urology to examine the effects of Tamm-Horsfall protein

on the zeta potential of calcium oxalate. Zeta potential distribution measurements, while qualitative and sometimes inconclusive, can be a powerful tool for studying colloidal and surface phenomena.

2.2 *Atomic Absorption Spectroscopy*

2.2.1 Theory of Atomic Absorption Spectroscopy

Atomic absorption spectroscopy (AAS) can be used to determine the concentration of an element in solution. The technique takes advantage of the principle that atoms emit or absorb light when their electrons undergo a change in energy level, as dictated by quantum mechanics. Welz and Sperling (1999) and Van Loon (1980) gave thorough descriptions of the operating principles of AAS. Their discussions are summarized in this section of the thesis.

The founder of AAS is generally believed to be Sir Alan Walsh of Australia, who developed the technique between 1952 and 1962. As mentioned above, AAS is based on the idea that atoms absorb electromagnetic radiation when their electrons undergo a transition from a lower energy state (ground state) into a higher energy state and emit electromagnetic radiation when their electrons drop from a higher energy state back to the ground state. The transition between the ground state and the excited state (and vice-versa) is known as the resonance transition. The absorbed or emitted radiation has a sharply defined frequency known as the resonance frequency. The resonance frequency is proportional to the energy difference between the two quantum mechanical states of electron transition. For a transition of an electron from energy level 1 to energy level 2, the resonance frequency is given by equation 2.5, where υ is the resonance frequency , w_{n1} and w_{n2} are the energy of electrons in states 1 and 2, respectively, and h is Planck's constant.

$$\upsilon = \frac{w_{n1} - w_{n2}}{h} \qquad [2.5]$$

In AAS, the concentration of atoms in an analyte is determined by passing a beam of energy (light) through a control volume and measuring how much of the energy is absorbed in the control volume. The basic equation (2.6) relates the energy absorbed to the number of free atoms per unit volume N, the spectral radiant intensity S_v, the speed of light i, and the atomic absorption coefficient, τ.

$$W_{abs} = \tau N i S_{\upsilon} \qquad [2.6]$$

In reality, it is easier to measure the change in radiant power over the absorption volume containing analyte atoms. The absorption is defined as the logarithm of the ratio of radiant power entering the absorption volume, Φ_0, vs. radiant power leaving the absorption volume, Φ_{tr}. The absorption, B, is linearly related to N, τ, and the length of the absorption layer, L, by equation 2.7. Equation 2.7 is known as the Beer-Lambert Law, and provides the foundation for modern day quantitative solution analysis using atomic absorption spectroscopy.

$$B = \log \frac{\Phi_0}{\Phi_{tr}} = 0.43 N L \tau \qquad [2.7]$$

Atomic absorption spectroscopy is a relative technique, which implies that some form of calibration is required. For calibration, standards containing the analyte atom at a known concentration are introduced to the spectrometer and the absorption

of each sample is measured. In this fashion, an absorption vs. concentration plot is constructed that should be linear, provided that appropriate standards were used for calibration. Once calibration is complete, the concentrations of samples may be determined by measuring the absorbance of the sample and relating this absorbance to concentration via the calibration plot.

2.2.2 Atomic Absorption Instrumentation

To be able to operate effectively, atomic absorption spectrometers need six key components: a nebulizer/atomizer, a burner, a radiation source, a monochromator, a detector, and a data processor. The matter train consists of the nebulizer and the burner/flame while the radiation train consists of the radiation source, the flame, the monochromator, and the detector. The schematic in Figure 2.3 shows the layout of an AA spectrometer.

In the matter train, the test solution is drawn through tubing into a pneumatic nebulizer where it is aspirated and mixed with fuel and oxidant (such as acetylene and air, respectively) before being injected into the burner. Once the analyte enters the flame, the liquid vaporizes and compounds are produced. As the compounds pass into the hotter regions of the flame, they are (ideally) broken down into individual atoms. Concurrently, radiation of the resonance frequency is generated in a hollow cathode lamp (HCL). This radiation is then passed through the flame directly (single beam spectrometer) or split into two beams with one beam passing through the flame and another beam used as a reference (double beam spectrometer). A monochromator, often a diffraction grating, isolates the resonance frequency from the light exiting the flame and passes this energy on to a photo-electric detector where it can be

transformed into an electrical output and analyzed by a computer or other data processor to determine the concentration of analyte.

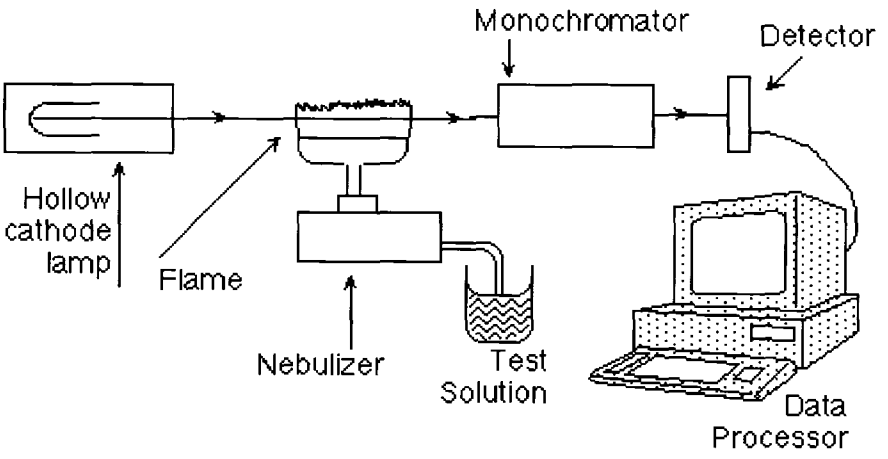

Figure 2.3: Layout of an atomic absorption spectrometer system (New Mexico State University: Department of Chemistry and Biochemistry).

2.3 Laboratory Flotation

Laboratory flotation machines are designed to roughly simulate the processing conditions which take place in industrial flotation. While the Syncrude BEU has been used previously in ore processability studies, the most popular techniques currently used are the Denver Cell, the Agitair unit, and the Laboratory Hydrotransport Extraction System (LHES or "the loop").

The Denver Cell and the Agitair unit are both batch processing units that provide sources of mechanical energy and aeration. These units are essentially small scale simulations of the mechanical flotation cells used as scavenger banks in industrial bitumen extraction operations. A rotary agitator is used to mix and aerate the slurry. The Denver Cell uses the corners of the cell as baffles while the Agitair unit has a baffle structure placed inside the cell (in addition to the corners). A

schematic of what occurs inside the Denver and Agitair cells during operation is shown in Figure 2.4.

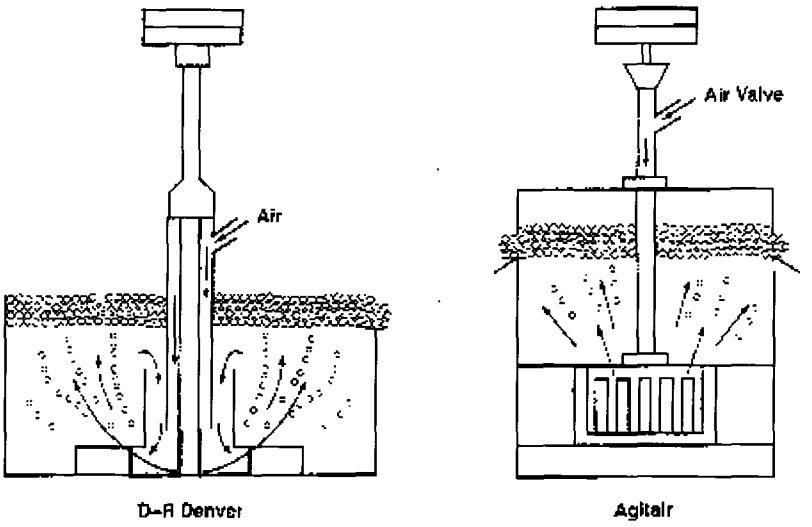

Figure 2.4: Schematic of Denver Cell and Agitair unit operation (Gray and Masliyah, 2002).

More recently, attempts have been made to simulate the conditions inside the hydrotransport line. This led to the development of the LHES. The LHES re-circulates oil sands slurry through a looped pipe to simulate the residence time and transport conditions which exist in industrial hydrotransport. A small froth formation zone allows for the intermittent formation and collection of froth during operation of the loop.

3 Zeta Potential Distribution Measurements

3.1 Experimental Techniques

3.1.1 Experimental Apparatus

A Zetaphoremeter III® from Sephy/Cad Instrumentation was used for all zeta potential and zeta potential distribution measurements. The Zetaphoremeter, or "zeta-meter", operates on the principles of electrophoresis. The device consists of an electrophoresis cell, components for particle illumination and observation, a computer, and an interface unit between the computer and the electrophoresis cell. As it is easiest to describe each piece of the instrument in the terms of how it operates, more thorough descriptions of each component and its role are given in the experimental procedure (Section 3.1.3).

3.1.2 Materials

Ultra-pure water produced by a Millipore water system (resistivity 18.2 MΩ cm) was used in the preparation of all solutions and subsequent suspensions or emulsions. Reagent grade $CaCl_2 \cdot 2H_2O$ and $MgCl_2 \cdot 6H_2O$ (Fisher and BDH, respectively) were the source of divalent cations while reagent grade HCl (Fisher) and NaOH (BDH or Fisher) were used as pH modifiers. High purity KCl (99.999%, Aldrich) was used as the background electrolyte in all zeta potential distribution measurements. Bicarbonate ions were obtained from reagent grade $NaHCO_3$ (ACP Chemicals).

Solvent extracted bitumen from facies 11 oil sand from Syncrude Canada's North Mine was used in this study. Montmorillonite clay (Panther Creek, CO) was obtained from Ward's Minerals. Cation exchange capacity measurements were performed by the Department of Earth and Atmospheric Sciences at the University of

Alberta. The exchangeable amounts of various ions (in meq/100 g) from the clay are given in Table 3.1

Table 3.1: Exchangeable amounts of various ions from montmorillonite clay.

Na	Mg	Ca	K	Total
54.95	9.26	26.70	1.48	92.39

The data in the table show that this montmorillonite was predominantly a sodium clay.

3.1.3 Experimental Procedure

A pre-requisite for the preparation of final samples for zeta potential distribution measurement was the preparation of concentrated emulsions/suspensions of the components under study (in this case bitumen and montmorillonite). To prepare a bitumen emulsion, approximately 1 g of bitumen was smeared onto the bottom of a 100 mL beaker. Approximately 60 mL of 1 mM KCl solution was then added to the beaker. The mixture was then taken to a sonic dismembrator (Fisher model 500) where the contents were emulsified for approximately 15 minutes at 70-75% power, producing a dark bitumen emulsion. Particle size distributions of the bitumen emulsion were obtained using a Malvern Mastersizer 2000. The d_{10}, d_{50}, and d_{90} after 20 minutes, 1 hour, and 4 hours of creaming (i.e. sitting) time are shown in Table 3.2.

To prepare a montmorillonite suspension, powdered montmorillonite and 60 mL of 1 mM KCl solution were added to a 100 mL beaker. Since the objective was dispersion of montmorillonite clumps rather than a true size reduction, sonic dismembration was unnecessary. Wetting of the clay was achieved through a

combination of manual stirring and agitation in an ultrasonic bath (Fisher model FS30). The montmorillonite suspension was then left undisturbed for approximately 1 hour to allow the coarse particles to settle and the fine particles (used in the measurements) to remain suspended in the top layer. The particle size distribution measured by the Mastersizer 2000 for the suspended clay is given in Table 3.2. The final sample used for zeta potential distribution measurement was created by adding small amounts (<1 mL) of the concentrated emulsion and/or suspension to 40-60 mL of solution with the desired ion concentration and pH. No settling time was allowed between the creation of this sample and the zeta potential distribution measurement. Unless noted otherwise, the pH of the bitumen-montmorillonite mixtures was adjusted to 8.5 using either NaOH or HCl. This pH was chosen as it falls in the middle of the conventional industrial operating pH range (Masliyah, 2004). After the pH was adjusted, small amounts of concentrated bitumen and montmorillonite emulsion/suspension were added to the solution while the solution was mixed with a magnetic stirrer (Fisher). Zeta potential distribution measurement of each sample commenced immediately after the sample was prepared. This was done to avoid any transient effects such as solution chemistry changes, differential settling of the samples, etc. While the sample was being stirred by a magnetic stirrer, a portion of the sample was drawn by syringe and tube into a rectangular quartz electrophoresis cell bordered on the ends by a pair of palladium-coated electrodes mounted in solvent resistant Kynar. A laser illuminator was used to illuminate droplets/particles within the stationary layer of the sample. An electric field was then applied to the cell by the interface unit, and the movement of 40-120 particles in the stationary layer was traced in 10 increments using a CCD camera mounted onto a microscope. The direction of

the electric field was then reversed, and the particle movement was traced in 10 increments in the opposite direction.

Table 3.2: Particle size distribution results (d_{10}, d_{50}, and d_{90}) of a bitumen emulsion and a montmorillonite suspension.

	d_{10} (μm)	**d_{50} (μm)**	**d_{90} (μm)**
Bitumen (20 min. cream time)	1.8	19.9	49.2
Bitumen (1 hr. cream time)	1.0	17.9	43.5
Bitumen (4 hr. cream time)	0.6	9.1	38.1
Montmorillonite (1 hr. settling time)	2.1	4.9	26.6

The initiation, reverse, and cessation of the electric field were automatically controlled by a computer program activated by the operator. The images captured by the microscope and camera were then transferred to the computer where a software program provided with the instrument calculated the electrophoretic mobility distribution based on the velocity of the particles. The electrophoretic mobility distribution is a histogram with the electrophoretic mobility as the abscissa and the percentage of the total particles possessing that mobility as the ordinate. The software converted the mobility distributions into zeta potential distributions using the Smoluchowski equation and also determined the average zeta potential value from the distribution. Smoluchowski's equation was applicable as the κa values in all the tests

were >> 1 (see Appendix B for a confirmation calculation). Verification that each measurement was performed at the stationary layer was provided by a level sensor connected to the computer via the interface unit. Data pertaining to the pH and conductivity of the sample received by the interface unit was also provided on screen.

The concentrations of bitumen and montmorillonite in the samples prepared for zeta potential measurements were much lower than the concentrations encountered during an industrial bitumen extraction process. To alleviate concerns that these dilute conditions would not allow for adequate interaction between bitumen and montmorillonite, all binary mixtures of bitumen and montmorillonite were conditioned using an ultrasonic bath (Fisher model FS30). After an initial zeta potential distribution measurement of the sample was completed, the mixtures were covered in paraffin wax and conditioned in the ultrasonic bath for approximately three minutes. The zeta potential distribution was then measured again. Any shift in the peak position(s) in comparison to the previous measurement was noted. This process was repeated until additional conditioning time no longer had any effect on the peak position(s). All binary mixtures were conditioned for at least nine minutes to ensure that ample time was given to allow for any hetero-coagulation to occur.

With the exception of the special experiments performed in section 3.5, the temperature of the room in which the equipment and samples were kept was maintained at 23°C ± 2°C.

3.1.3.1 Special Considerations at 35°C

The experimental procedure for the zeta potential distribution measurements performed at 35°C was largely the same as at 23°C with a few exceptions. All experimental apparatus and samples were moved into a closed, un-ventilated room.

Several electrical space heaters were placed inside the room to bring the temperature up to 35°C. With the temperature of all samples, experimental equipment, and the ambient air at 35°C, interference with the measurements from natural convection currents was minimized.

3.2 Average Zeta Potential as a Function of pH

Section 2.1.2.1 explained why an adequate separation of the peak positions of the suspended components, measured individually, is a pre-requisite for the technique of zeta potential distribution measurements to apply. As changes to the pH of the suspending medium can change the zeta potential of suspended particles/droplets, it was necessary to determine the pH range where the technique could be used in this study. This was accomplished by measuring the average zeta potential of bitumen and montmorillonite in 1 mM KCl and combinations of 1 mM KCl and 1 mM $CaCl_2$ or $MgCl_2$ at various pH values. The results for bitumen and montmorillonite are shown in Figures 3.1 and 3.2, respectively.

The iso-electric points of bitumen in all three electrolytes fell within the range 2.5-3.5. The zeta potential of bitumen in 1 mM KCl dropped sharply from -10 mV to -60 mV as pH increased from 3 to 4.5 respectively. After pH 4.5, increases in pH caused a more gradual shift of the zeta potential to more negative values, with a final zeta potential of approximately -80 mV at pH 11 (the maximum operating pH of the instrument). It is likely that as more NaOH was added to increase the pH of the system, an abundance of negatively charged surfactants was produced from the bitumen. These surfactants impose a negative charge to the interface of the bitumen and the aqueous medium, making the zeta potential more negative.

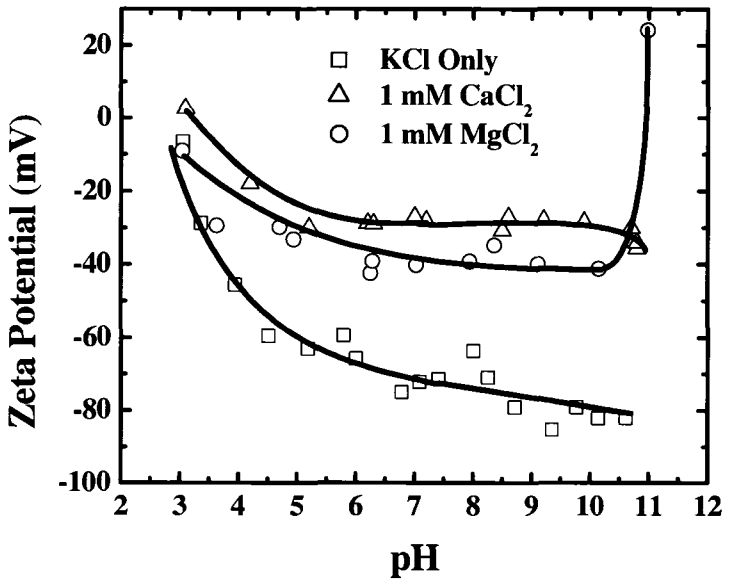

Figure 3.1: Average zeta potential of bitumen at various pH values in three electrolytes.

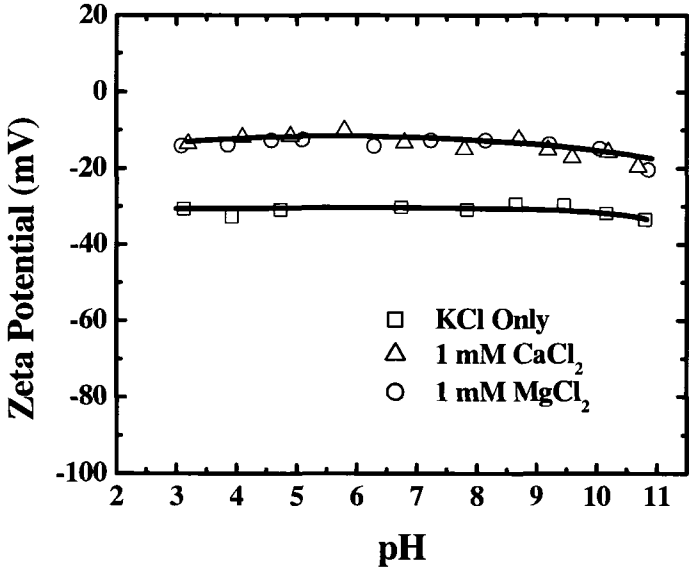

Figure 3.2: Average zeta potential of montmorillonite at various pH values in three electrolytes.

A similar trend was observed when the suspending medium contained both 1 mM KCl and 1 mM $CaCl_2$. In this case, the zeta potential also dropped sharply in the pH range 3 to 4.5, decreasing from 5 mV to -20 mV respectively. The zeta potential at pH 11 was approximately -37.5 mV. These zeta potential values are comparatively lower in magnitude than those obtained in KCl alone. This result indicates that calcium affects the surface or Stern Layer of bitumen in some way that renders it less negative. Compression of the electrical double layer due to the increase of total salinity also contributes to such a reduction.

Magnesium affected the zeta potential of bitumen in much the same way as calcium for pH values below 11. The shape of the trend-line when magnesium was present followed the trend when calcium was present closely, although the values were slightly more negative. The major difference between the cases when calcium or magnesium was present was observed at pH 11. While the zeta potential of bitumen in the presence of calcium remained negative, the zeta potential in the presence of magnesium increased sharply to the point where it experienced an iso-electric point between pH 10.5 and 11 and then carried a positive potential of approximately 20 mV near pH 11. It is likely that at this pH some form of magnesium adsorption onto bitumen, possibly in the form of precipitates, occurred. Precipitation behavior of calcium and magnesium solutions is discussed further in Chapter 4.

While the zeta potential of bitumen was strongly affected by changes to the solution pH, Figure 3.2 shows that the zeta potential of montmorillonite was less affected by changing solution pH. The zeta potential of montmorillonite in 1 mM KCl varied from -31 mV at pH 3 to -34 mV at pH 11. A similar lack of dependence of the zeta potential on pH was observed in the solutions containing 1 mM KCl with 1

mM of the di-valent cations. In both solutions, the zeta potential ranged from approximately -14 mV at pH 3 to -20 mV at pH 11. As before, the decrease in the magnitude of the average zeta potential in the presence of di-valent cations can be attributed to surface and Stern Layer interactions combined with an increase in double layer compression.

3.3 The Effects of Di-valent Cations on Slime Coating

3.3.1 Measurements in 1 mM KCl

Zeta potential distribution measurements of bitumen and montmorillonite were performed in 1 mM KCl at pH 8.5 to determine whether hetero-coagulation occurred in the absence of di-valent cations. This measurement would be used as a basis for evaluating the effects of calcium and magnesium in later tests. These tests have also been performed previously by Liu et al. (2002).

The zeta potential distributions of bitumen and montmorillonite measured individually and in a 1:1 mixture by mass are shown in Figure 3.3. Two separate and distinct peaks were observed for bitumen and montmorillonite in Figure 3.3(a). The peak for bitumen was located at approximately -70 mV while the peak for montmorillonite was at approximately -30 mV. Note that these values correspond well to the values obtained for bitumen and montmorillonite as a function of pH from Figures 3.1 and 3.2. Since a difference of approximately 40 mV existed between the peaks of bitumen and montmorillonite with a blank space between the distribution tails of bitumen and montmorillonite, the technique of zeta potential distributions was applicable for this case.

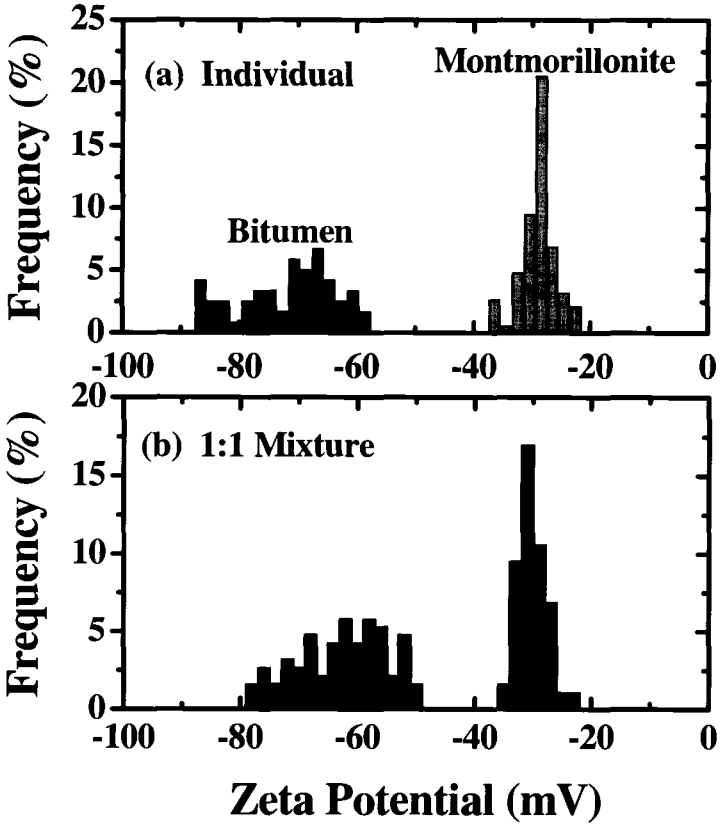

Figure 3.3: Zeta potential distributions of bitumen and montmorillonite in 1 mM KCl at pH 8.5 measured individually (a), and as a 1:1 mixture (b).

Figure 3.3(b) shows the zeta potential distribution obtained from a binary mixture of bitumen and montmorillonite at a 1:1 mass ratio in 1 mM KCl at pH 8.5. Two peaks are present in this figure, and the peak positions are close to those of the two components measured individually. One peak lies at approximately -60 mV while the other lies at -32.5 mV. These peaks can be inferred to belong to bitumen and montmorillonite, respectively. Recalling the theory behind zeta potential distribution measurements from section 2.1.2.1, it is evident that both bitumen and montmorillonite were present. This implies that no slime coating of montmorillonite onto bitumen occurred in 1 mM KCl at pH 8.5. This result is also in-line with the

theory in terms of the prediction that the distance between the peaks will narrow as a result of hydrodynamic interactions when a binary mixture is present. In other words, the zeta potential distribution peak of bitumen shifted to a less negative value (-70 to -60 mV) while the zeta potential distribution peak of montmorillonite shifted to a more negative value (-30 to -32.5 mV), closing the absolute distance between the two peaks.

3.3.2 Measurements in 1 mM KCl and 1 mM $CaCl_2$

As discussed in the literature review, the presence of calcium in flotation water has been shown to have a detrimental impact on bitumen flotation (Kasongo et al., 2000). It has also been shown through zeta potential distribution measurements that the presence of 1 mM of calcium ions induces a montmorillonite slime coating on bitumen (Liu et al., 2002). Liu's tests were repeated in this study to establish a baseline for further testing with bicarbonate and to familiarize the author with the experimental procedure. The results of these experiments are shown in Figure 3.4.

The results obtained in Figure 3.4 are very similar to those obtained by Liu et al. The zeta potential distribution peaks of bitumen and montmorillonite measured separately in this electrolyte were at approximately -35 mV and -12.5 mV, respectively (Fig. 3.4(a)). The space between the two distributions is approximately 10 mV. This is comparatively lower than the roughly 20 mV between the bitumen and montmorillonite distributions for the case with KCl alone.

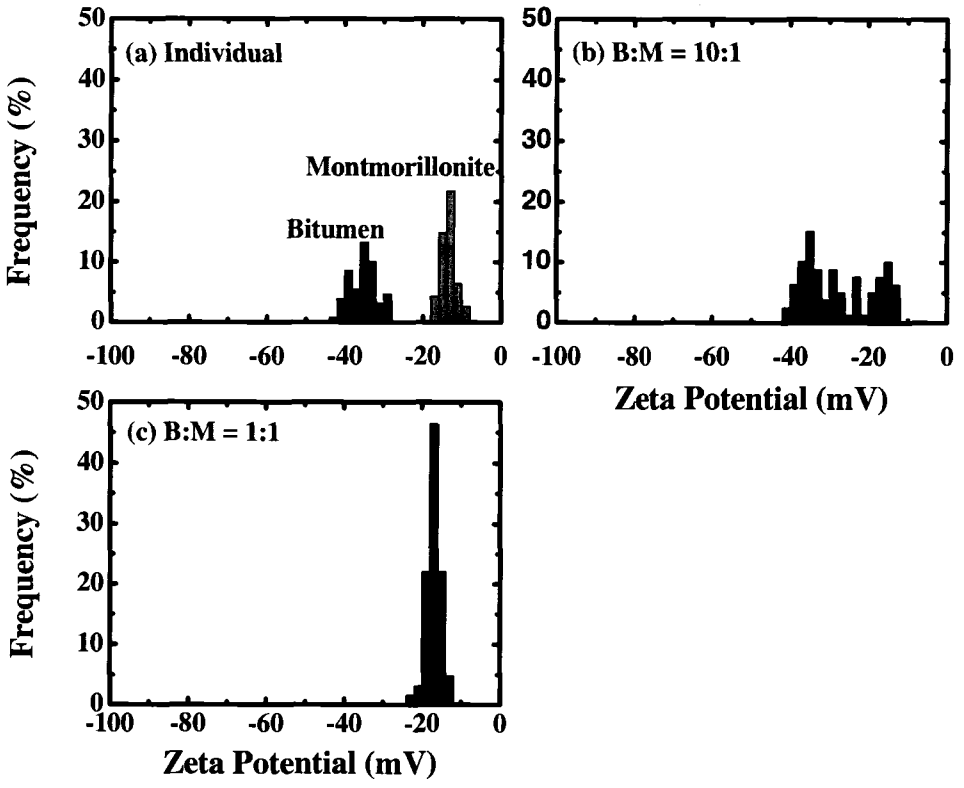

Figure 3.4: Zeta potential distributions of bitumen and montmorillonite in 1 mM KCl and 1 mM $CaCl_2$ at pH 8.5 individually (a), with a 10:1 B:M ratio (b), and with a 1:1 B:M ratio (c).

Similar to the work of Liu et al., bitumen and montmorillonite were co-added to aqueous solutions to create measurement samples containing various ratios of bitumen to montmorillonite (B:M). Liu et al. used bitumen to montmorillonite ratios of 20:1, 2:1, and 1:1. In this study, B:M ratios of 10:1 and 1:1 were used. Figure 3.4(b) shows the zeta potential distributions observed with a 10:1 B:M ratio in this electrolyte. This distribution appears to be very similar to that obtained by Liu for a B:M ratio of 20:1. Although two peaks are present, there is an increased frequency of

particles between the two peaks. It would therefore be acceptable to view this distribution as a large, slightly bi-modal distribution. Considering the fact that the space in-between the two individual distributions is lower in this electrolyte than in the electrolyte containing only KCl, there are three possible explanations for this distribution. The first explanation is that no physico-chemical interactions exist between bitumen and montmorillonite. In this instance, the peaks would have shifted closer to each other due to the hydrodynamic factors discussed previously. The points between the two peaks would be simply a result of data scatter. The second possibility is that a weak attraction existed between bitumen and montmorillonite. Most of the bitumen droplets and clay particles would exist freely. The data points in-between the two modes would result from the few bitumen-clay aggregates that existed. The third possible explanation, and the explanation put forth by Liu et al., is that a strong interaction existed between bitumen and montmorillonite, but an insufficient amount of clay was available for complete coverage of the bitumen. The clay may have partially coated the first few bitumen droplets that it came into contact with, and then left many other bitumen droplets free of clay.

In order to improve our understanding of bitumen-montmorillonite interactions in this electrolyte, an experiment was performed where bitumen and clay were co-added to the aqueous solution at a B:M ratio of 1:1 (Fig. 3.4(c)). The objective was to provide an abundance of clay particles to overcome the inconclusive interpretation problems experienced with a 10:1 B:M ratio. Similar to the results of Liu, a single peak centered at approximately -17.5 mV was observed. The peak corresponding to bitumen disappeared from the distribution, indicating that no bitumen surfaces were present in the mixture. The only surfaces present would have been montmorillonite coated bitumen and free montmorillonite particles. This result

confirms that a strong attraction does exist between bitumen and montmorillonite in the presence of 1 mM $CaCl_2$ and 1 mM KCl at pH 8.5.

3.3.3 Measurements in 1 mM KCl and 1 mM $MgCl_2$

The previous work done on bitumen-montmorillonite interactions has focused on the detrimental role of calcium in inducing a slime coating of montmorillonite onto bitumen. The effects of magnesium on bitumen-montmorillonite interactions have not been previously established. Examining the effects of magnesium by using zeta potential distribution measurements was the next goal of this research work.

Aqueous solutions were prepared containing 1 mM KCl and 1 mM $MgCl_2$. The experiments performed with calcium were repeated with the new solution containing magnesium. The results are shown in Figure 3.5. The zeta potential distributions of bitumen and montmorillonite measured individually (Fig. 3.5(a)) appeared quite similar to those obtained in the presence of calcium. The peak for bitumen was located at approximately -35 mV and the peak for montmorillonite was located at about -10 mV. Again, there is a gap of approximately 10 mV between the tail ends of the bitumen distribution and the montmorillonite distribution. When bitumen and montmorillonite were mixed together at a 10:1 B:M ratio (Fig. 3.5(b)), a broad and single modal distribution was obtained with a peak position near -25 mV. This peak position lay between the individual peak positions of bitumen and montmorillonite.

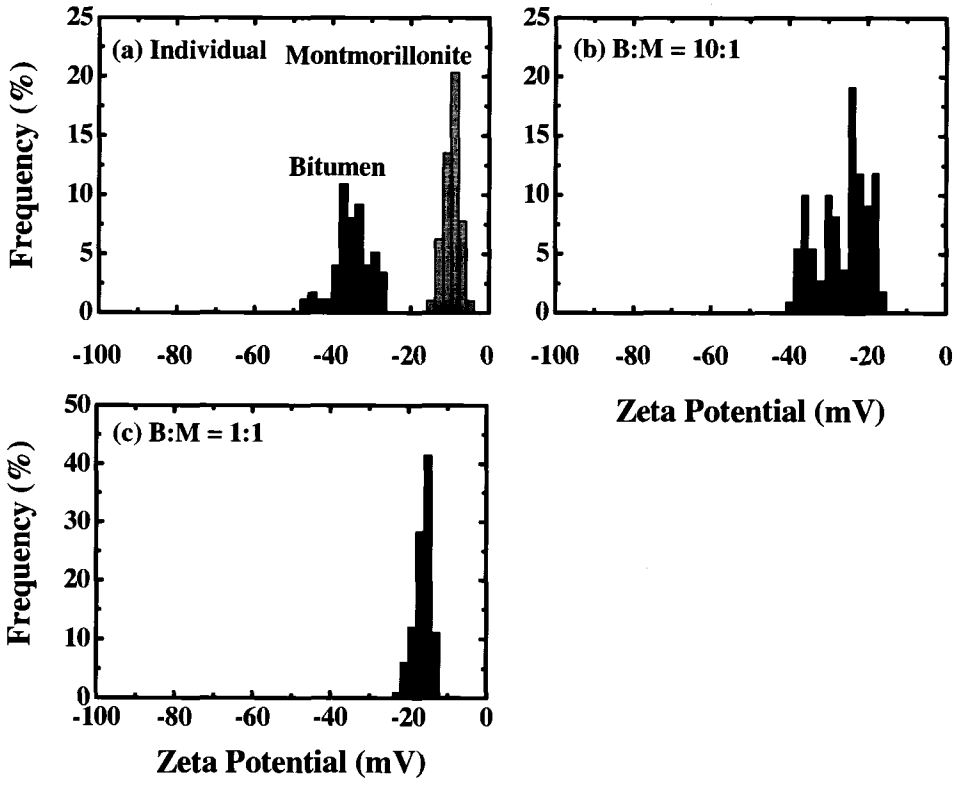

Figure 3.5: Zeta potential distributions of bitumen and montmorillonite in 1 mM KCl and 1 mM $MgCl_2$ at pH 8.5 individually (a), with a 10:1 B:M ratio (b), and with a 1:1 B:M ratio (c).

After considering the theory of zeta potential distributions, it is likely that there are strong attractive forces between bitumen and montmorillonite. In this case, it is also likely that there is an insufficient number of montmorillonite particles available for the bitumen surfaces to be completely covered. When bitumen and montmorillonite are present at a B:M ratio of 1:1, the zeta potential distributions show a single peak residing near -15 mV. As this zeta potential value is close to that of the independent montmorillonite value, it can be concluded that there is a complete slime

coating of bitumen by montmorillonite. The results appear to suggest that both calcium and magnesium have a similar detrimental effect of inducing slime coating of montmorillonite clay onto bitumen.

3.3.4 Measurements in 1 mM KCl, 0.5 mM $CaCl_2$, and 0.5 mM $MgCl_2$

It was also of interest to determine whether a solution containing a mixture of calcium and magnesium, with the total di-valent ion concentration of 1 mM, would induce the same slime coating effect as solutions containing either 1 mM calcium or 1 mM magnesium. This measurement was important from an industrial standpoint, as industrial extraction water contains significant levels of both calcium and magnesium (among other ions). Zeta potential distributions showing the interactions between bitumen and montmorillonite in the solutions containing equi-molar concentrations of calcium and magnesium (0.5 mM each) and 1 mM KCl are shown in Figure 3.6. The results closely resemble those obtained from the measurements performed in either 1 mM calcium or 1 mM magnesium. The individual peaks for bitumen and montmorillonite are at approximately -35 and -15 mV, respectively (Fig. 3.6(a)). The gap between the tails of the individual distributions is very small, at approximately 7.5 mV. Figure 3.6(b) shows that when bitumen and montmorillonite are present together at a B:M ratio of 10:1, a uni-modal distribution is obtained which has a peak centered at approximately -17.5 mV. The distribution does have a significant tail leading towards more negative values. It thus appears that some bitumen remains partially free of clay attachment. This situation, when considering the theory of zeta potential distribution measurements, could be explained by either the strong-attraction/absence of sufficient particles scenario or the weak attraction scenario.

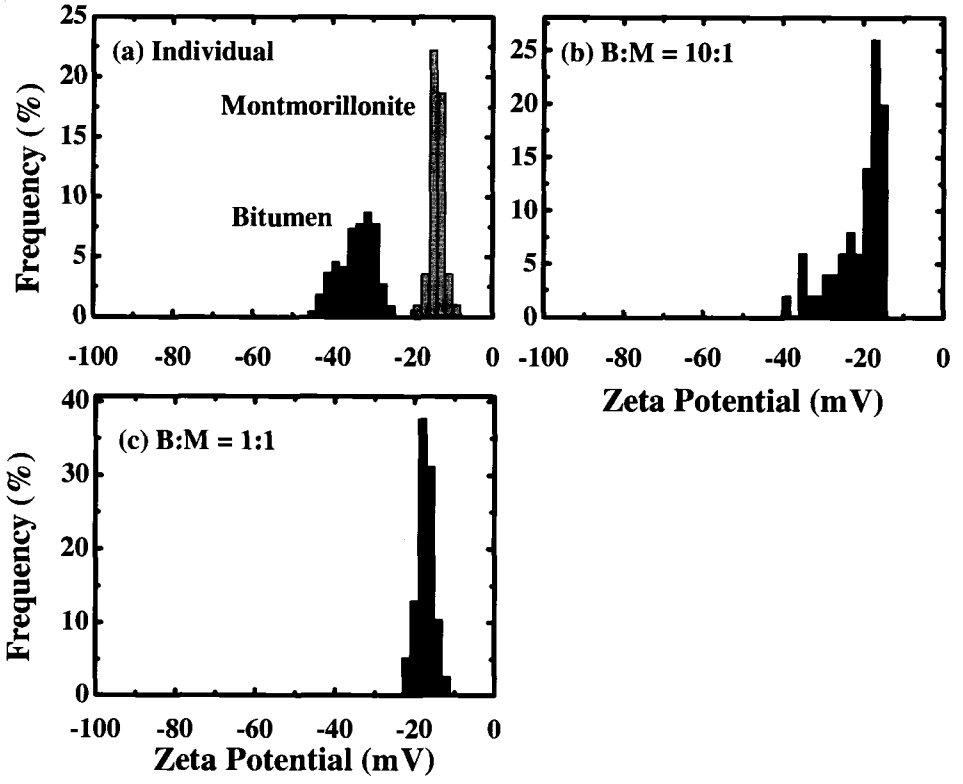

Figure 3.6: Zeta potential distributions of bitumen and montmorillonite in 1 mM KCl, 0.5 mM $CaCl_2$, and 0.5 mM $MgCl_2$ at pH 8.5 individually (a), with a 10:1 B:M ratio (b), and with a 1:1 B:M ratio (c).

Adjustment of the B:M ratio from 10:1 to 1:1 clarifies the explanation. As can be seen in Figure 3.6(c), one peak exists that is centered at around -20 mV when the B:M ratio is 1:1. This result indicates a strong attraction between bitumen and montmorillonite in the mixed di-valent electrolyte solution.

3.3.5 Tests Performed Using Bitumen Extracted from Ore

For the zeta potential distribution results presented so far, solvent extracted bitumen has been used exclusively. It was of interest to determine whether bitumen which had not undergone the solvent extraction process would behave in the same manner as solvent extracted bitumen.

To obtain bitumen without using solvent extraction, a small amount of good processing ore (see Chapter 5 for details on ore composition) was placed in the bottom of a 100 mL beaker. Potassium chloride solution (1 mM) at room temperature was added until the combined volume of ore and solution was approximately 70 mL. The contents of the beaker were then agitated using the sonic dismembrator until a bitumen in water emulsion formed. The sample was left to sit for one hour to allow the coarse solids to settle. The bitumen used for the tests was withdrawn from the top portion of the sample. This top portion of the sample undoubtedly contained some suspended fine solids as well. As such, the "bitumen" obtained from good processing ore is referred to as "ore bitumen" in this section.

The tests were conducted in 1 mM KCl with and without the addition of 1 mM $CaCl_2$. The objective was to determine whether calcium would induce slime coating with this bitumen in the same way as it did with solvent extracted bitumen. Figure 3.7 shows the results obtained in 1 mM KCl. Individually, ore bitumen and montmorillonite have two separate peaks. The peak for ore bitumen is located at around -37.5 mV while the peak for montmorillonite is located at -25 mV. Interestingly, the zeta potential distribution of the bitumen from this good processing ore resembled the zeta potential distribution previously published (Liu, 2005) from emulsified froth collected from poor processing ore in tailings water also collected from the processing of a poor ore. It should also be noted that the zeta potential

distribution peak observed here for ore bitumen, at -37.5 mV, is significantly less negative than the -70 mV observed for solvent extracted bitumen in Figure 3.4. The association of bitumen with the fine particles from the ore may play a role in reducing the magnitude of the zeta potential. There is some over-lap between the tail ends of the distributions for ore bitumen and montmorillonite. The zeta potential distribution for the 1:1 mixture of ore bitumen and montmorillonite is shown in Figure 3.7(b). The broad, bi-modal distribution obtained closely resembles the two super-imposed distributions from Figure 3.7(a). As such, it is apparent that little or no slime coating of montmorillonite onto ore bitumen occurred in 1 mM KCl at pH 8.5.

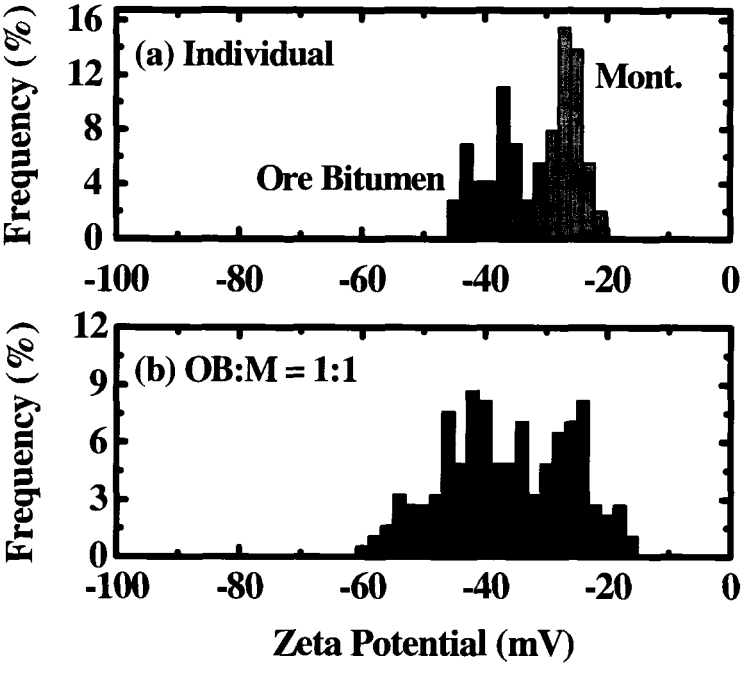

Figure 3.7: Zeta potential distributions of a bitumen/fines mixture extracted from a good processing ore and montmorillonite in 1 mM KCl measured individually (a), and in a 1:1 mixture (b).

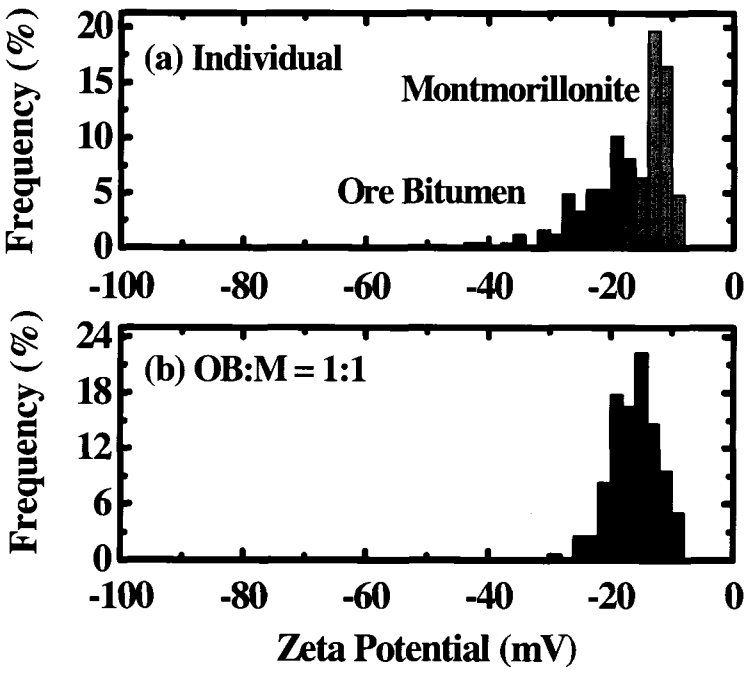

Figure 3.8: Zeta potential distributions of a bitumen/fines mixture extracted from a good processing ore and montmorillonite in 1 mM KCl with 1 mM $CaCl_2$ measured individually (a), and in a 1:1 mixture (b).

The distributions obtained for the individual components and a 1:1 binary mixture when 1 mM of calcium ions were added are shown as Figs. 3.8(a) and 3.8(b), respectively. The zeta potential peaks of ore bitumen and montmorillonite both became less negative when calcium ions were added, shifting to -20 mV and -12.5 mV, respectively. There is again a significant over-lap between the tail ends of the ore bitumen and montmorillonite distributions. The fact that the peak for ore bitumen was not nearly as pronounced as the peak for montmorillonite, combined with the fact that there was such significant over-lap in the individual measurements in Figure 3.8(a), means that it is extremely difficult to interpret the results from the binary

mixture in Figure 3.8(b). Unfortunately, what exactly occurred in the binary mixture is unclear. It may be that no slime coating occurred and the two peaks shifted closer together due to the hydrodynamic interactions. It is also possible that some degree of slime coating did occur, and that the apparent single peak on Figure 3.8(b) is truly the peak of montmorillonite coated ore bitumen. This lack of a conclusion suggests the need for future work on this issue using other experimental techniques.

3.4 Negation of Slime Coating

The work in Section 3.3 has established the negative impact of dissolved calcium and magnesium on bitumen/montmorillonite interactions. The di-valent cations induce a slime coating of montmorillonite particles on bitumen droplets. The montmorillonite slime coating decreases the probability of successful bitumen-air bubble attachment and could lead to a reduction in bitumen recovery and/or froth quality in a bitumen extraction system.

From an industrial standpoint, it becomes imperative to establish a method of negating or minimizing the amount of slime coating. Several approaches may be used. One approach involves cation attenuation. In this approach, the detrimental cations such as calcium or magnesium are precipitated/chelated/complexed such that they cannot induce slime coating. Another method would be to add powerful dispersants to the system to over-power the attraction between bitumen and montmorillonite in systems containing di-valent cations. The next portion of this thesis will examine the effects of two process aids on bitumen-montmorillonite interactions: sodium bicarbonate and high concentrations of sodium hydroxide.

3.4.1 Sodium Bicarbonate

Metal bicarbonates or carbonates have been proposed as process aids in several patents (Globus, 1978; Humphreys, 1998). The effect of sodium bicarbonate on the zeta potentials of bitumen and montmorillonite in the presence of either calcium or magnesium was of interest. An enhancement of the negative surface potential of either bitumen or montmorillonite would indicate a dispersion or a cation attenuation effect. Zeta potential distributions on mixtures of bitumen and montmorillonite would determine the net effect of bicarbonate on hetero-coagulation behavior in the presence of calcium or magnesium.

The dosage of sodium bicarbonate was based on the desired level of the bicarbonate anion in solution. Two bicarbonate concentrations were chosen: 7.1 mM and 16.4 mM. Sodium bicarbonate was added to solutions containing 1 mM KCl and a desired level of either $CaCl_2$ or $MgCl_2$. The pH of the solutions was adjusted to 8.5 using diluted NaOH or HCl prior to zeta potential distribution measurement.

3.4.1.1 Effect of Sodium Bicarbonate in the Presence of Calcium

Figure 3.9 shows the zeta potential distributions of bitumen and montmorillonite measured separately in a 1 mM KCl and 1 mM $CaCl_2$ solution without bicarbonate addition (a), and with 7.1 mM of added bicarbonate ions (b). Without bicarbonate addition, the zeta potential distribution peaks for bitumen and montmorillonite lie at -35 mV and -12.5 mV, respectively. With the addition of 7.1 mM of bicarbonate, both the bitumen and montmorillonite peaks shifted to become more negative (-45 mV and -25 mV, respectively).

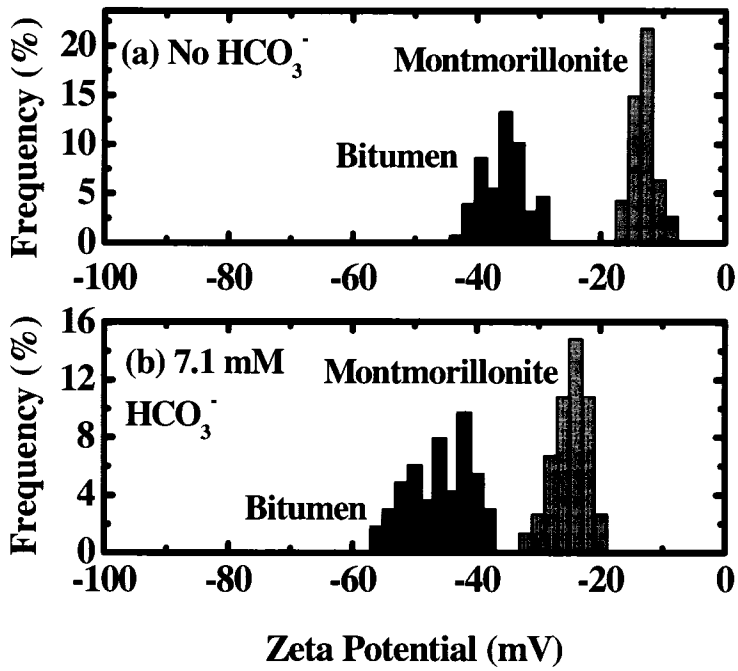

Figure 3.9: Zeta potential distributions of bitumen and montmorillonite measured separately in 1 mM KCl and 1 mM $CaCl_2$ without added bicarbonate (a), and with 7.1 mM of bicarbonate (b).

Zeta potential distributions obtained from 1:1 mixtures of bitumen and montmorillonite without and with the addition of 7.1 mM of bicarbonate are shown in Figures 3.10(a) and 3.10(b), respectively. Two independent peaks, centered at approximately -55 mV and -27.5 mV, exist in the distribution obtained with bicarbonate addition. By comparison, only one peak exists (closer the peak position of montmorillonite) when bicarbonate is absent. The significance of this measurement lies in the possibility that the addition of bicarbonate, at 7.1 mM, might be effective in preventing slime coating when added to process waters containing up to 1 mM calcium. On an industrial level, this might indicate that pre-treatment of

calcium loaded process water with a bicarbonate containing compound might improve bitumen recoveries and/or froth qualities in the extraction plant.

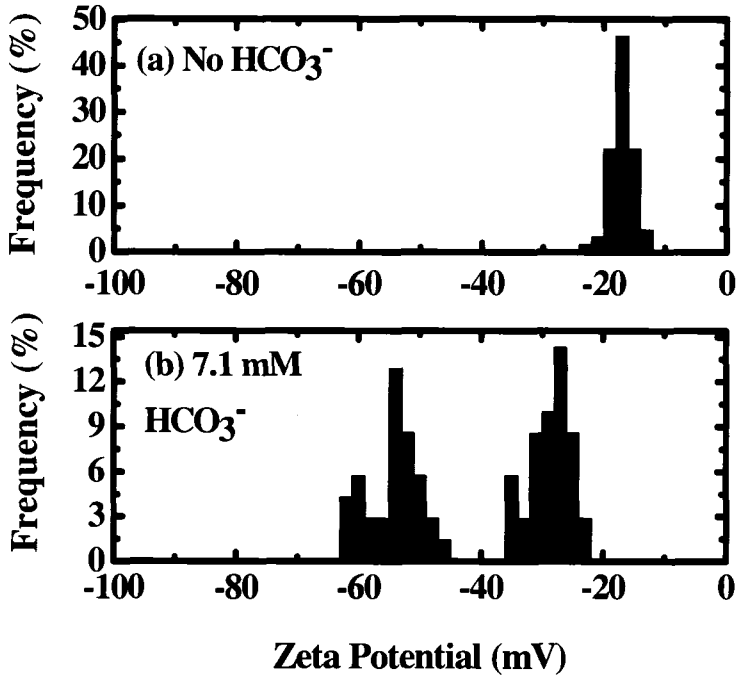

Figure 3.10: Zeta potential distributions of 1:1 binary mixtures of bitumen and montmorillonite in 1 mM KCl and 1 mM $CaCl_2$ without added bicarbonate (a), and with 7.1 mM of bicarbonate (b).

The bicarbonate concentration was increased to 16.4 mM to observe any trends resulting from an increase in bicarbonate concentration. A comparison of Figures 3.11(b) and 3.9(b) shows that the increase in bicarbonate concentration from 7.1 mM to 16.4 mM makes both the bitumen and montmorillonite individual zeta potentials more negative, shifting them from -45 to -55 mV and from -25 to -27.5 mV, respectively. Figure 3.12(b) shows that, for the 1:1 mixture, two independent peaks are present when 16.4 mM of bicarbonate is added to the system while only one peak

exists when bicarbonate is absent (Fig. 3.12(a)). The two peaks present in the binary mixture with 16.4 mM bicarbonate addition are also comparatively more negative than those measured in the 7.1 mM bicarbonate solution (-62.5 mV vs. -55 mV and -35 mV vs. -27.5 mV).

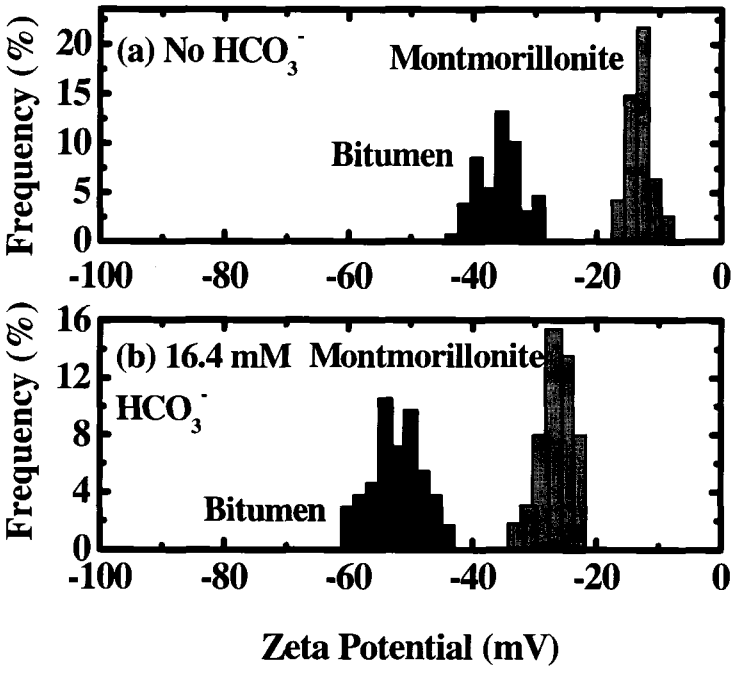

Figure 3.11: Zeta potential distributions of bitumen and montmorillonite measured separately in 1 mM KCl and 1 mM $CaCl_2$ without added bicarbonate (a), and with 16.4 mM of bicarbonate (b).

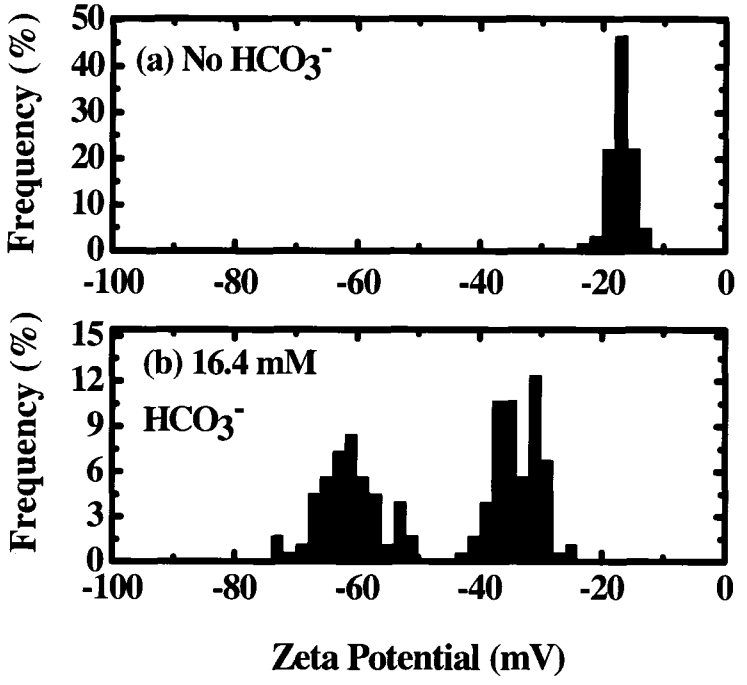

Figure 3.12: Zeta potential distributions of 1:1 binary mixtures of bitumen and montmorillonite in 1 mM KCl and 1 mM $CaCl_2$ without added bicarbonate (a), and with 16.4 mM of bicarbonate (b).

A more subtle observation from the results performed with bicarbonate addition is that the positions of both peaks in the mixtures shift to become more negative with respect to the peaks of the components measured individually. This is different from the other instance where two peaks were present both in the individual measurements and the binary mixture. In the measurements performed in KCl alone (Fig. 3.3), the bitumen peak shifted to become less negative while the montmorillonite peak shifted to become more negative. Although the reasons for this difference are not clear, it provides a clue that the current theory behind the interpretation of zeta potential distributions may not be entirely correct, particularly for the case of a binary

mixture of non-interacting components. This remains a topic for future work. What cannot be argued is that the presence of two peaks in Figures 3.10(b) and 3.12(b) indicates that both bitumen and montmorillonite were present, suggesting that slime coating did not occur in either case.

There are two main possibilities for why bicarbonate appears to be effective at preventing slime coating in the presence of calcium. The first possibility is the classic water softening scenario. In this case, sodium bicarbonate would dissolve in water and the dissolved bicarbonate ions would react with free calcium ions. With free calcium ions removed from the solution, the necessary building blocks of the bridge between bitumen and montmorillonite would be depleted. The role of bicarbonate in the precipitation of calcium is further elucidated in Chapter 4. The second possibility is that the bicarbonate addition increases the magnitude of the zeta potentials on bitumen and clay so that the electrostatic repulsive force between the two components is sufficient to over-power the attractive force induced by the presence of calcium. A combination of the two effects is also possible. A more thorough study of the effects of bicarbonate addition on process water chemistry and the surface chemistry of various oil sands components would be a valuable future endeavor.

3.4.1.2 Effect of Sodium Bicarbonate in the Presence of Magnesium

A set of experiments identical to those performed in Section 3.4.1.1 was performed with the exception that magnesium was added as the di-valent cation in place of calcium. The individual measurements of bitumen and montmorillonite in 1 mM KCl and 1 mM $MgCl_2$ with and without 7.1 mM of bicarbonate are shown in Figure 3.13(b) and 3.13(a), respectively.

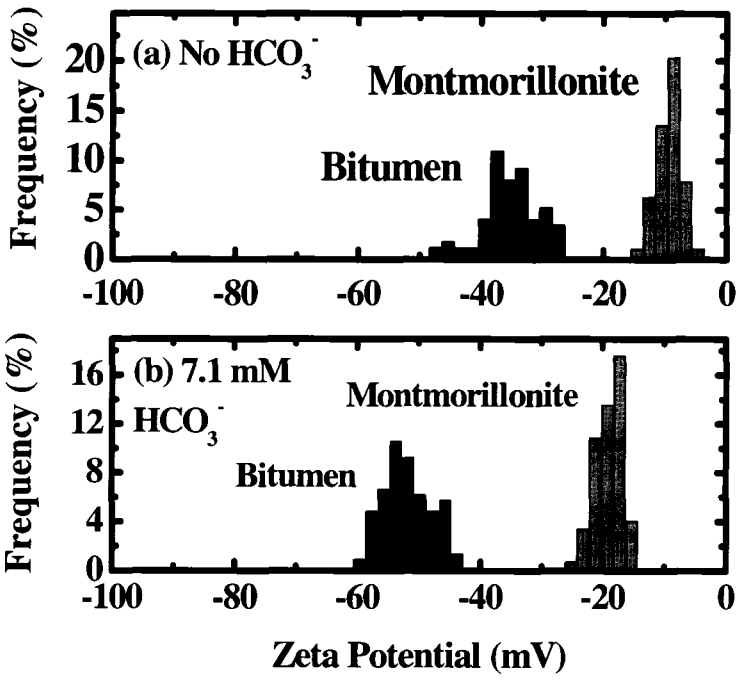

Figure 3.13: Zeta potential distributions of bitumen and montmorillonite measured separately in 1 mM KCl and 1 mM $MgCl_2$ without added bicarbonate (a), and with 7.1 mM of bicarbonate (b).

Without bicarbonate addition, the peaks for bitumen and montmorillonite lie at -35 mV and -10 mV, respectively. With the addition of 7.1 mM of bicarbonate, the peaks shifted to the more negative values of -52.5mV for bitumen and -20 mV for montmorillonite. Interestingly, the 1:1 binary mixture of bitumen and montmorillonite in the solution containing 7.1 mM of bicarbonate still gave one peak located near -25 mV, as shown in Figure 3.14(b). This result indicates that even with the presence of 7.1 mM of bicarbonate, slime coating of montmorillonite onto the bitumen occurred. This observation contrasts strongly with the case where calcium was present. At the same bicarbonate level, slime coating induced by calcium was

prevented even when the total molar concentration of the bad acting di-valent cation was the same.

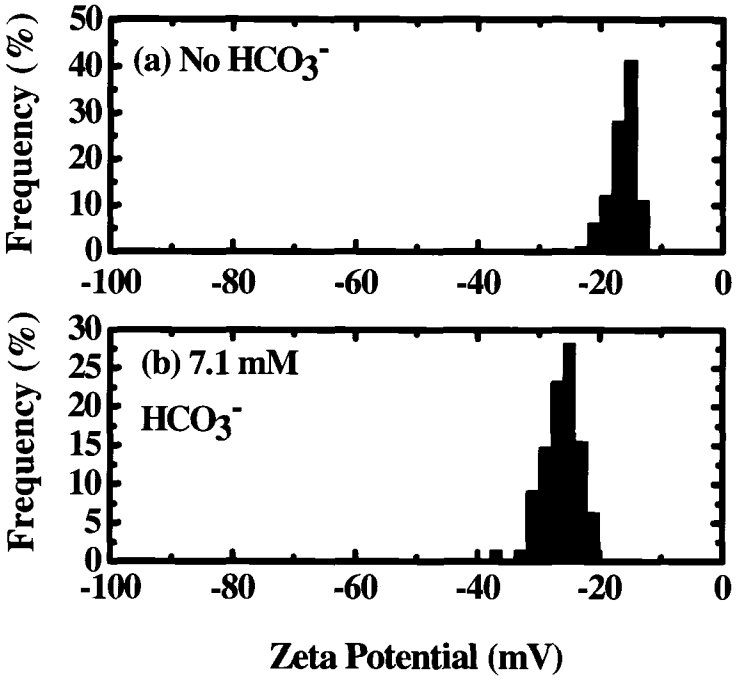

Figure 3.14: Zeta potential distributions of 1:1 binary mixtures of bitumen and montmorillonite in 1 mM KCl and 1 mM $MgCl_2$ without added bicarbonate (a), and with 7.1 mM of bicarbonate (b).

The bicarbonate concentration was increased from 7.1 mM to 16.4 mM to determine whether any effects would be realized with a higher dosage of sodium bicarbonate. Figure 3.15(b) shows two distinct peaks for bitumen and montmorillonite (measured separately) in this electrolyte, with the bitumen peak located near -50 mV and the montmorillonite peak located near -30 mV. The binary 1:1 mixture of the two components in this electrolyte (Fig. 3.16(b)) still gives one peak located at -32.5 mV, near the individual peak for montmorillonite.

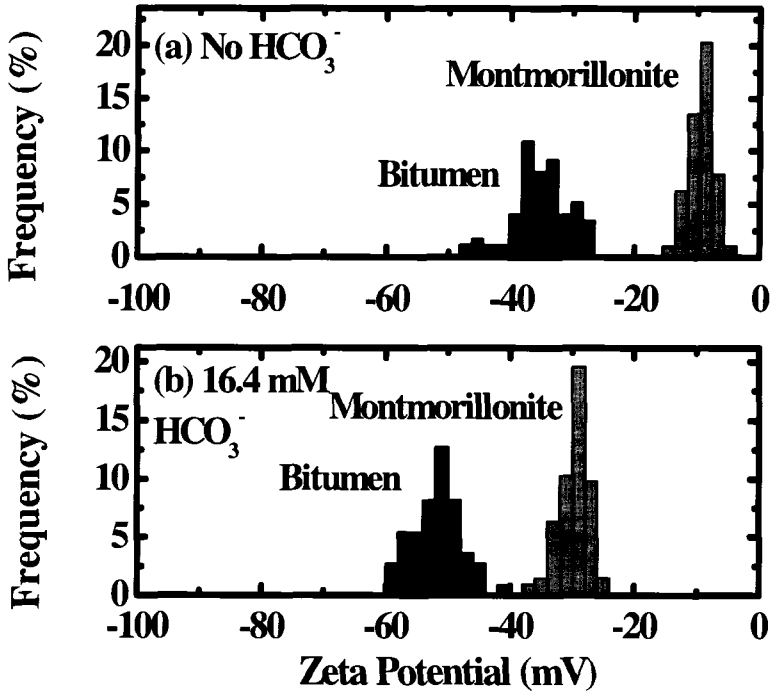

Figure 3.15: Zeta potential distributions of bitumen and montmorillonite measured separately in 1 mM KCl and 1 mM $MgCl_2$ without added bicarbonate (a), and with 16.4 mM of bicarbonate (b).

From these observations, it is apparent that sodium bicarbonate is not an effective preventive agent for slime coating when magnesium is present. As process waters used in bitumen extraction often contain magnesium as well as calcium, this finding is significant from an industrial standpoint.

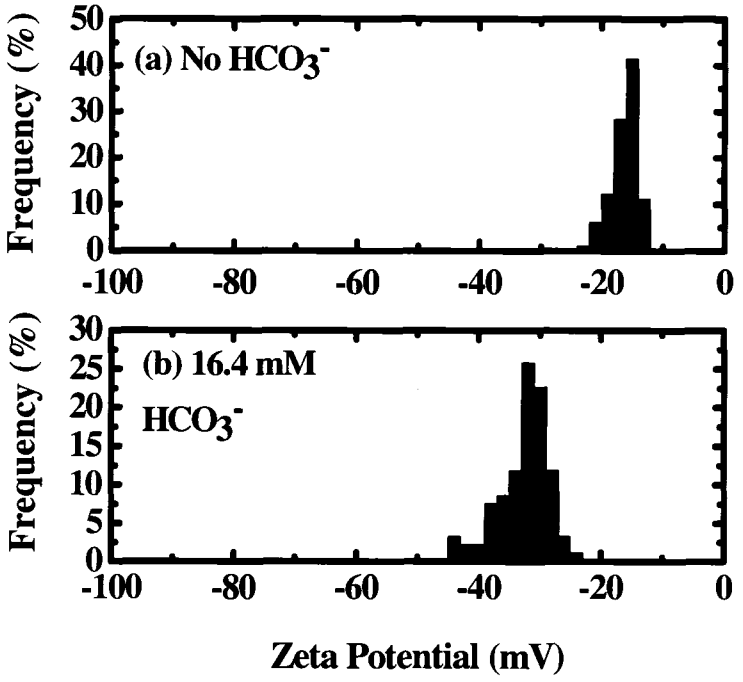

Figure 3.16: Zeta potential distributions of 1:1 binary mixtures of bitumen and montmorillonite in 1 mM KCl and 1 mM $MgCl_2$ without added bicarbonate (a), and with 16.4 mM of bicarbonate (b).

When considering the reasons why bicarbonate is not an effective slime coating preventive agent for systems containing magnesium, it is helpful to recall the reasons given as to why bicarbonate was effective for systems containing calcium. For the case of magnesium, it is known that bicarbonate does not precipitate with magnesium at these bicarbonate levels and at pH 8.5. Again, this possibility is further explored in Chapter 4. It is also possible that magnesium induces a stronger bridging force between bitumen and montmorillonite than calcium does. The dispersant effect of bicarbonate would thus be insufficient to overpower the attractive force created by the presence of magnesium. These findings further support the need for more

research into the effect of bicarbonate and other surface modifiers on water chemistry and the surface chemistry of the different oil sands components.

3.4.1.3 Effect of Sodium Bicarbonate in the Presence of Calcium and Magnesium

As mentioned in the previous sections, process water used in industrial bitumen extraction operations often contains significant amounts of both calcium and magnesium. It was of interest to determine if bicarbonate would be effective at preventing slime coating in the case where the solution contained equi-molar amounts of calcium and magnesium (0.5 mM each).

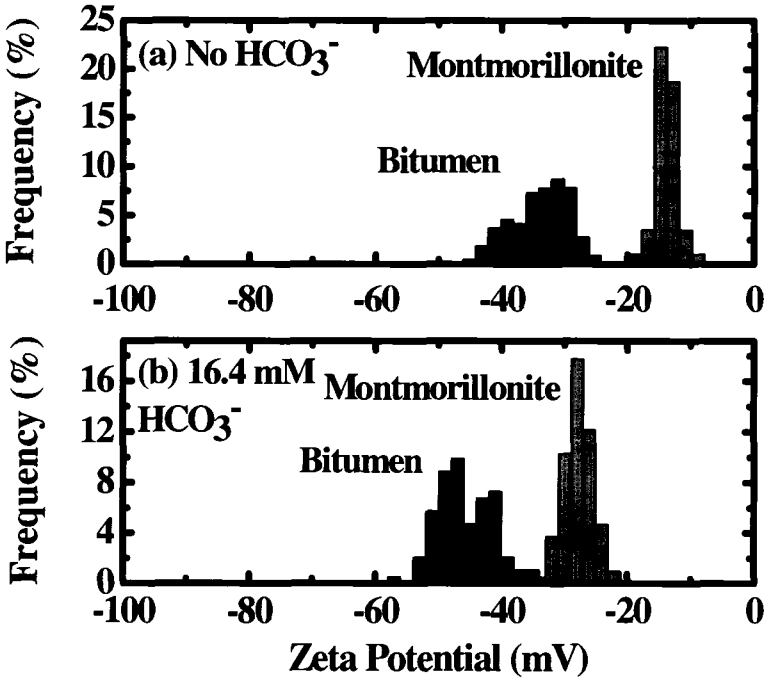

Figure 3.17: Zeta potential distributions of bitumen and montmorillonite measured separately in 1 mM KCl with 0.5 mM $CaCl_2$ and 0.5 mM $MgCl_2$ without added bicarbonate (a), and with 16.4 mM of bicarbonate (b).

The individual zeta potential distributions of bitumen and montmorillonite, measured separately, in the mixed electrolyte with and without 16.4 mM of added bicarbonate are shown in Figure 3.17. Predictably, the zeta potentials of both bitumen and montmorillonite have again shifted to more negative values (bitumen from -35 mV to -47.5 mV and montmorillonite from -15 mV to -27.5 mV). The tails of bitumen and montmorillonite overlap slightly for the case with bicarbonate addition. The distribution representing the 1:1 binary mixture with 16.4 mM bicarbonate (Fig. 3.18(b)) is wide, yet single-modal, with a peak near -30 mV. There is a significant tail, however, which extends from the peak into the negative values until approximately -60 mV. This small tail indicates that the bicarbonate addition did have a marginal impact on the amount of slime coating that occurred. The significant peak near the zeta potential value for montmorillonite indicates that most bitumen remained slime coated. Viewed from an industrial perspective, it appears that the addition of bicarbonate to waters containing a mixture of calcium and magnesium would likely have only a minor impact on bitumen recovery or froth quality.

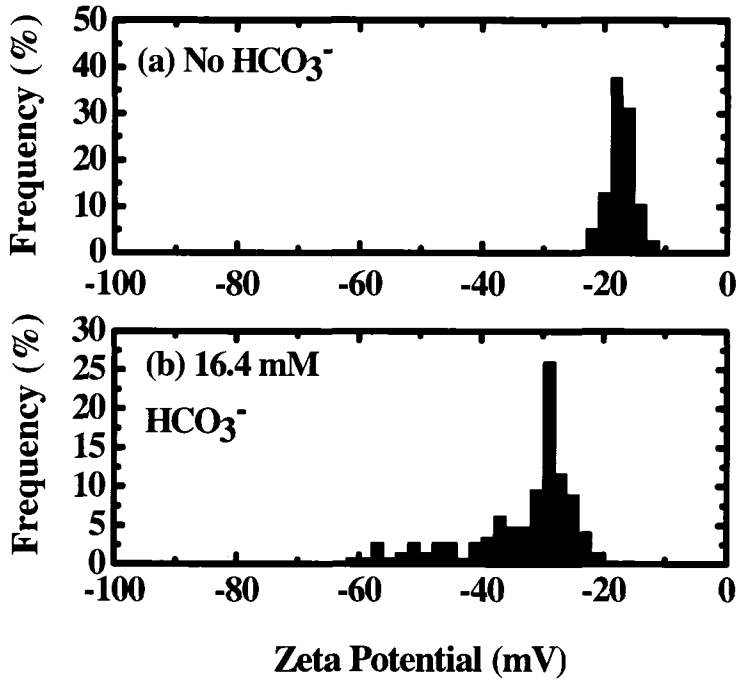

Figure 3.18: Zeta potential distributions of 1:1 binary mixtures of bitumen and montmorillonite in 1 mM KCl with 0.5 mM $CaCl_2$ and 0.5 mM $MgCl_2$ without added bicarbonate (a), and with 16.4 mM of bicarbonate (b).

3.4.1.4 Sodium Bicarbonate as a Remedial Agent

The experiments from section 3.4.1.1 have shown that the addition of sodium bicarbonate to process water containing calcium can help eliminate slime coating of montmorillonite onto bitumen. In those experiments, the bicarbonate was added to the solution prior to the addition of bitumen or montmorillonite. To further elucidate the role of bicarbonate, a test was performed where bicarbonate was added to the system after slime coating was allowed to occur. This test evaluated the efficacy of bicarbonate as a remedial agent (i.e. once the problem had already occurred) rather than as a preventive agent. For this test, a 1:1 binary suspension of bitumen and

montmorillonite was created in an electrolyte containing 1 mM KCl and 1 mM $CaCl_2$ at pH 8.5. The mixture was agitated ultrasonically prior to an initial zeta potential distribution measurement. This initial zeta potential distribution measurement, shown in Figure 3.19(a), served to confirm that slime coating had indeed occurred. A prescribed amount of sodium bicarbonate powder was then added to the suspension. The suspension was stirred until the added powder had dissolved completely. Ultrasonic agitation was again applied prior to the second zeta potential distribution measurement. The results of this measurement are shown in Figure 3.19(b).

Compared with Figure 3.19(a), Figure 3.19(b) has a significantly higher frequency of particles lying in the zeta potential range representing the individual bitumen distribution (-45 to -60 mV). Clearly, the addition of bicarbonate in this fashion had some effect on the degree of hetero-coagulation between bitumen and montmorillonite in the system. Recalling the theory of zeta potential distribution measurements, this distribution resembles a mixture between the cases of "strong attraction with insufficient number of coating particles" and "weak attraction". Strong attraction with an insufficient number of coating particles is ruled out by the distribution shown in Figure 3.19(a). At the same time, the bi-modal distribution characteristic of a weak attraction is not present. It is thus likely that the attraction between bitumen and montmorillonite was weakened by the addition of bicarbonate, but not to an extent that a significant number of bitumen droplets became completely free of montmorillonite. Had a significant number of bitumen droplets became completely free of montmorillonite, a distribution similar to the pre-treated case (Fig. 3.19(c)) would have likely been observed.

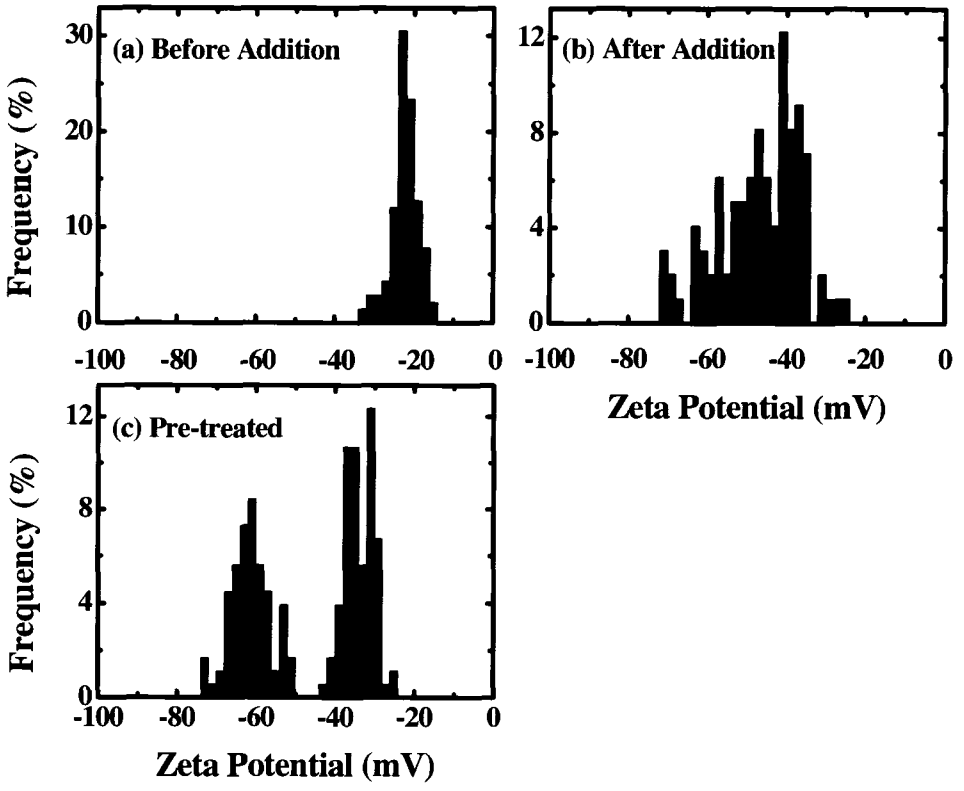

Figure 3.19: Zeta potential distributions of bitumen and montmorillonite in 1 mM KCl and 1 mM $CaCl_2$ at pH 8.5 with a 1:1 B:M ratio (a), of the same mixture after 16.4 mM bicarbonate addition (b), and from the previous results with 16.4 mM bicarbonate pre-treatment (c).

Comparison of Figures 3.19(c) and 3.19(b) shows that in industrial operations, it is more advantageous to use bicarbonate in a preventive fashion rather than a remedial fashion. The two strong, independent peaks in Figure 3.19(c) show that very little hetero-coagulation occured between bitumen and montmorillonite when the water is pre-treated with bicarbonate. The broad single distribution observed in

Figure 3.19(b) shows that a significant amount of bitumen remains at least partially slime coated when bicarbonate is used as a remedial agent.

3.4.2 Sodium Hydroxide

As the reader will learn in Chapter 4, magnesium begins to precipitate out of solution at a pH of approximately 10.5. According to the theory of slime coating, removal of the magnesium ion "bridge" between bitumen and montmorillonite should help prevent slime coating. A set of zeta potential tests was performed to observe whether pre-treating a 1 mM $MgCl_2$ solution with 12.5 mM of NaOH would prevent slime coating.

The measured pH of the 1 mM $MgCl_2$ solution with 12.5 mM of added NaOH was 11.8. Although this pH value was outside the specified operating range of the instrument, the experiments were performed in the hopes of revealing trends. The individual zeta potential distributions for bitumen and montmorillonite are shown in Figure 3.20(a). In contrast to all the previous cases, the zeta potential distribution of montmorillonite lies at more negative values than that of bitumen. The zeta potential distribution peak for montmorillonite was at approximately -50 mV while the peak for bitumen was near + 20 mV. The positive zeta potential value for bitumen in this electrolyte is in agreement with the results obtained in Figure 3.1, where the zeta potential of bitumen was measured as a function of pH.

Recalling the slime coating theory of Sun, who predicted that oppositely charged surfaces attract each other (Sun, 1943), it can be predicted that the positively charged bitumen would hetero-coagulate with negatively charged montmorillonite due to the electrostatic attraction between the two. The zeta potential for the 1:1 binary mixture of the two components appears to confirm this prediction. As shown

in Figure 3.20(b), a single peak exists near -45 mV, which is representative of the peak for montmorillonite alone. The results of this test show that high levels of hydroxide addition increase the probability of slime coating. This adverse effect is in addition to the danger of a strong bitumen emulsion forming in the abundance of surfactants produced by the addition of such a large amount of hydroxide ions. Oil sands operations thus have another reason to use caustic soda prudently in bitumen extraction plants.

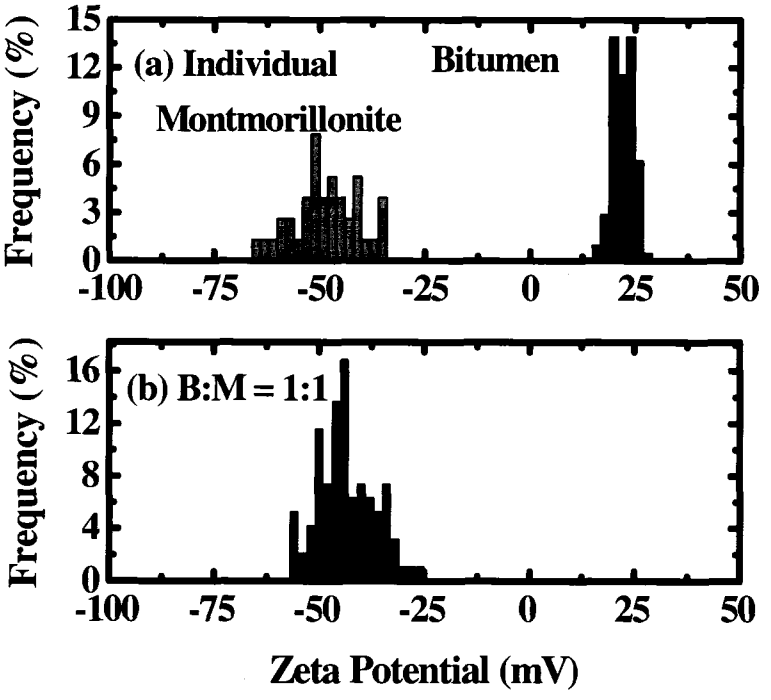

Figure 3.20: Zeta potential distributions of bitumen and montmorillonite in 1 mM KCl with 1 mM $MgCl_2$ and 12.5 mM NaOH measured individually (a), and in a 1:1 mixture (b).

3.5 Slime Coating at Higher Temperatures

Since it is well known that increases in temperature improve bitumen recovery, it was of interest to determine if increased temperatures play a role in preventing slime coating. An attempt was made to re-perform several of the experiments where slime coating was observed at 23°C to determine if the additional thermal energy could prevent slime coating.

Frequently, but not always, transient results for bitumen were obtained in this elevated temperature environment. In cases where transient behavior was observed, the zeta potential distribution observed after ultrasonic agitation or a few zeta potential measurements would be less negative than the original measurement. An example of this sort of behavior is shown in Figure 3.21. In this case, the measurement was bitumen in 1 mM KCl with 1 mM $MgCl_2$ at pH 8.5. The two results shown on the graph are obtained from a freshly prepared sample and the same sample after approximately 5 minutes of ultrasonic agitation. The zeta potential distribution shifts to become less negative after ultrasonic agitation, with the center of the distribution shifting from approximately -35 mV before agitation to approximately -15 mV after agitation.

This sort of behavior clearly poses a problem when it comes to interpreting results for binary mixtures. For instance, would observing a single peak for a binary mixture actually signal that slime coating had occurred, or would it represent two individual peaks that happen to over-lap because of the shift? While the zeta potential distribution technique does not appear to be applicable at high temperatures because of this dilemma, another question arises; why does the measured zeta potential of bitumen change with the combination of high temperature and agitation?

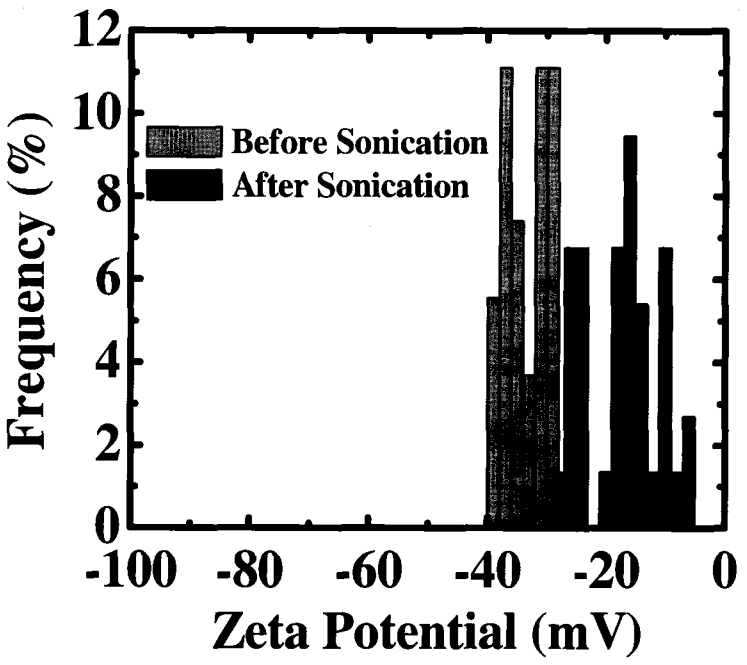

Figure 3.21: Zeta potential distribution "shift" of bitumen in 1 mM KCl and 1 mM $MgCl_2$ at 35°C.

The word to be considered here is "measured". The viscosity of bitumen is lower than at 35°C than at 23°C. This viscosity reduction makes it more likely that emulsified bitumen droplets will break apart when they are subjected to hydrodynamic shear. The true zeta potential of bitumen will, of course, not change when the particle size decreases; the zeta potential is dependent solely on the surface and solution chemistries of the particle and suspending medium. The velocity of a particle moving during electrophoresis will, however, decrease slightly due to the increase in the surface area and the resulting increase in the drag force acting on the droplet.

At this time, it would be prudent to remind the reader of two mathematical expressions which relate the electrophoretic mobility to the zeta potential:

Smoluchowski's Equation (Eq. 2.2) and Henry's Solution (Eq. 2.3). Smoluchowski's Equation, the equation used in this study to covert mobility to zeta potential, states that the velocity of a particle during electrophoresis is proportional to the di-electric constant of the supporting electrolyte, the zeta potential of the particle, the applied electrical field strength, and the reciprocal of the viscosity. Henry's Solution states that the velocity is proportional to all the factors mentioned for the Smoluchowski Equation but also contains an additional factor which is a function of particle size.

Several graphs were constructed to give a visual description of how the Smoluchowski Equation differs from Henry's Solution for various particle sizes. The di-electric constant, viscosity, and inverse debye length used for the calculations were those from a 1 mM solution of a 1:1 electrolyte such as KCl at 35°C (Chemical Rubber Company, 2005; Israelachvili, 1992).

By examining Figure 3.22, one can see that for a true constant zeta potential of -60 mV, Smoluckowski's Equation gives an electrophoretic moblility of -5.7 micron/sec/V/cm regardless of the particle size (when all other variables are held constant). Henry's Solution gives similar results except for very small sized particles (< 1 micron). Below 1 micron, the electrophoretic mobility obtained via Henry's Solution decreases sharply even though the true zeta potential of the particle remains the same.

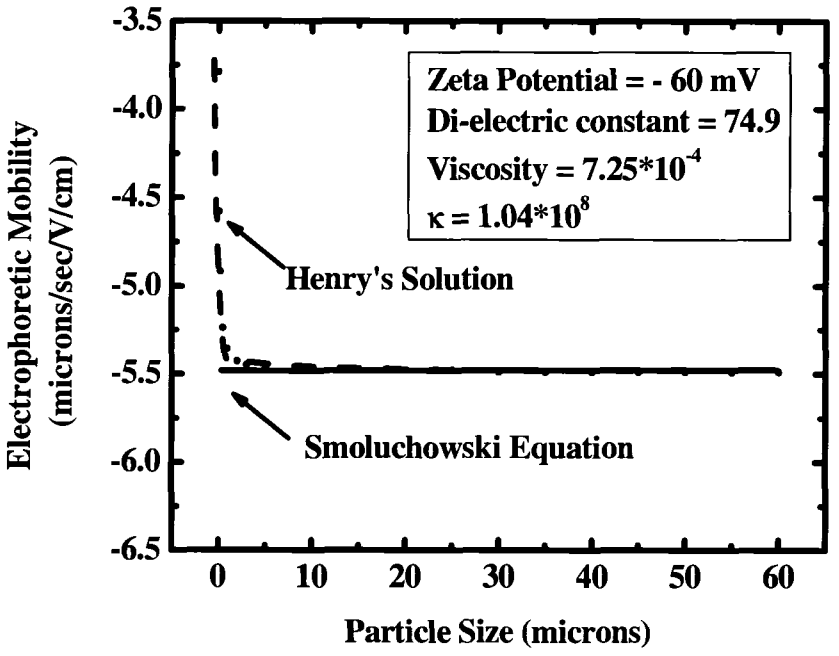

Figure 3.22: Effects of particle size on electrophoretic mobility calculated using Smoluchowski's Equation and Henry's Solution at a constant true zeta potential of -60 mV.

Examining the same phenomenon from a different perspective, one can plot the zeta potential vs. particle size for a constant electrophoretic mobility. This perspective is plotted for a constant electrophoretic mobility of -5.7 micron/sec/V/cm for both the Smoluchowski Equation and Henry's Solution in Figure 3.23. Again, both the Smoluchowski Equation and Henry's Solution give approximately the same result ($\approx$ -60 mV) except for the case of very small sized particles. For very small sized particles (< 1 micron), Smoluchowski's Equation still returns a value of – 60 mV while for Henry's Solution the values become much more negative.

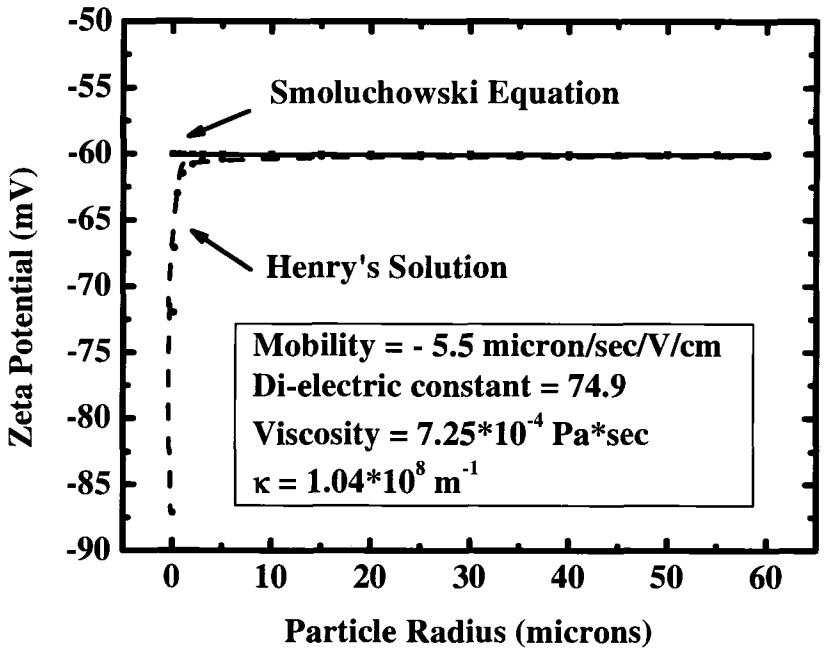

Figure 3.23: Effects of particle size on zeta potential calculated using Smoluchowski's Equation and Henry's solution at a constant electrophoretic mobility of – 5.7 micron/sec/V/cm.

When the theory discussed above and the zeta potential results obtained at 35°C are considered together, it becomes apparent that the shift in the zeta potential values observed in the tests may be an artifact of the experiment rather than a true change in the zeta potential of the bitumen droplets themselves. Figure 3.22 shows that as the size of the bitumen droplet decreased, the true zeta potential of the bitumen droplet may have remained the same even though the electrophoretic mobility of the droplet decreased. In order for the technique of zeta potential distribution measurement to be used effectively for bitumen at high temperatures, the use of Henry's Solution is required. Henry's Solution, however, requires knowledge of the particle size. The zetaphoremeter is incapable of determining particle size. The size

must thus be measured using a laser device such as the Malvern Mastersizer® or other similar instruments. Such an instrument would surely impart more shear to the emulsion and might further reduce the bitumen droplet size. It would become extremely difficult to be confident about any true size measurement or zeta potential measurement at this point.

3.6 Summary

1) The zeta potential of bitumen became progressively more negative as pH increased. The only exception was the case where 1 mM magnesium was present. In this case, an iso-electric point was observed near pH 10.5. The zeta potential of montmorillonite was not pH dependent.

2) No slime coating of montmorillonite onto bitumen was observed in 1 mM KCl. Slime coating was observed when 1 mM of calcium or magnesium ions were added to the KCl solutions. Slime coating was more pronounced at lower bitumen to montmorillonite ratios.

3) Sodium bicarbonate was an effective slime coating preventive agent for the case where calcium was present, but not when magnesium was present. Sodium bicarbonate did not act as effectively when used as a remedial agent.

4) Adding high levels of sodium hydroxide in an attempt to precipitate magnesium and prevent slime coating in the presence of magnesium only

made slime coating more pronounced because of the positive charges imparted to bitumen.

5) Attempts to measure the zeta potential distributions at an elevated temperature (35°C) were unsuccessful as inconsistent values were obtained. It is believed that the size of the emulsified bitumen droplets was constantly changing during measurements at this temperature. As such, erroneous results were obtained.

4 Precipitation of Calcium and Magnesium Ions from Solutions

4.1 Experimental Techniques

4.1.1 Experimental Apparatus

A SpectrAA 220 FS atomic absorption spectrometer (Varian) was used for determination of soluble calcium and magnesium concentrations in the test solutions. The instrument was used in flame mode with air and acetylene as the oxidant and fuel, respectively. Any sample with an absorbance outside the range of the calibration plot was diluted with a micro-diluter (Hamilton Microlab 500 Series) or the Sample Introduction Pumping System (SIPS) provided with the AAS equipment.

4.1.2 Materials

Ultra-pure water from a Millipore water system (resistivity of 18.2 MΩ cm) was used in the preparation of all solutions. Reagent grade $CaCl_2 \cdot 2\ H_2O$ (Fisher) and $MgCl_2 \cdot 6H_2O$ (BDH) were used as the source of di-valent cations. Reagent grade HCl (Fisher) and NaOH (BDH or Fisher) were used as pH modifiers. Bicarbonate ions were obtained from reagent grade $NaHCO_3$ (ACP Chemicals).

4.1.3 Experimental Procedure

Stock solutions of 1 mM $CaCl_2$ and 1 mM $MgCl_2$ were prepared by adding the appropriate amount of the metal chloride salts to ultra-pure water. For the solutions with bicarbonate, sodium bicarbonate was also added to the stock solution. Approximately 50 mL of stock solution was dispensed from the volumetric flask into 100 mL beakers. At this point, NaOH or HCl was added to the stock solution to bring

the pH to the desired value. After the pH was at the desired value, the solution was poured from the beaker into a 50 mL plastic centrifuge tube. Plastic tubes were selected over glass tubes to ensure that the adsorption of metal ions onto container surfaces was minimized (Majer and Khalil, 1981). The contents of the centrifuge tubes were immediately centrifuged for 20 minutes at 3000 rpm in an IEC HN-SII centrifuge to allow for separation of the precipitates from the supernatant. The supernatant was poured into a new, clean centrifuge tube and set aside until the AAS measurements were performed.

The AAS measurements were performed immediately after all the samples were prepared to ensure that the measured levels of dissolved cations were comparable to those present in the zeta potential distribution measurements. In the zeta potential distribution measurements, the bitumen and montmorillonite were added to the solution immediately after the pH was adjusted to 8.5. It was of concern that the sample composition could change over time due to adsorption of calcium or magnesium ions on the plastic surfaces, reaction with gases trapped in the air gap of the centrifuge tube, etc. An additional consideration was that in real oil sands extraction plants, process aids such as sodium hydroxide or sodium bicarbonates/carbonates are generally added to the oil sands ore or process water immediately prior to their introduction into the hydrotransport line or flotation system. By performing the measurements immediately after the solutions were prepared, it was possible to obtain a glimpse of what might be occurring in a real extraction plant.

An absorbance/concentration plot was generated using the operating software for the instrument. Commercial standards or acidized chloride solutions were used as the calibration standards. The computer software managed and controlled sample injection, absorbance measurement, and concentration calculations.

4.2 Precipitation in Solutions Containing 1 mM $CaCl_2$

The concentration of calcium ions in solution was measured at various pH values for a solution containing no added bicarbonate, a solution with 7.1 mM of added bicarbonate, and a solution with 16.4 ppm of added bicarbonate. The concentration of soluble calcium in solution as a function of pH is shown in Figure 4.1.

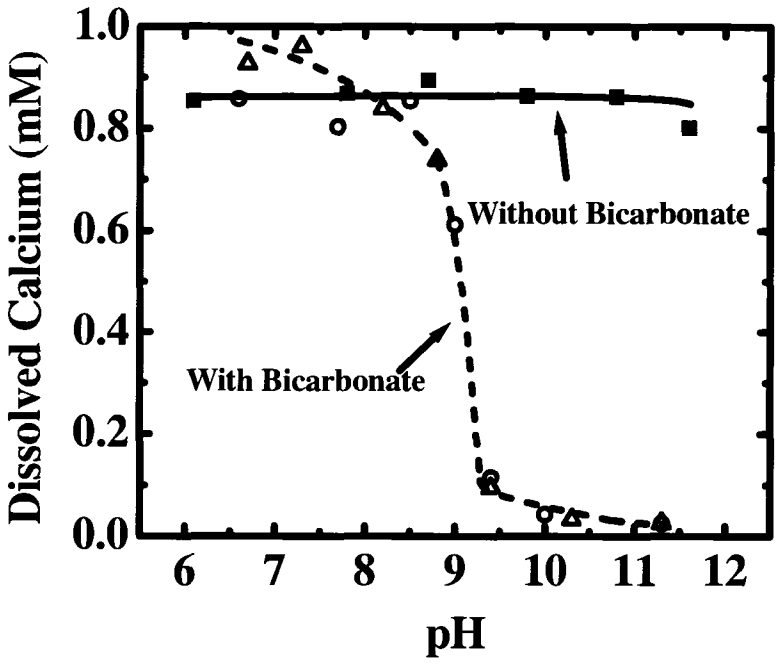

Figure 4.1: Solubility of calcium as a function of pH with and without bicarbonate addition. The total amount of added calcium was 1 mM. The square symbols represent the case without bicarbonate addition, the open circles represent the case with 7.1 mM bicarbonate, and the open triangles represent 16.4 mM bicarbonate.

It is apparent from the solid line in Figure 4.1 that very little precipitation of calcium occured when no bicarbonate was added. From pH 6 to 11.5, the level of calcium in solution was nearly constant at approximately 0.85 mM. When sodium bicarbonate was added in a sufficient quantity to provide either 7.1 mM or 16.4 mM

of bicarbonate ions to solution, precipitation of calcium began to occur at a pH of approximately 8.5 (as illustrated by the dashed line). At pH values around 9.5, only about 0.10 mM of calcium remained in solution. At pH values above 10, less than 0.05 mM of calcium remained. The sharpest decline in the level of calcium in solution occurred between the pH values of 8.5 and 9.25.

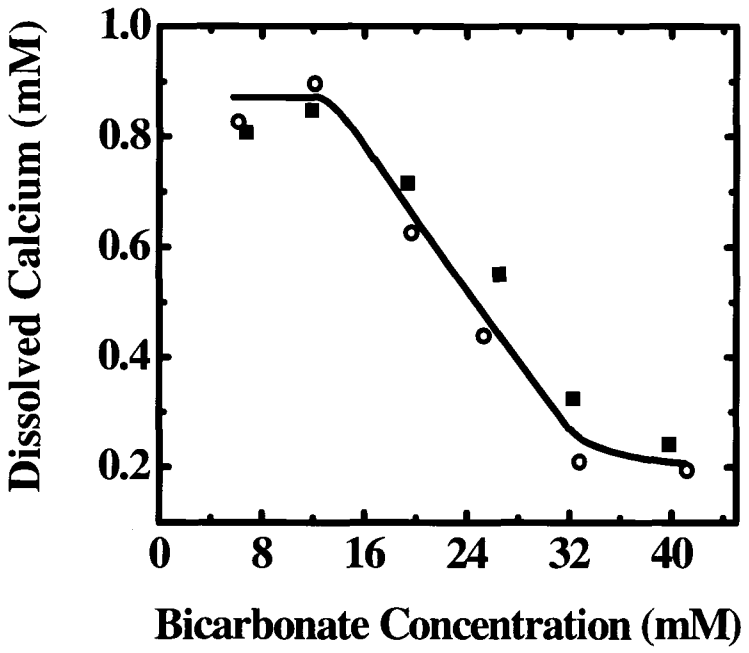

Figure 4.2: Solubility of a 1 mM $CaCl_2$ solution at pH 8.5 as a function of bicarbonate concentration. The squares and the open circles represent the two experimental runs.

To further explore the effects of bicarbonate at pH 8.5, a set of tests was conducted where the pH was kept constant at 8.5 and bicarbonate was added at dosages ranging from 6 mM to 40 mM. Because the decline in the level of calcium in this pH region was very sharp, two runs were performed to verify that the trend

observed was real and not due to errors in pH adjustment or measurement. The trendline in Figure 4.2 shows that at a constant pH of 8.5, the concentration of calcium remaining in the solutions dropped from above 0.8 mM at a bicarbonate dosage of 6 mM to below 0.3 mM at a bicarbonate dosage of 40 mM. These two figures indicate that dissolved calcium can be sequestered both by changing the level of bicarbonate in solution or making an adjustment to the solution pH.

4.3 Precipitation in Solutions Containing 1 mM $MgCl_2$

Identical experiments to those performed with 1 mM $CaCl_2$ solutions were performed using 1 mM $MgCl_2$ solutions. The addition of bicarbonate appeared to have no effect on the precipitation behavior of magnesium, as shown in Figures 4.3 and 4.4. For the cases with no bicarbonate and the cases with 7.1 and 16.4 mM of added bicarbonate, precipitation began to occur near pH 10.5. It would appear that magnesium hydroxide is the phase that precipitates out at the same pH in all three cases. Similar to the case for calcium, the precipitation of magnesium happens over a very narrow pH range. The concentration of magnesium drops from around 0.85 mM at pH 10.5 to less than 0.4 mM at pH 11.3.

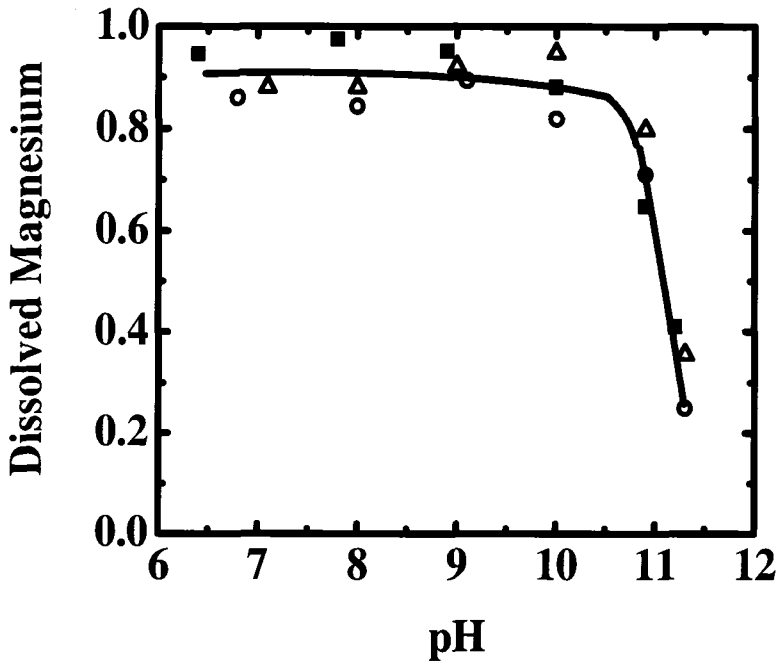

Figure 4.3: Solubility of magnesium as a function of pH with and without bicarbonate addition. The total amount of added magnesium was 1 mM. The square symbols represent the case without bicarbonate addition, the open circles represent the case with 7.1 mM bicarbonate, and the open triangles represent 16.4 mM bicarbonate.

Figure 4.4 shows the results when the pH was kept constant at 8.5 and the added bicarbonate level changed from 7 mM to 40 mM. The trend-line remains horizontal at around 0.9 mM, indicating the absence of magnesium precipitation even at very high bicarbonate concentrations.

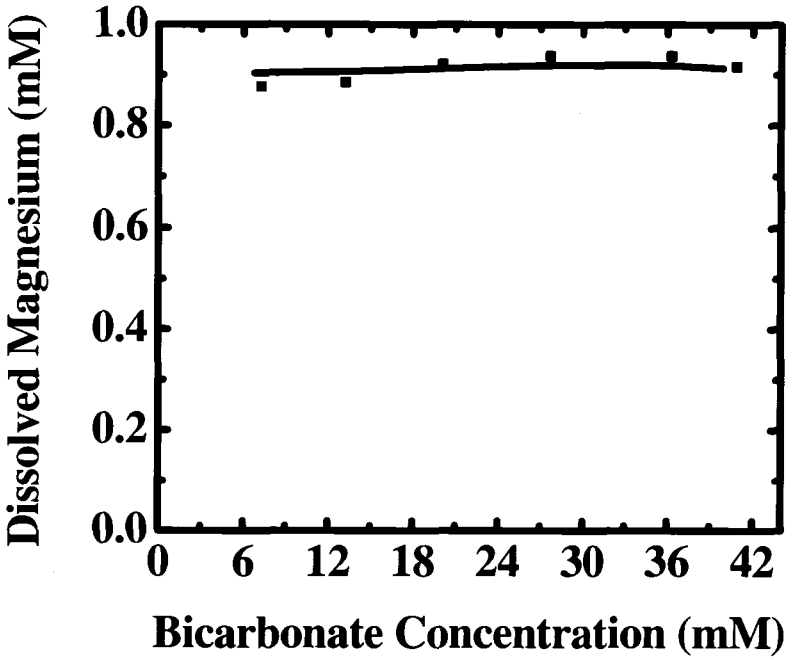

Figure 4.4: Solubility of a 1 mM $MgCl_2$ solution at pH 8.5 as a function of bicarbonate concentration.

4.4 Relationship with Zeta Potential Distribution Results

Certain correlations arise when comparing the results from this chapter with those from Chapter 3 on zeta potential distributions. The atomic absorption results indicate that in the absence of bicarbonate, virtually no calcium or magnesium precipitates from solutions containing 1 mM of those cations. The dissolved calcium and magnesium would thus be available to form a "bridge" between bitumen and montmorillonite as predicted by the theory of slime coating. The atomic absorption tests showed that the addition of bicarbonate at pH 8.5 or higher could precipitate calcium, but not magnesium. Correspondingly, bicarbonate appeared to prevent slime coating in the presence of calcium but not magnesium.

While it may be convenient to "put two and two together" in light of these comparisons, a more thorough examination of the results shows that the AA results may not be directly correlated to the zeta potential results. For instance, the zeta potential distribution results showed that 7.1 mM and 16.4 mM of added bicarbonate prevented slime coating in the presence of calcium at pH 8.5. However, Figure 4.2 shows that at pH 8.5, around 0.8 mM and 0.7 mM of calcium are present in solutions containing 7.1 mM and 16.4 mM of bicarbonate, respectively. While these considerations don't rule out the possibility that precipitation of calcium contributes to the prevention of slime coating, they indicate that other phenomena may also be contributing. An example of one such phenomenon would be the formation of calcium complexes (rather than precipitates) with species released from bitumen emulsions used in zeta potential distribution tests. Such complexes might not be able to induce slime coating. Another possibility is that a critical concentration of free calcium (greater than 0.7 or 0.8 mM) in solution may be required before slime coating can occur.

4.5 Summary

1) Without bicarbonate addition, precipitation of calcium does not occur even at pH values as high as 11.5. When bicarbonate is added at either 7.1 mM or 16.4 mM levels, calcium precipitation begins to occur at around pH 8.5.
2) At a constant pH of 8.5, an increased amount of calcium may be precipitated by adding more bicarbonate into solutions.

3) Bicarbonate addition does not aid in the precipitation of magnesium. Magnesium precipitates out as magnesium hydroxide at pH values above 10.5.

4) While precipitation of calcium may explain why bicarbonate can prevent slime coating in the presence of calcium, but not magnesium, there are likely other phenomena playing a role as well.

5 Processability of Ores Doped with Di-Valent Ions and Montmorillonite

5.1 Experimental Techniques

5.1.1 Experimental Apparatus

A laboratory flotation Denver Cell (Geneq) was used for all the flotation tests. In order to accommodate the elevated temperature requirements of the experiments, a 1 L flotation cell containing its own water jacket was constructed in house by the machining staff of the Department of Chemical and Materials Engineering. This modified device allowed for the addition of air, mechanical energy, and heat simultaneously, creating conditions analogous to those in real bitumen extraction systems.

5.1.2 Materials

Two oil sand ores were used in the flotation tests. The "good processing" ore was a facies 11 ore obtained from Syncrude Canada Ltd. Ore D, the "poor processing" ore, was also obtained from Syncrude Canada Ltd. The compositions of the ores are listed in Table 5.1. The bitumen, mineral, and water contents of the ores, averaged over two samples of each ore, were determined using the Dean and Stark method which will be described in Appendix A. The particle size distributions of the solids collected from the Dean and Stark analyses were determined using a Malvern Mastersizer 2000®. The volume % of solids passing 45 microns is analogous to the fines content of the ore. The -45 micron fraction listed in Table 5.1 is the average of four samples from each ore.

Great care was taken to minimize the amount of de-hydration and weathering that occurred in the ore prior to its use in extraction tests. Ore samples, once received by our laboratory, were stored inside of tightly sealed plastic bags (no air gap) inside a household freezer. It is likely that a small amount of ore weathering occurred before the ore was brought to our lab (i.e. between the mine face and our laboratory). This weathering, however, was beyond our control.

Table 5.1: Ore characteristics.

	% by Mass			-45 μm
	Bitumen	Mineral	Water	% Volume
Good Ore	14.2	81.5	3.39	12.8
Poor Ore	9.64	87.0	2.28	39.1

The montmorillonite used for this part of the study was the same montmorillonite used in the zeta potential distribution measurements (Section 3.1.2)

Slurry water was prepared using ultra-pure water from a Millipore water system with a resistivity of 18.2 MΩ·cm. Reagent grade $CaCl_2 \cdot 2H_2O$ was added to the ultra-pure water for the tests performed with calcium addition. Laboratory compressed air was used as the air source.

5.1.3 Experimental Procedure

Sealed plastic bags containing 600 g of oil sand were taken out of a household freezer and allowed to de-frost at room temperature for approximately 1 hour. De-frosted samples were mixed by hand inside the plastic bag to break up any lumps and to identify rocks which needed to be removed in order to prevent damage to the

Denver Cell. The water jacket used to circulate heated water around the flotation cell was powered on and set to the test temperature 30 minutes to 1 hour prior to the start of the test. Cellulose extraction thimbles (Whatman) were placed inside of glass jars and the combined weight of each thimble-jar pair was recorded. Using a scoopula, 450 g of oil sand was weighed out into a beaker. For the tests with 3% (by mass) clay addition, 13.5 g of montmorillonite was placed in a separate glass beaker.

After the flotation cell and the slurry water were heated to the desired temperature, 300 mL of de-ionized or calcium doped de-ionized water was added to the flotation cell. If the test was being performed with clay addition, the clay was then added and stirred manually to disperse any lumps prior to adding 450 g of oil sand to the cell. The oil sand was conditioned using mechanical energy (1800 rpm rotational speed) and aeration (150 mL/min) in the Denver Cell for 5 minutes. At the end of 5 minutes, the air was turned off but agitation was allowed to continue un-interrupted. Another 650 mL of slurry flood water was carefully added to the flotation cell, and a primary froth was skimmed into the extraction thimble(s) continuously for 10 minutes. After 10 minutes, air addition resumed at a volumetric flow rate of 50 mL/min. A secondary froth was then collected for 8 minutes after which the air and agitation were discontinued and no more froth was collected.

The tailings water was then decanted from the flotation cell and placed in a 1 L glass beaker. The top of the glass beaker was sealed with laboratory wax to prevent the entrance of air or exit of moisture from the beaker. The beaker was allowed to cool to room temperature and the pH of the cool slurry was measured with a pH probe (Accumet or Orion). Two 50 mL tailings aliquots were then taken and placed into two 50 mL plastic centrifuge tubes (Fisher). The tubes were centrifuged at 3000 rpm for 20 minutes in an IEC HN-SII centrifuge. After the 20 minutes the top layer of

each tube was withdrawn and placed into 25 mL teflon centrifuge tubes and centrifuged at 20000 rpm for 1 hour in a Beckman Allegra 64 R Centrifuge. The clear layer was then removed and placed in another clean 50 mL plastic centrifuge tube to await calcium and magnesium determination by AAS.

An assay of the froth collected was obtained using a Dean and Stark method. The detailed procedures of this method are outlined in Appendix A. Calcium and magnesium contents in the tailings water were determined using the same procedure as that described in section 4.1.3 of this thesis.

A matrix of flotation tests was performed on both good and poor processing ores at 35°C and 65°C. Table 5.2 lists the three test conditions used at each temperature and for each ore type.

Table 5.2: Manipulated variables in the flotation tests.

Test Name	**Clay Addition (% by mass of ore)**	**Calcium in Slurry Water (mM)**
Blank	0	0
Clay	3%	0
Clay + Calcium	3%	1

Two replicates were performed at each set of conditions to take into account the experimental error that is inherent in flotation tests performed with natural ores.

5.2 Low Temperature Experiments

A temperature of 35°C was chosen to observe the impact of montmorillonite and calcium on low-temperature extraction systems.

5.2.1 Good Ore Processability

The effects of clay addition and the co-addition of clay and calcium on the primary and total recoveries obtained from the good processing ore at 35°C are shown in Figure 5.1. The average recovery values are indicated by the histogram bars while the error bars indicate the data spread (maximum and minimum) values used to calculate the average.

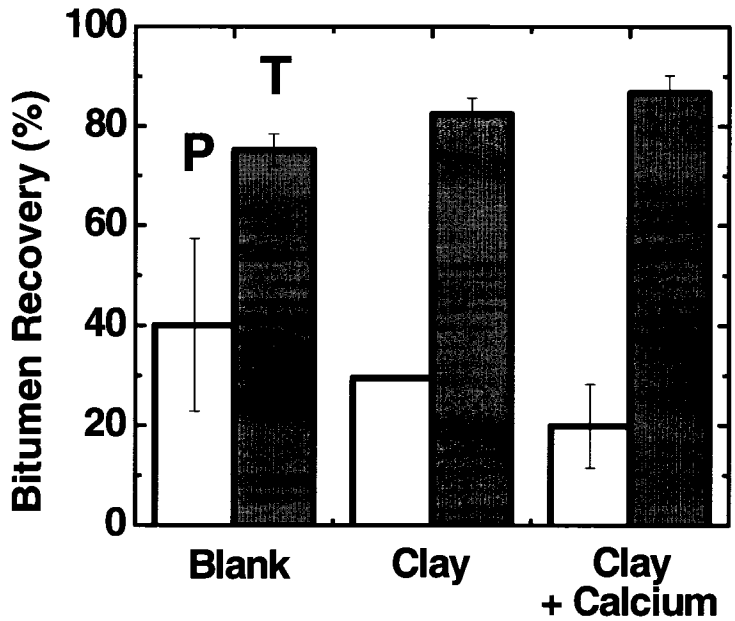

Figure 5.1: Primary (white) and total (gray) recovery from a good processing ore at 35°C.

In all cases, a larger portion of the bitumen was recovered during the secondary stage. The average primary recovery for the blank tests was 40.1%. The average primary recovery decreased to 29.6% and 19.9% when clay and a combination of clay and calcium were added to the system, respectively. In spite of this apparent trend, the error bars representing the variance between replicate tests is quite large for the blank

and the co-addition of clay and calcium. As a result of this variance, one cannot be certain that this perceived trend is actually caused by the addition of clay or calcium ions. Similar results are apparent when observing the total recovery results. While the average total recovery actually increased from 75.2% to 82.4% when clay was added and to 86.7% when clay and calcium were co-added, the range of the error bars lie within each other. Without taking the error bars into account, it is possible that the average primary recovery dropped with the addition of clay or the combination of clay and calcium because of montmorillonite slime coating on bitumen. Aeration of these slime coated droplets may not have been possible in the primary stage but may have been possible at longer periods of time (in the secondary stage). This would explain why there was no drastic decrease in total bitumen recovery. The slight increase in total recovery observed by adding montmorillonite clay or a combination of montmorillonite and calcium may be due to the increase of pH caused by the clay addition (see section 5.2.3).

Previous work (Baptista, 1989b) has shown that the nature of the exchangeable cations on the clays plays an important role in determining whether or not the clays will adversely affect processability. Baptista found that clays that were calcium saturated were more detrimental to recovery than sodium saturated clays. Table 3.1 showed that the major exchangeable ion in the clays used in these tests was sodium. This may also help explain why more drastic reductions in bitumen recovery were not observed.

From an industrial standpoint, the quality of froth produced during the flotation process is also very important. One key indicator of froth quality is the weight ratio of bitumen to solids in the froth. The bitumen/solids (B/S) ratios obtained from the good ore at 35°C are shown in Figure 5.2. Similar to the results for

recovery, there exists a large amount of variance between replicate data sets. The large and over-lapping error bars make it hard to differentiate between true differences in the average and scatter. The B/S ratios of the secondary froth, however, appear to be slightly higher than the B/S ratios of the primary froth for all cases.

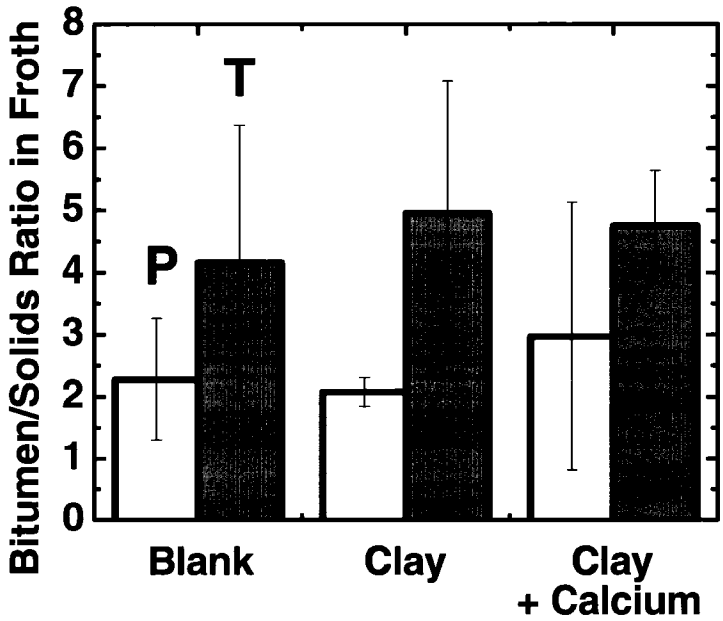

Figure 5.2: The bitumen/solids ratio of the primary (white) and secondary (gray) froths from a good processing ore at 35°C.

5.2.2 Poor Ore Processability

The primary and total recoveries obtained from the poor ore processed at 35°C are shown in Figure 5.3.

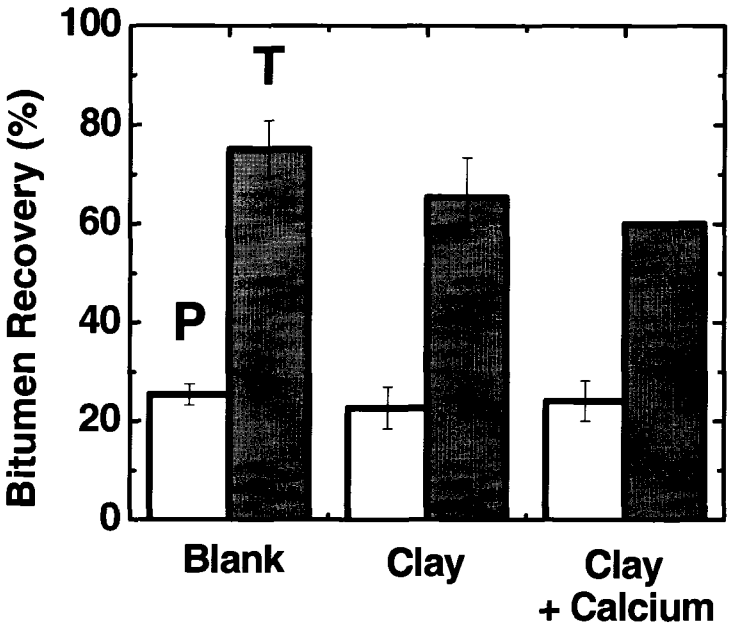

Figure 5.3: Primary (white) and total (gray) recovery from a poor processing ore at 35°C.

The average primary recovery for all three conditions ranged from 22.7% for the case with 3% clay to 25.4% for the blank. The average total recovery dropped when clay and the combination of clay and calcium were added, falling from 75.1% to 65.4% and 60.0%, respectively. Despite this apparent decrease, the large error bars make it difficult to draw definitive conclusions from the data. If one were to ignore the error bars, it becomes apparent that slime coating may have occurred and may have affected total bitumen recovery. It is also worth noting that the primary and total recoveries were generally lower for the poor processing ore than for the good processing ore. The poor processing ore contained a much higher amount of fines which may have inhibited bitumen recovery by a number of mechanisms. These mechanisms include the consumption of natural surfactants by solid matter, fine

particle interference with bitumen recession from sand grains, and impediment of air bubble-bitumen attachment caused by clay slime coatings on bitumen droplets or air bubbles.

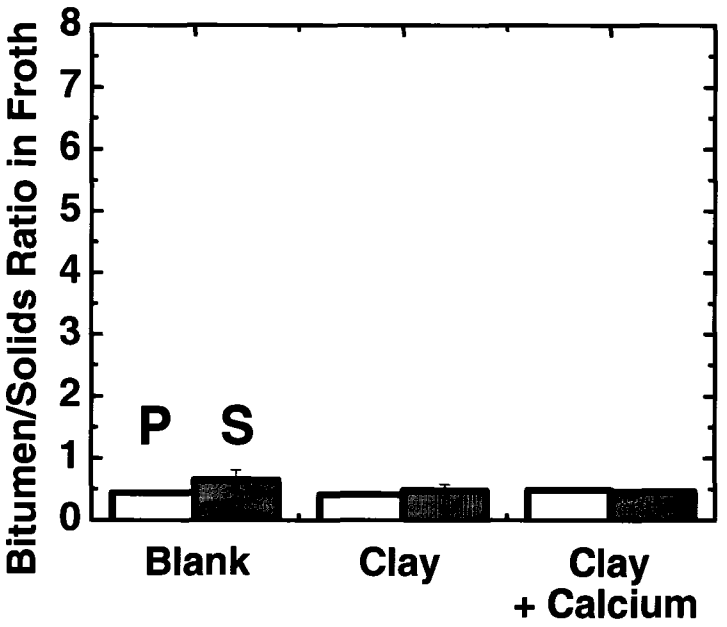

Figure 5.4: The bitumen/solids ratio of the primary (white) and secondary (gray) froths from a poor processing ore at 35°C.

The bitumen/solids ratios obtained from the poor processing ore (Fig. 5.4) were also far below those obtained from the good processing ore. While the B/S ratios for the good processing ore were all above 2, the same ratios for the poor ore were all below 0.7. This is not un-expected when the mechanisms listed in the previous paragraph are considered. Specifically, it is possible that some partially slime coated bitumen droplets were aerated and achieved enough buoyancy to float into the froth. Other possibilities include true flotation of hydrophobic or bi-wetable

solids and mechanical entrainment of suspended fine particles with rising bitumen-air aggregates.

5.2.3 Tailings Water Chemistry

The results of the pH and AAS measurements performed on the tailings water from each test are summarized in Tables 5.3 and 5.4 for good ore and poor ore, respectively.

Table 5.3: Analysis of the tailings water from tests performed at 35°C using good ore.

	[Ca] ppm	[Mg] ppm	pH
Blank	0.136	0.0983	6.7
Clay Only	0.0485	0.175	8.9
Clay + Calcium	0.454	0.134	8.8

The results show that only trace amounts of calcium or magnesium (< 1 ppm) were present in the tailings water after extraction was completed regardless of the type of ore processed or whether clay or calcium were added. This is a particularly interesting finding for the cases where the slurry water was doped with 1 mM (40 ppm) of calcium. It is obvious that nearly all of the calcium added to the water was consumed during the test. Possible consumers of calcium include ion exchange in the montmorillonite, reaction of calcium with surfactants produced, or adsorption of calcium onto other mineral or bitumen surfaces. Clearly, more study is needed in this area.

Table 5.4: Analysis of the tailings water from tests performed at 35°C using poor ore.

	[Ca] ppm	[Mg] ppm	pH
Blank	0.0205	0.115	8.0
Clay Only	0.019	0.435	8.8
Clay + Calcium	0	0.366	8.2

In contrast, the pH of the tailings water did change with ore type and the presence of calcium and/or clay. For the good processing ore, the pH of the tailings water for the blank test was 6.7. The pH rose to 8.9 and 8.8 when clay or the combination of clay and calcium were added, respectively. The increasing of pH by montmorillonite addition has been observed previously (Fong et al., 2004) and was attributed in some way to the presence of exchangeable ions specific to montmorillonite. The change in pH was not so drastic for the poor ore. The tailings water from the blank tests had an average pH of 8.0 while the addition of clay or a combination of clay and calcium resulted in pH increases to 8.8 and 8.2, respectively. The difference between the pH values corresponding to the blank tests for the good and poor ores may be related to differences in the mineralogical composition or connate water chemistry of the ores.

5.3 High Temperature Experiments

In order to observe the impact of montmorillonite and calcium on bitumen extraction at higher temperatures, the same flotation tests were repeated at 65°C.

5.3.1 Good Ore Processability

Figure 5.5 shows the effects of clay addition and the co-addition of clay and calcium on the processability of the good ore at 65°C. It is obvious that there is a large and statistically significant drop in bitumen recovered during the primary stage when clay or a combination of clay and calcium are present during flotation. The primary recovery drops from approximately 77% for the blank to 26% and 28% for the case with clay addition and with clay and calcium addition, respectively. The drop in recovery may be attributable to clay slime coating of bitumen or air bubbles, consumption of surfactants generated by mineral surfaces, or entrapment of bitumen in clay structures as described by Baptista (Baptista, 1989b). Despite this drastic reduction in primary recovery, the total recovery obtained after combining the secondary froth with the primary froth hovers around 80% for all three cases. If bitumen-trapping clay structures, described by Baptista, did form during the test, they would have formed during the conditioning when the ratio of clay to bitumen was high prior to the addition of flood water. Such clay-bitumen structures may have been broken apart when the flood water was introduced following the conditioning stage. It is important, however, to remember that no air was added to the slurry from the time the flood water was added until the secondary flotation stage began. As a result, the previously trapped bitumen that was freed during the flood water addition would have remained suspended in the middlings phase until the second aeration stage began. This may explain why the total recovery during all three test conditions is similar.

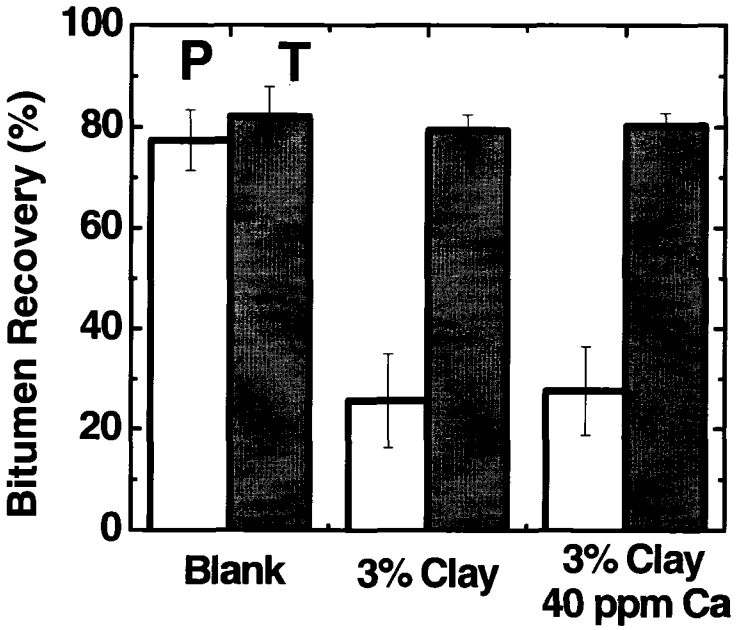

Figure 5.5: Primary (white) and total (grey) recovery from a good processing ore at 65°C.

The fact that a drastic reduction in bitumen recovery was observed at 65°C but not at 35°C opens the door for further discussion on the role of temperature in bitumen extraction. This result implies that temperature may have just as great an impact on bitumen recovery as ore characteristics for certain ores. For instance, the recoveries obtained from the blank at 35°C and the two poisoned good processing ores at 65°C were comparable. It is also possible that the difficulties encountered during processing at the lower temperature were so severe (even in the good ore) that the addition of clay or clay with calcium could not possibly make any difference.

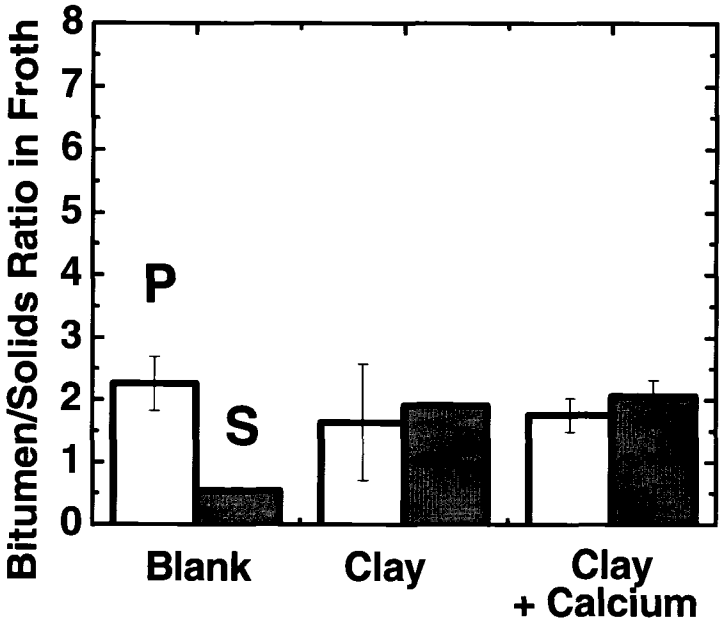

Figure 5.6: The bitumen/solids ratio of the primary (white) and secondary (gray) froths from a good processing ore at 65°C.

A slightly different trend is present in the results illustrating the bitumen/solids ratios of the froth from these tests (Fig. 5.6). The values for the bitumen/solids ratios from the primary froths all lie within the range 1.64-2.26, which could be considered to be within the experimental error range. Interestingly, the bitumen/solids ratio for the secondary froth actually increases when clay or a combination of clay and calcium are added. When the whole flotation process is considered, this result is not un-expected. In the blank test, almost all of the bitumen was recovered during the primary stage, leaving very little bitumen available for secondary flotation. As a result, the overall mass of solids reporting to the secondary froth likely did not change, but its percentage of the total froth increased due to the absence of bitumen.

5.3.2 Poor Ore Processability

The results of the flotation tests performed on poor ore at 65°C are shown in Figure 5.7.

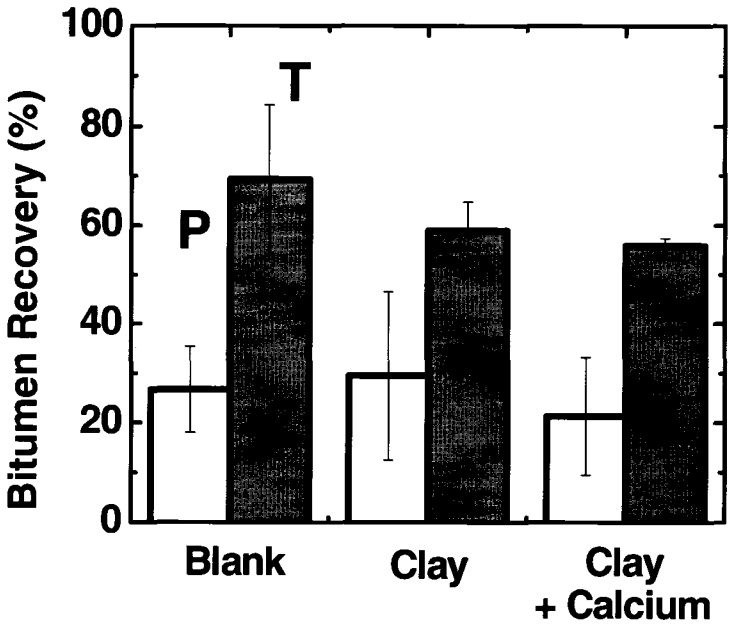

Figure 5.7: Primary (white) and total (grey) recovery from a poor processing ore at 65°C.

In contrast to the good processing ore, the primary and total recoveries of the poor processing ore do not change drastically with the addition of clay or a combination of clay and calcium. The average primary recovery changes from 26.7% to 29.5% when clay is added and to 21.3% when clay and calcium are co-added. All of these values lie within the range of the error bars. The addition of clay caused a decrease in total recovery from 69.3% to 59.0% while a clay and calcium co-addition depressed the recovery to 55.9%. Again, the error bars are wide and differences in the average values may not be statistically significant.

The recoveries obtained for the poor ore at 65°C are comparable to those obtained at 35°C. Contrary to what is generally believed, it appears that increasing the temperature will not necessarily improve recovery for all ores. The subject of the role of temperature in bitumen recovery thus remains an item for further exploration.

Previous work studying the parameters affecting ore processability has been based on the hypothesis that a good processing ore could be "poisoned" by adding clays and di-valent ions such that it would act as a poor processing ore (Kasongo et al., 2000). The recovery from the poisoned good processing ore could then be compared to the recovery from a poor processing ore. Comparison of Figure 5.5 with Figure 5.7 shows that this hypothesis is reasonable when only primary recovery is considered. The primary recovery obtained from the blank tests with the poor processing ore is close to those obtained when clay or a combination of clay and calcium are added to a good processing ore. In spite of this correlation, the hypothesis does not hold true when total recovery is considered. The total recoveries obtained from all three test conditions from the poor processing ores were all below 70% while the recoveries obtained from the poisoned good processing ores were all around 80%.

Comparisons of the bitumen/solids ratios obtained from the two different ores further supports the position that the poisoning of good processing ores does not entirely re-create the processability of poor ores. Figure 5.8 clearly shows that the B/S ratios from the poor ore were below 1 for all the froths (primary and total) obtained from all three flotation conditions. The B/S ratios from the good ore, meanwhile, were all above 1.5 with the exception of the secondary froth from the good processing ore (discussed in section 5.3.1). The addition of clay or a combination of clay and calcium to the good processing ore did not produce B/S ratios similar to those obtained from the poor processing ore.

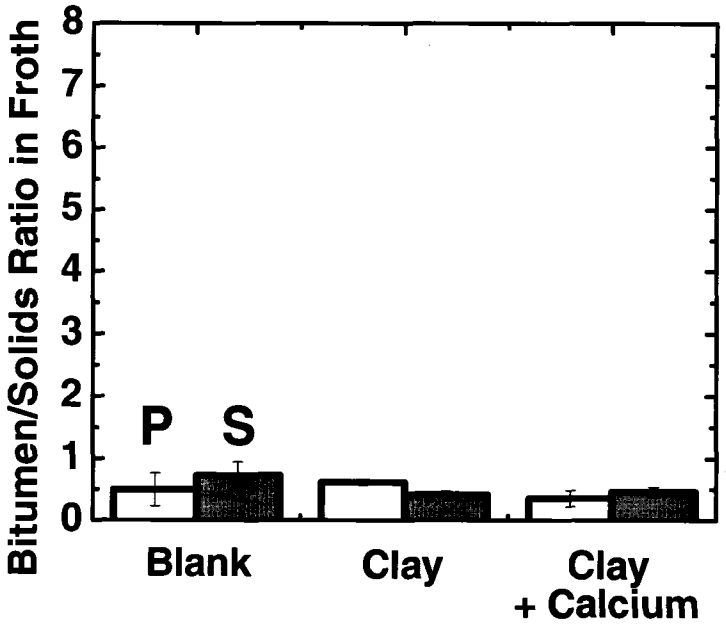

Figure 5.8: The bitumen/solids ratio of the primary (white) and secondary (gray) froths from a poor processing ore at 65°C.

5.3.3 Tailings Water Chemistry

The results of the pH and AAS measurements performed on the tailings water from each test are summarized in Tables 5.5 and 5.6 for good ore and poor ore, respectively. Recall that the extraction tests were performed at 65°C. Again, the residual levels of calcium in the tailings water were very low (< 0.5 ppm). The pH of the slurry increased with the addition of montmorillonite. For the good ore, the pH increased from 6.7 to 8.4 and 8.2 for the tests performed with clay addition and the co-addition of clay and calcium, respectively. For the poor ore, the pH increased from 7.6 to 8.3 and 8.2 for the tests with clay addition and the co-addition of clay and calcium, respectively.

Table 5.5: Analysis of the tailings water from tests performed at 65°C using good ore.

	[Ca] ppm	[Mg] ppm	pH
Blank	0.164	0.120	6.7
Clay Only	0.105	0.235	8.4
Clay + Calcium	0.495	0.159	8.2

Table 5.6: Analysis of the tailings water from tests performed at 65°C using poor ore.

	[Ca] ppm	[Mg] ppm	pH
Blank	0.023	0.151	7.6
Clay Only	0.126	0.447	8.3
Clay + Calcium	0.113	0.262	8.2

5.4 Summary

1) A large drop in primary recovery was observed when clay or a combination of clay and calcium was added to the good ore at 65°C. This decrease was not observed at 35°C. The processing temperature strongly affected the processability of this ore.

2) For the poor ore processed at 35°C or 65°C, total recovery appeared to drop slightly with the addition of clay or the co-addition of clay and calcium. The

primary recoveries and froth qualities obtained were similar in all cases. The processing temperature did not impact the processability of this ore.

3) The processability of poor ores can not always be re-created by doping good ores with clays or di-valent ions.

4) AAS results incidated that virtually all of the calcium added to the flotation system was consumed by various slurry components.

5) The addition of montmorillonite to the flotation slurry increased the pH of the system, which may have offset some of the detrimental effects of montmorillonite on bitumen recovery.

6) The montmorillonite used in these experiments was primarily a sodium clay (rather than a calcium clay), and this may explain why more drastic reductions in bitumen recovery were not observed.

6 Conclusions and Recommendations for Future Work

6.1 Summary of the Current Work

It is commonly believed that the so-called "poor processing" ores may be characterized by high levels of fine particles and di-valent cations. The fine particles are believed to consist mainly of clays while calcium and magnesium are commonly viewed as the most problematic di-valent cations.

Zeta potential distribution measurements have shown that calcium can induce a slime coating of montmorillonite clay onto bitumen (Liu et al., 2004b; Liu et al., 2002). A similar slime coating effect was not observed with kaolinite clay or in the absence of calcium. It was speculated that such a coating would inhibit bitumen aeration and thus bitumen flotation. Flotation results have shown that montmorillonite clay and calcium act synergetically to depress bitumen recovery (Kasongo et al., 2000)

In this work, zeta potential distributions were used to examine the effects of magnesium, sodium bicarbonate, and sodium hydroxide on slime coating of montmorillonite onto bitumen. Atomic absorption spectroscopy was used to examine how the levels of calcium and magnesium in a 1 mM solution change with pH or the level of sodium bicarbonate added to the solution. Flotation tests were performed to determine whether a direct correlation existed between slime coating tendency and bitumen recovery or froth quality.

6.1.1 Zeta Potential Distributions

The average zeta potential of bitumen became increasingly negative as pH increased. Additions of 1 mM of $CaCl_2$ or $MgCl_2$ caused the zeta potential to become less negative. An iso-electric point was observed at a pH of approximately 11.5 when magnesium was present. This was attributed to adsorption of magnesium hydroxide precipitates on the surface of bitumen. The zeta potential of montmorillonite did not change with pH, although the addition of calcium or magnesium did make the zeta potential less negative.

No slime coating of montmorillonite on bitumen was observed in an electrolyte solution containing 1 mM KCl. Slime coating was observed when 1 mM of calcium ions, magnesium ions, or 0.5 mM of both calcium and magnesium ions were added to the 1 mM KCl solutions. The slime coating was more pronounced at lower bitumen to montmorillonite mass ratios. The addition of 7.1 or 16.4 mM of sodium bicarbonate to the solutions prevented slime coating when calcium was present, but showed little effect when magnesium was present. The removal of calcium from the solution limits the calcium that can act as a "bridge" between bitumen and montmorillonite. It was also possible that the dispersing effect of sodium bicarbonate was enough to overpower the attraction induced by calcium but not the attraction induced by magnesium. Sodium bicarbonate was also more effective at preventing slime coating than reversing slime coating when calcium was present.

The addition of 12.5 mM of NaOH to a solution containing 1 mM KCl and 1 mM $MgCl_2$ caused the zeta potential of bitumen to become positive. The zeta potential of montmorillonite remained negative. Slime coating was observed in this case and was attributed to the attraction between the oppositely charged components.

Attempts to perform zeta potential distribution measurements at 35°C were unsuccessful as transient results were obtained. It is likely that the size of bitumen droplets continuously changed during the measurements at high temperature.

6.1.2 Atomic Absorption Spectroscopy

Atomic absorption spectroscopy (AAS) measurements showed that little precipitation of calcium occurred in the pH range 6-11.5 without sodium bicarbonate addition. Calcium precipitation began to occur near pH 8.5 when 7.1 mM or 16.4 mM of sodium bicarbonate was added. At a constant pH of 8.5, the amount of calcium precipitated increased as the level of bicarbonate addition increased.

The addition of sodium bicarbonate had little effect on solutions containing 1 mM $MgCl_2$. The disappearance of soluble magnesium, in all cases, began near pH 10.5.

The precipitation behavior can help explain why sodium bicarbonate is effective in preventing slime coating in the presence of calcium, but not magnesium.

6.1.3 Denver Cell Flotation

A large, statistically significant drop in bitumen recovery was observed only when the good processing ore was doped with clay or clay and calcium at 65°C. It is likely that slime coating or bitumen-trapping clay structures were responsible for this effect. A depression in recovery was not noted for this ore at 35°C, which indicates that temperature may be a stronger factor affecting bitumen recovery than the presence of clays or di-valent cations. For the poor processing ore, the total recovery appeared to decrease slightly with the addition of clay or the combination of clay and calcium. The results showing that froth quality from the blank tests with the poor ore

was lower than those with the doped good ore means that the processability of poor ores may not always be replicated by doping good ores with clay or di-valent cations.

In all flotation tests, very little residual calcium and magnesium was observed in the tailings water. Furthermore, the addition of montmorillonite to flotation increased the pH of the tailings water. The fact that the di-valent concentration was low and pH remained high despite the addition of the detrimental ions and clays may help explain why more drastic reductions in bitumen recovery or froth quality were not generally observed. The concept that calcium clays are more detrimental to recovery than sodium clays (used in this study) may also explain why more drastic reductions in froth quality or recovery were not observed in this work.

6.2 Recommendations for Future Work

An on-going problem in oil sands research is that there is no laboratory test method that can accurately re-create the process conditions experienced in industrial operations. For example, the hydrodynamics, residence time, and slurry flow patterns experienced in industrial operations are un-likely to be the same as those experienced in a Denver flotation cell or even a laboratory hydrotransport extraction system. Without a laboratory system that accurately re-creates real industrial conditions, one cannot be sure that the trends observed when clay, di-valent cations, or process aids are added to lab tests will translate into similar trends in industrial operations.

This work has shown that montmorillonite clay, when added to a good processing ore at 65°C, drastically decreased primary bitumen recovery. At the same time, the same clay added to a poor processing ore at the same temperature did not have a drastic effect on bitumen recovery. It would be a valuable exercise to add one particular clay (e.g. the same sodium montmorillonite used in this study) to many

different ore types such as marine ores, estuarine ores, transition ores, oxidized ores, etc. to see how the clay affects the processability of the various ore types. This exercise might help identify other ore components that are responsible for poor processability or conversely for good processability. Alternatively, it might be useful to modify the clay and see how it affects the processability of a given ore. In particular, it would be helpful to transform the sodium clay used in this study into the calcium form and then use it in processability studies to see if a different trend is observed.

The zeta potential and flotation experiments performed in this study were all carried out in de-ionized water with the manipulated variables being the levels of di-valent ions and clays added. The water used in industrial operations contains a plethora of dissolved ions and surfactants and is much more complex than the fluids used in this study. For the industrial operators, it would be of interest to determine whether slime coating occurs in various process waters (as process waters are not all alike). Furthermore, extraction tests can also be carried out with process water rather than de-ionized water.

Continuing on with the topic of water chemistry, it would be a useful exercise to "trace the path" of calcium, magnesium, and bicarbonate (or carbonate) ions in bitumen extraction to determine whether they adsorb preferentially on bitumen, sand, or clay surfaces, or if they react with dissolved species in the water before they make it to any surface.

Finally, the nature and role of dissolved organics in the water is not well understood. A better understanding of what these species are, where they migrate to, and what they do would fill an important piece in the processability puzzle.

References

Baptista, M. (1989a). Role of the Exchangeable Cations and Iron-amorphous Coatings of the Oil Sand Solids in Oil Sand Processing - Part 2. Pilot and Plant Tests. *AOSTRA Journal of Research, 5*(3), 243-256.

Baptista, M. (1989b). Role of the Exchangeable Cations of Oil Sand Clays in Oil Sand Processing - Part 1. Batch Tests. *AOSTRA Journal of Research, 5*(3), 237-241.

Basu, S., Nandakumar, K., Lawrence, S., and Masliyah, J. (2004). Effect of calcium ion and montmorillonite clay on bitumen displacement by water on a glass surface. *Fuel, 83*(1), 17-22.

Bensebaa, F., Kotlyar, L., Sparks, B., and Chung, K. (2000). Organic Coated Solids in Athabasca Bitumen: Characterization and Process Implications. *Canadian Journal of Chemical Engineering, 78*(4), 610-616.

Boeve, E., Cao, L., De Bruijn, W., Robertson, W., Romijn, J., and Schroder, F. (1994). Zeta Potential Distribution on Calcium Oxalate Crystal and Tamm-Horsfall Protein Surface Analyzed with Doppler Electrophoretic Light Scattering. *The Journal of Urology, 152*(2), 531-536.

Camp, F. (1976). *The Tar Sands of Alberta, Canada.* Denver, CO: Cameron Engineers.

Canadian Energy Research Institute. (2004). *Oil Sands Supply Outlook: Potential Costs of Crude Bitumen and Synthetic Crude Oil in Canada, 2013-2017.* Calgary.

Chemical Rubber Company. (2005). *CRC Handbook of Chemistry and Physics.* Binghamton, NY: Knovel.

Chong, J., Ng, S., Chung, K., Sparks, B., and Kotlyar, L. (2003). Impact of fines content on a warm slurry extraction process using model oilsands. *Fuel, 82*(4), 425-438.

Clark, K., and Pasternack, D. (1932). Hot Water Separation of Bitumen from Alberta Bituminous Sand. *Industrial and Engineering Chemistry, 24*, 1410-1416.

Connah, M. (2002). High Resolution Zeta Potential Measurements: Analysis of Multi-component Mixtures. *Journal of Dispersion Science and Technology, 23*(5), 663-669.

Czarnecka, E., and Gillott, J. (1980). Formation and Characterization of Clay Complexes with Bitumen from Athabasca Oil Sand. *Clays and Clay Minerals, 28*(3), 197-203.

Drelich, J., Lelinski, D., Hupka, J., and Miller, J. (1995). The role of gas bubbles in bitumen release during oil sand digestion. *Fuel, 74*(8), 1150-1155.

Eslinger, E., and Pevear, D. (1988). *Clay Minerals for Petroleum Geologists and Engineers*. Tulsa, OK: Soc. of Economic Paleontologists and Mineralogists.

Everett, D. (1988). *Basic Principles of Colloid Science*. London, UK: Royal Society of Chemistry.

Flynn, M., Bara, B., Czarnecki, J., and Masliyah, J. (2001). An Investigation of the Effect of Air Addition During Oil Sand Conditioning. *Canadian Journal of Chemical Engineering, 79*(3), 468-470.

Fong, N., Ng, S., Chung, K., Tu, Y., Li, Z., Sparks, B., et al. (2004). Bitumen recovery from model systems using a warm slurry extraction process: effects of oil sands components and process water chemistry. *Fuel, 83*(14-15), 1865-1880.

Globus, A. (1978). Process for Recovery of Bituminous Material from Tar Sands. United States: Guardian Chemical Corporation,.

Government of Alberta: Department of Energy. (2004). *Talk about Oil Sands: Fact Sheet*. Retrieved May 13, 2005, from http://www.energy.gov.ab.ca/152.asp

Gray, M., and Masliyah, J. (2002). Paper presented at the Extraction and Upgrading of Oilsands Bitumen: Intensive Short Course, Fort McMurray, AB.

Grim, R. (1968). *Clay Mineralogy*. New York, NY: McGraw-Hill.

Gu, G., Xu, Z., Nandakumar, K., and Masliyah, J. (2003). Effects of physical environment on induction time of air-bitumen attachment. *International Journal of Mineral Processing, 69*(1-4), 235-250.

Hall, E., and Tollefson, E. (1982). Stabilization and Destabilization of Mineral Fines-Bitumen-Water Dispersions in Tailings from Oil Sand Extraction Plants that use the Hot Water Process. *Canadian Journal of Chemical Engineering, 60*(6), 812-821.

Humphreys, R. (1998). Tar Sands Extraction Process. Canada: Geopetrol Equipment Ltd,.

Hunter, R. (1981). *Zeta Potential in Colloid Science: Principles and Applications.* New York, NY: Academic Press.

Hunter, R. (2001). *Foundations of Colloid Science* (2 ed.). Oxford, UK: Oxford University Press.

Israelachvili, J. (1992). *Intermolecular and Surface Forces* (2 ed.). San Diego, CA: Academic Press.

Ives, K. (Ed.). (1984). *The Scientific Basis of Flotation.* The Hague, The Netherlands: Martinus Nijhoff Publishers.

Johnson, S., Franks, G., Scales, P., Boger, D., and Healy, T. (2000). Surface chemistry-rheology relationships in concentrated mineral suspensions. *International Journal of Mineral Processing, 58*(1-4), 267-304.

Kasongo, T., Zhou, Z., Xu, Z., and Masliyah, J. (2000). Effect of Clays and Calcium Ions on Bitumen Extraction from Athabasca Oil Sands Using Flotation. *Canadian Journal of Chemical Engineering, 78*(4), 674-681.

King, R. (Ed.). (1982). *Principles of Flotation.* Johannesburg, South Africa: South African Institute of Mining and Metallurgy.

Klassen, V., and Mokrousov, V. (1963). *An Introduction to the Theory of Flotation* (J. Leja and G. Poling, Trans. 2 ed.). London, UK: Butterworths.

Kotlyar, L., Sparks, B., and Schutte, R. (1995). Role of Bicarbonate Ions in the Stability of Ultra-Fines Suspensions. *Journal of Environmental Science and Health A, 30*(6), 1277-1288.

Liu, J., Xu, Z., and Masliyah, J. (2003). Studies on Bitumen-Silica Interactions in Aqueous Solutions by Atomic Force Microscopy. *Langmuir, 19*(9), 3911-3920.

Liu, J., Xu, Z., and Masliyah, J. (2004a). Interaction betwen Bitumen and FInes in Oil Sands Extraction System: Implication to Bitumen Recovery. *Canadian Journal of Chemical Engineering, 82*(4), 655-666.

Liu, J., Xu, Z., and Masliyah, J. (2004b). Role of Fine Clays in Bitumen Extraction from Oil Sands. *AIChE Journal, 50*(8), 1917-1927.

Liu, J., Zhou, Z., Xu, Z., and Masliyah, J. (2002). Bitumen-Clay Interactions in Aqueous Media Studied by Zeta Potential Distribution Measurement. *Journal of Colloid and Interface Science, 252*(2), 409-418.

Majer, J., and Khalil, S. (1981). Adsorption of Calcium and Magnesium Ions on Surfaces. *Analytica Chimica Acta, 126*, 175-183.

Masliyah, J. (1994). *Electrokinetic Transport Phenomena.* Edmonton, AB: Alberta Oil Sands Technology and Research Authority.

Masliyah, J., Zhou, Z., Xu, Z., Czarnecki, J., and Hamza, H. (2004). Understanding Water-Based Bitumen Extraction from Athabasca Oil Sands. *Canadian Journal of Chemical Engineering, 82*(4), 628-654.

Moran, K., Yeung, A., and Masliyah, J. (2000). Factors Affecting the Aeration of Small Bitumen Droplets. *Canadian Journal of Chemical Engineering, 78*(4), 625-634.

New Mexico State University: Department of Chemistry and Biochemistry. Retrieved April 18, 2005, from http://www.chemistry.nmsu.edu/Instrumentation/AAS_schematic.gif

Ng, S., Warszynski, P., Zembala, M., and Malysa, K. (2000). Bitumen-Air Aggregates Flow to Froth Layer: II. Effect of Ore Grade and Operating Conditions on Aggregate Composition and Bitumen Recovery. *Minerals Engineering, 13*(14-15), 1519-1532.

Petrucci, R., and Harwood, W. (1997). *General Chemistry: Principles and Modern Applications* (7 ed.). Upper Saddle River, NJ: Prentice-Hall.

Radler, M. (2002). Worldwide reserces increase as production holds steady. *Oil and Gas Journal, 100*(52), 113-145.

Sanford, E. (1983). Processability of Athabasca Oil Sand: Interrelationship Between Oil Sand Fine Solids, Process, Aids, Mechanical Energy and Oil Sand Age After Mining. *Canadian Journal of Chemical Engineering, 61*(4), 554-567.

Sanford, E., and Seyer, F. (1979). Processibility of Athabasca tar sand using a batch extraction unit: the role of NaOH. *CIM Bulletin, 72*(803), 164-169.

Schramm, L. (1989). The influence of suspension viscosity on bitumen rise velocity and potential recovery in the hot water flotation process for oil sands. *Journal of Canadian Petroleum Technology, 28*(3), 73-80.

Schramm, L., and Smith, R. (1985). The Influence of Natural Surfactants on Interfacial Charges in the Hot-Water Process for Recovering Bitumen from the Athabasca Oil Sands. *Colloids and Surfaces, 14*(1), 67-85.

Schramm, L., and Smith, R. (1989). Some Parametric Studies of Oil Sand Conditioning in the Hot Water Flotation Process. *AOSTRA Journal of Research, 5*, 87.

Schramm, L., Smith, R., and Stone, J. (1984). The Influence of Natural Surfactant Concentration on The Hot Water Process for Recovering Bitumen from the Athabasca Oil Sands. *AOSTRA Journal of Research, 1*, 5-13.

Schramm, L., Stasiuk, E., and Turner, D. (2003). The influence of interfacial tension in the recovery of bitumen by water-based conditioning and flotation of Athabasca oil sands. *Fuel Processing Technology, 80*(2), 101-118.

Schramm, L., Stasiuk, E., Yarranton, H., Maini, B., and Shelfantook, B. (2003). Temperature Effects From the Conditioning and Flotation of Bitumen From Oil Sands in Terms of Oil Recovery and Physical Properties. *Journal of Canadian Petroleum Technology, 42*(8), 55-61.

Skvarla, J. (1996a). Detection of the heterocoagulation-stability transition in binary colloidal systems by electrophoretic light scattering. Silica-silica/aminopropyl system. *Colloids and Surfaces A, 110*(2), 135-139.

Skvarla, J. (1996b). Evaluation of mutual interactions in binary mineral suspensions by means of electrophoretic light scattering (ELS). *International Journal of Mineral Processing, 48*(1-2), 95-109.

Smith, R., and Schramm, L. (1992). The influence of mineral components on the generation of natural surfactants from Athabasca oil sands in the alkaline hot water process. *Fuel Processing Technology, 30*(1), 1-14.

Sparks, B., Kotlyar, L., O'Carroll, J., and Chung, K. (2003). Athabasca oil sands: effect of organic coated solids on bitumen recovery and quality. *Journal of Petroleum Science and Engineering, 39*(3-4), 417-430.

Sun, S. (1943). The Mechanism of Slime-coating. *Transactions of the AIME, 153*, 479-492.

Takamura, K., and Chow, R. (1983). A mechanism for initiation of bitumen displacement from oil sand. *Journal of Canadian Petroleum Technology, 22*(6), 22-30.

Towson, D. (1979). The Oil Sands of Alberta: source of Canada's future oil supply? *Journal of Canadian Petroleum Technology, 18*(4), 10-12.

USCINCPAC. (2002). *Asian Oil Imports: A Special Report*: Headquarters, United States Commander In Chief Pacific.

Van Loon, C. (1980). *Analytical Atomic Absorption Spectroscopy: Selected Methods.* New York, NY: Academic Press.

van Olphen, H. (1977). *An Introduction to Clay Colloid Chemistry.* New York, NY: John Wiley and Sons.

Velde, B. (1977). *Clays and Clay Minerals in Natural and Synthetic Systems.* Amseterdam: Elsevier.

Velde, B. (1992). *Introduction to Clay Minerals.* London, UK: Chapman and Hall.

Wallace, D., Tipman, R., Komishke, B., Wallwork, V., and Perkins, E. (2004). Fines/Water Interactions and Consequences of the Presence of Degraded Illite on Oil Sands Extractability. *Canadian Journal of Chemical Engineering, 82*(4), 667-677.

Wallwork, V., Xu, Z., and Masliyah, J. (2004). Processability of Athabasca Oil Sand Using a Laboratory Hydrotransport Extraction System (LHES). *Canadian Journal of Chemical Engineering, 82*(4), 687-695.

Welz, B., and Sperling, M. (1999). *Atomic Abosrption Spectrometry* (3 ed.). Weinheim, Germany: Wiley-VCH.

Xu, Z., Liu, J., Choung, J., and Zhou, Z. (2003). Electrokinetic study of clay interactions with coal in flotation. *International Journal of Mineral Processing, 68*(1-4), 183-196.

Zhou, Z., Xu, Z., and Masliyah, J. (2000). Effect of Natural Surfactants Released from Athabasca Oil Sands on Air Holdup in a Water Column. *Canadian Journal of Chemical Engineering, 78*(4), 617-624.

Appendix A

Appendix A: Analysis of Froth and Calculation of Bitumen Recovery and the Bitumen/Solids Ratio

Dean and Stark Procedure:

1) The cellulose thimbles containing the froth samples were hung inside of glass round bottom flasks containing approximately 250 mL of toluene. The flasks were placed into mantle heaters where the toluene was re-fluxed with a condenser and water trap assembly. Water and some toluene condensates were collected in the trap while the remaining condensed toluene was allowed to drip over the thimbles containing froth. The mantle heaters were turned off after all toluene dripping through the thimbles was clear, indicating that all the bitumen in the thimble had dissolved.

2) The water in the traps was collected and weighed (m_w). The thimbles containing solids from the froth were placed in a vacuum oven at 80°C overnight to remove the remaining toluene. Dry thimbles were removed from the vacuum oven and the weight of solids was obtained by comparing the dried thimble to the original weight of the thimble and jar (m_s).

3) After the contents had cooled to room temperature, the diluted bitumen samples remaining in the bottom of the round bottom flasks were transferred to 250 mL volumetric flasks and topped up to the 250 mL mark with additional toluene. The flasks were shaken and inverted, and 50 mL from each flask were transferred to 50

mL plastic centrifuge tubes (Fisher). The tubes were centrifuged at 3000 rpm for 20 minutes (IEC HN-SII) to enable the remaining suspended fine solids to settle. Glass fiber filter pads (Whatman) were weighed and placed on a watch glass. A glass pipette was used to evenly spread 5 mL of the centrifuged diluted bitumen from the centrifuge tubes onto the filter papers. The filter papers were hung in a fume hood and allowed to dry for 20-30 minutes. The filter papers were then re-weighed and the difference between the two weights was used to determine the bitumen content of the froth (m_b).

The expression for percent bitumen recovery is

$$\%\,\mathrm{Recovery} = \frac{m_b}{(m_{ore})(grade)} * 100\% \qquad [A.1]$$

where m_b is the mass of bitumen recovered, m_{ore} is the mass of ore used for the test, and "grade" is the bitumen fraction of the ore. The bitumen to solids ratio (B/S ratio) is defined as the mass of bitumen divided by the mass of solids (m_s) recovered during the test.

$$B/S = \frac{m_b}{m_s} \qquad [A.2]$$

Appendix B

Appendix B: Sample calculation for κa and the applicability of the Smoluchowski equation.

Sample Electrolyte: 1 mM KCl, 1 mM $MgCl_2$ at pH 8.5 (modified using NaOH)

Recalling equation 1.11,

$$\kappa = \left(\frac{2000 I^2}{\varepsilon \varepsilon_0 RT} \right)^{1/2} \left(0.5 \sum c_i z_i^2 \right)^{1/2}$$

we can calculate the value κ in m^{-1}. In this solution, the ionic strengths are approximately as follows:

Table B.1: Ionic composition of the sample electrolyte.

K^+	Na^+	OH^-	Cl^-	Mg^{2+}
0.001 M	$3.16 \cdot 10^{-6}$ M	$3.16 \cdot 10^{-6}$ M	0.003 M	0.001 M

Assuming the system temperature is at 25°C, equation 1.11 simplifies to the following (Hunter, 2001), where κ is given in nm^{-1}:

$$\kappa = 3.288 * \left(0.5 \sum c_i z_i^2 \right)^{1/2} \qquad [B.1]$$

Thus, for our sample electrolyte, $\kappa = 0.208\ nm^{-1}$. The values of κa for the various components used in our studies are listed in Table B.2.

Table B.2: κa values for the components used in the sample electrolyte at 25°C.

	Bitumen (20 minutes cream time)	Bitumen (1 hour cream time)	Bitumen (4 hours cream time)	Montmorillonite (1 hour settling time)
κ	$0.208\ nm^{-1}$	$0.208\ nm^{-1}$	$0.208\ nm^{-1}$	$0.208\ nm^{-1}$
a	$1 \cdot 10^4$ nm	$9 \cdot 10^3$ nm	$4.6 \cdot 10^3$ nm	$2.5 \cdot 10^3$ m
κa	2080	1872	957	520

As all κa values listed are >>1, Smoluchowski's equation can be correctly used to convert the electrophoretic mobility values in this study to zeta potential values.